

# Nanoscale

Accepted Manuscript



This is an *Accepted Manuscript*, which has been through the Royal Society of Chemistry peer review process and has been accepted for publication.

*Accepted Manuscripts* are published online shortly after acceptance, before technical editing, formatting and proof reading. Using this free service, authors can make their results available to the community, in citable form, before we publish the edited article. We will replace this *Accepted Manuscript* with the edited and formatted *Advance Article* as soon as it is available.

You can find more information about *Accepted Manuscripts* in the [Information for Authors](#).

Please note that technical editing may introduce minor changes to the text and/or graphics, which may alter content. The journal's standard [Terms & Conditions](#) and the [Ethical guidelines](#) still apply. In no event shall the Royal Society of Chemistry be held responsible for any errors or omissions in this *Accepted Manuscript* or any consequences arising from the use of any information it contains.

Cite this: DOI: 10.1039/c0xx00000x

www.rsc.org/xxxxxx

**ARTICLE TYPE**

# Future prospects of luminescent nanomaterials based security ink: from synthesis to anti-counterfeiting applications

**Pawan Kumar,<sup>a,b</sup> Satbir Singh<sup>a,b</sup> and Bipin Kumar Gupta<sup>\*b</sup>***Received (in XXX, XXX) XthXXXXXXXXXX 20XX, Accepted Xth XXXXXXXXXXXX 20XX*

DOI: 10.1039/b000000x

Counterfeiting of valuable documents, currency and branded products is a challenging problem that has serious economic, security and health ramifications for governments, businesses and consumers all over the world. It is estimated that counterfeiting represents a multi-billion dollar underground economy with counterfeit products being produced at large scale every year. Counterfeiting is an increasingly high-tech crime and it calls for high-tech solutions to prevent and deter the acts of counterfeiting. The present review briefly outlines and addresses the key challenges in this area, including above concerns for anti-counterfeiting applications. This article describes a unique combination of all possible kinds of security ink formulations based on lanthanide doped luminescent nanomaterials, quantum dots (semiconductor and carbon based), metal organic frameworks as well as plasmonic nanomaterials for their possible use in anti-counterfeiting applications. Moreover, in this review, we have briefly discussed and described the historical background of luminescent nanomaterials, basic concepts and detailed synthesis methods with their characterizations. Furthermore, we have also discussed about the strategy adopted for the fabrication and design of luminescent security inks, various security printing techniques and their anti-counterfeiting applications.

## 1. Introduction

Luminescent materials have found a wide range of applications in all walks of daily life, including advanced optical displays, solid state lighting, X-ray intensification, scintillation and many more.<sup>1</sup> Therefore, enormous efforts have been devoted to explore novel luminescent materials so far, which is the need of the hour. These materials are generally characterized by the emission of light in the visible range, but can exist in other spectral regions also (such as ultraviolet or infrared) with energy beyond thermal equilibrium.<sup>1-3</sup> The ever-growing demand for newer luminescent materials has motivated scientific and technological efforts to improve the existing features of luminescent materials and to provide encouragement for the development of new effective luminescent nanomaterials having desired shape, size, morphology and optical properties etc.<sup>4</sup> These nanomaterials have a wide range of applications such as photovoltaic, bio-medical, anti-counterfeiting, solid state lighting and display technologies etc. One of their extremely important uses is for the development of security ink for anti-counterfeiting applications. These nanomaterials can easily be applied inexpensively to different surfaces and have been implemented widely as security inks to protect high-value merchandise, documents, pharmaceuticals and currency.<sup>5</sup> Counterfeiting is an ever growing global problem that challenges companies, governments and customers.<sup>6</sup> Anti-counterfeiting techniques that make genuine items harder to copy

45

and easier to authenticate them are therefore important for the protection of brands and valuable documents.<sup>7</sup> Luminescent tags are most popular security elements for protecting authentic articles.<sup>7</sup> One way to incorporate luminescent nanomaterials as luminescent security elements is to print them with luminescent inks.<sup>8</sup> Nowadays, these printed luminescent security elements usually comprise only solid or halftone single ink color patterns.<sup>9</sup> Typical examples are bank notes that show luminescent parts under UV light.<sup>9</sup> Procedures for producing full color images by printing luminescent inks exist.<sup>10</sup> These methods use several luminescent inks with different luminescent colors to form a full color image by luminescence.<sup>7</sup> However, they are either colorimetrically inaccurate or use complex halftoning algorithms.<sup>7</sup> Many luminescent inks and markers used, for example as security inks, are made of lanthanide compounds.<sup>11</sup> The distinctive character of the emission from lanthanide ions and particularly, their unique spectral fingerprints, enable the use of emissions and colors from lanthanide blends as security labels, markers or tags.<sup>7</sup>

The counterfeiting in fields of medicine and edible items can severely endanger human health. During the last decade, millions of dollars have been spent worldwide by governments and industries to safeguard their products and currencies from being counterfeited.<sup>12</sup> The efforts have yielded positive results but still there is further demand to develop improved anti-counterfeiting

Nanoscale Accepted Manuscript

nanomaterials and to build a suitable strategy for fabrication and design of security ink to deter counterfeiting.

Here, we present a review which is deeply focused on the synthesis of strategic luminescent nanomaterials, their morphology/microstructural characterizations, fabrication of security ink and its application against counterfeiting. During the past decades, a number of anti-counterfeiting technologies such as simple markers, plasmonic security labels, holograms, security inks were developed as a shield against counterfeiting.<sup>13-18</sup> Merely a few review articles have been reported where development of anti-counterfeiting technologies are discussed collectively using lanthanide doped luminescent nanomaterials, quantum dots (semiconductor and carbon based), luminescent metal organic frameworks as well as plasmonic nanomaterials based security inks at a single platforms. The present review article systematically describes in details the historical background of luminescent materials, basic concepts, luminescent mechanism, synthesis methods with their characterizations, fabrication of luminescent inks, security printing techniques and anti-counterfeiting applications using various types of luminescent nanomaterials: lanthanide doped luminescent nanomaterials (downconversion / downshift, upconversion and dual mode), quantum dots (semiconductor and carbon dots), luminescent metal organic frameworks and plasmonic nanomaterials.

### 1.1 Historical background and basic concepts of luminescent materials

The materials that glow in dark after exposure of light are known as '*phosphor*' since the early 17<sup>th</sup> century. The phosphor is a Greek word which means '*light bearer*'. There are many ancient reports related to minerals that glow in the dark. Most distinguished of them was Bolognian phosphor (impure barium sulfate; BaSO<sub>4</sub>) discovered by a cobbler Vincenzo Cascariolo in 1602.<sup>19</sup> Before the discovery of Bolognian stone, it is believed that the Japanese had reportedly prepared the phosphorescent paint from seashells. This fact is documented in a 10<sup>th</sup> century Chinese document (Song dynasty) which credits the Japanese for preparing phosphors for the first time.<sup>20</sup> Similarly, the blue colour emission was also observed from infusion of a wood by Nicolas Monardes (a Spanish physician and botanist) in 1565 and was used to treat kidney and urinary diseases (Fig. 1a).<sup>19, 21-26</sup> Later on this wood was called lignum nephriticum. The extracts from this wood were further investigated by Boyle, Newton and others but the phenomena was not understood at that time.<sup>19, 27</sup>

Later, Edward D. Clarke, Professor of Mineralogy at the University of Cambridge reported an abnormal property of fluorite crystals in 1819. The crystals were highly transparent in nature and had dichroic behaviour. In these crystals, the reflected light was deep sapphire blue, whereas transmitted light was bright green as shown in Fig 1b. But Clarke was unable to explain that phenomenon. Later on a French Mineralogist Rene Just Haüy also discussed the double colour of some fluorite crystals in 1822. He explained the phenomenon as a type of opalescence (which is observed with opal, a naturally occurring hydrated silica glass, and results from light scattering): the two colors were complementary, violet being the dominant shade of the scattered

light and green the dominant shade of the transmitted (i.e., unscattered) light.

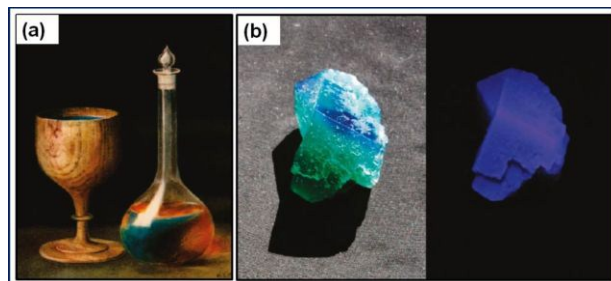


**Fig.1** (a) Absorption and fluorescence colours of infusions of lignum nephriticum in daylight (b) Twinned crystals of green fluorite (from Rogerley, Weardale, Durham County, England) illuminated with sunlight (left) and a UV lamp (right).<sup>19</sup> Reproduced with permission from ref. 19. Copyright 2014, American Chemical Society.

Although the explanation was incorrect<sup>19</sup> and a correct one was still a long way off Haüy's view and two minerals fluorite and opal were going to play a key role in understanding and naming of the fluorescence. After that, a famous paper titled, "on refrangibility of light" published by Sir G. G. Stokes, a physicist and professor of mathematics at Cambridge in 1852 proved to be ground breaking event in the history of photoluminescence.<sup>28</sup>

Later on in 1888, a German physicist, Eilhard Wiedemann was first to introduce the word '*Luminescence*' for both the fluorescence and phosphorescence phenomena. The *luminescence* term was taken from a Latin word *lumen*, which means light. Now a days, luminescence is defined as a phenomenon of spontaneous emission of radiation from an electronically excited species (or from a vibrationally excited species) not in thermal equilibrium with its environment.<sup>19, 29</sup> The fluorescence and phosphorescence can be distinguished on the basis of duration of emission after the end of excitation: fluorescence was considered as emission of light that disappear simultaneously after end of excitation whereas in phosphorescence the emitted light persists after the end of excitation.<sup>19</sup> But such distinction between fluorescence and phosphorescence is not appropriate because there are long-lived fluorescence (e.g., divalent europium salts) and short-lived phosphorescence (e.g., violet luminescence of zinc sulfide) whose durations are comparable (several hundreds of nanoseconds).<sup>19</sup> In 1929 Francis Perrin defined the phosphorescence as the phenomenon where the excited species passes through an intermediate state before emission.<sup>30</sup> More precisely, the fluorescence and phosphorescence can be defined in terms of the change in spin multiplicity. The spin multiplicity remains same in case of fluorescence whereas it changes from triplet to singlet or vice versa in case of phosphorescence.<sup>19</sup> The Schematic diagram (Jablonski diagram) for fluorescence and phosphorescence is shown in Fig.2.

The luminescence can also be classified on the basis of the source of excitation as shown in Table 1.

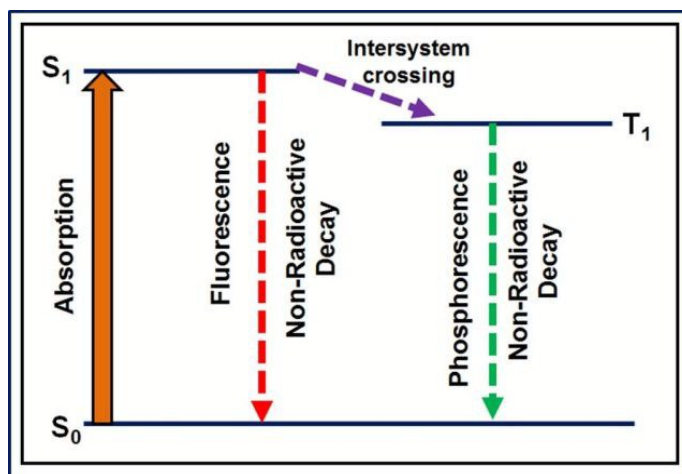


**Fig.2** Schematic diagram (Jablonski diagram) is showing difference between fluorescence and phosphorescence.

Type of Luminescence		Source of excitation	Examples
Biological	Bioluminescence	Luminescence produced by organisms	Firefly ( <i>Photinus pyralis</i> ), Glowworm ( <i>Lampyris noctiluca</i> )
Chemical	Chemiluminescence	Emission as a result of a chemical reaction	Luminol ( $C_8H_7N_3O_2$ )
Physical	Photoluminescence	Photons	Phosphor materials ( $YVO_4:Eu$ , $Y_2O_3:Eu$ , $GdVO_4:Er/Yb$ , $NaGdF_4:Eu$ , $NaYF_4:Eu$ etc.)
	Crystalloluminescence	Emission produced during crystallization	NaCl
	Electroluminescence	Emission as a result of an electric current passed through a substance	ZnS:Mn and ZnS:Cu
	Mechanoluminescence	Emission as a result of a mechanical action on a solid	Quartz glass, KBr and LiF
	Radioluminescence	Emission as a result of bombardment by ionizing radiation	$YBO_3:Eu$ , $Ba_2Si_5N_8:Eu$ ,
	Thermoluminescence	Emission as a result of heating	ZnS:Cu

**Table 1** Different types of luminescence depending upon the source of excitation.

## 1.2 Lanthanide doped luminescent nanomaterials

Recently, the lanthanide based luminescent nanostructures have been recognized worldwide for their better chemical and optical properties originating from their unique electronic structures as well as due to their wide range of applications in photovoltaics, bio-medical, anti-counterfeiting, solid state lighting and display technologies etc.<sup>31-59</sup> Lanthanide based luminescent nanomaterials are also known as nanophosphors. Generally, nanophosphors have one or more trivalent lanthanide ion doped in host lattice. There are 15 rare-earth elements including scandium and yttrium which can be used as trivalent ions in lanthanide based luminescent nanomaterials. The lanthanide based luminescent materials show sharp emission due to their intra-4f or 4f-5d electronic transitions. The lanthanide doped luminescent nanomaterials have many advantages over other luminescent materials (organic dye, quantum dots, plasmonic materials etc.) like sharp emission, broad excitation spectra, good thermal stability, low toxicity, a longer lifetime, better chemical stability and high photochemical stability etc.<sup>34</sup> The lanthanide doped luminescent materials can exhibit emission from ultraviolet (UV) to near infrared light region depending upon excitation. The lanthanide doped luminescent nanomaterials are further divided into two types depending upon their emission mechanism of luminescence as described below:

**1.2.1 Downconversion/downshift luminescence.** In this luminescence process, a high energy photon is converted into a low energy photon. This energy difference between emitted and absorbed photon is known as stoke shift. The schematic diagram for the downconversion luminescence process is shown in Fig.3.

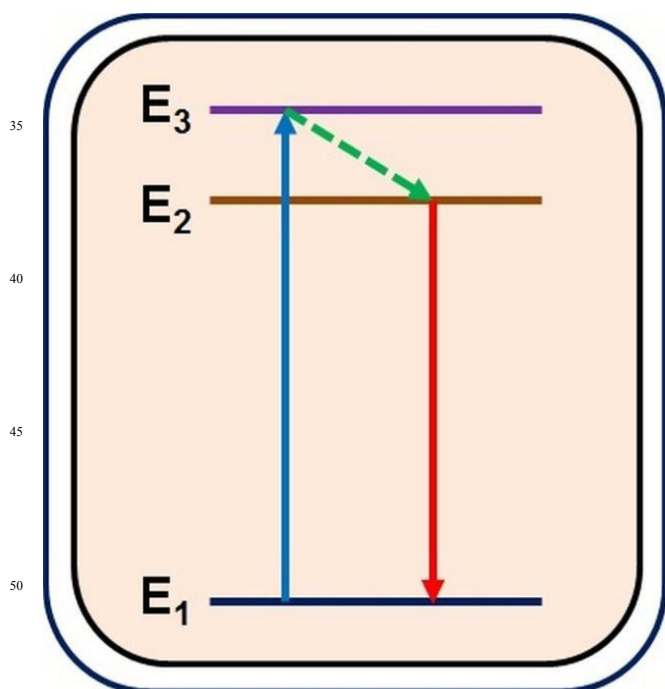


**Fig. 3** Schematic diagram for downconversion luminescence process.

The downconversion luminescent materials generally consist of host lattice doped with trivalent lanthanide ions. There are several types of lanthanide based host lattices such as oxides, fluoride, vanadate, oxy-sulfide and phosphate etc.<sup>34</sup> The lanthanide trivalent ions doped in rare-earth host lattice act as an activator. The role of host lattice is to absorb the energy (photons) and transfer it to the activator. Mostly in downconversion luminescent materials, host lattice also acts as sensitizer. For examples in Y<sub>2</sub>O<sub>3</sub> host lattice O<sup>2-</sup> acts as sensitizer while in case of GdVO<sub>4</sub>, VO<sub>4</sub><sup>3-</sup> acts as sensitizer. The emission efficiency in both the cases is higher due to efficient energy transfer energy from host to activator. The doping concentration of lanthanide ions is optimized so that the crystal structure of the host lattice with or without doping remains the same. In our earlier report, we have established that the optimum doping concentration of Eu<sup>3+</sup> in Y<sub>2</sub>O<sub>3</sub> host lattice is 5 mole%.<sup>15</sup> Besides the dopant concentration, the PL intensity is also influenced by some other factors, such as the host lattice, particle size, calcination temperature, environment, and synthesis condition.<sup>15,34,60-69</sup> The efficiency of downconversion can also be enhanced by doping of another lanthanide ion which acts as sensitizer. The sensitizer sufficiently transfers energy from host lattice to activator, resulting in enhancement of the luminescence efficiency. However, there are limited examples available in the literature of co-doping in case of downconversion. The Ce<sup>3+</sup> ion is most commonly used for co-doping in order to increase the luminescence efficiency of Ln<sup>3+</sup> (Ln = Eu, Tb, Dy, Sm) ions. There are many reports on downconversion luminescent nanomaterials reported in literature, where Ce<sup>3+</sup> act as sensitizer such as NaGdF<sub>4</sub>:Ce, Ln, BaYF<sub>5</sub>:Ce,Tb, YPO<sub>4</sub>:Ce,Tb, GdF<sub>3</sub>:Ce, Ln and Sr<sub>3</sub>Y<sub>2</sub>(BO<sub>3</sub>)<sub>4</sub>:Ce,Dy.<sup>69-74</sup> In all these luminescent materials discussed above, it is interesting to note that the excitation spectra are dominated by 4f-5d absorption of Ce<sup>3+</sup> ions, whereas the emission spectra are characteristic of Ln<sup>3+</sup> ions, indicating the energy transfer from Ce<sup>3+</sup> to Ln<sup>3+</sup> ions.<sup>34</sup>

**1.2.2 Upconversion luminescence.** In upconversion (UC) luminescence, a low energy photon is converted into a high energy photon by a non-linear process. Conceptually, in upconversion process, two or more photons are absorbed and converted into higher energy photons (generally NIR, visible and UV). In general, upconversion utilizes sequential absorption of multiple photons through the use of long lifetime and real ladder-like energy levels of trivalent lanthanide ions embedded in an appropriate inorganic host lattice to produce higher energy photons. This energy difference between emitted and absorbed photon is known as anti-Stokes shift.<sup>38</sup> The upconverting phosphors are generally inorganic host lattice doped with emitters Er<sup>3+</sup>, Tm<sup>3+</sup>, Ho<sup>3+</sup> and Yb<sup>3+</sup> (trivalent lanthanide ions) which produce emission when they are in excited states. The emission wavelength can be tuned by appropriate selection of trivalent lanthanide ions. There are three main mechanisms for upconversion process: excited state absorption, energy transfer upconversion and photon avalanche.<sup>45</sup> The schematic diagrams for upconversion process is shown in Fig.4 a-g. The schematic diagram for excited state absorption upconversion mechanism for single lanthanide ion doped luminescent materials is

Cite this: DOI: 10.1039/c0xx00000x

www.rsc.org/xxxxxx

ARTICLE TYPE

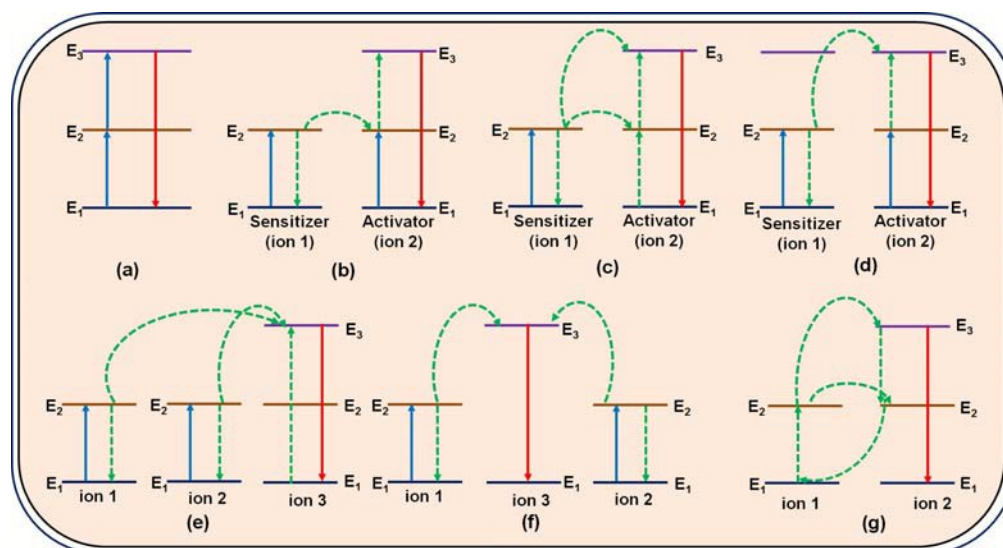


Fig. 4 Schematic diagram for upconversion process.

20

demonstrated in Fig. 4 a. The excited state absorption mechanism is a successive absorption of two photons as shown in Fig. 4 a. When the lanthanide ion is excited with a suitable energy photons from ground state ( $E_1$ ) to higher energy level ( $E_2$ ), another photon promotes the excited ion to higher energy state ( $E_3$ ). The upconversion occurs when photons drop from excited state ( $E_3$ ) to ground state ( $E_1$ ). The energy-transfer upconversion process is most efficient process. The five different types of energy-transfer upconversion process are shown in Fig. 4 b-f. In excited state absorption (Fig. 4b), the sensitizer ions absorbed the photons and transit from ground state ( $E_1$ ) to excited state ( $E_2$ ). The energy transfer occurs from sensitizer ion to activator ion, which is at excited state ( $E_2$ ). The energy transfer promotes activator ions from lower energy state ( $E_2$ ) to higher energy state ( $E_3$ ). In successive energy transfer (Fig. 4c), only sensitizer ion absorbs photons and promotes activator ion to energy level ( $E_2$ ) and energy level ( $E_3$ ) by two successive energy transfers. The sensitizer and activator ions both are of similar nature in cross-relaxation upconversion (Fig. 4d). The activator and sensitizer ions absorbed photons in their excited state ( $E_2$ ). The energy transfer process then promotes the activator ion to its excited state  $E_3$  while the sensitizer reverts to the ground state.<sup>45</sup> Fig. 4 e & f demonstrates that the energy transfer upconversion involves the cooperative effect. In these cases, luminescence nanomaterials have more than one ions that take part in sensitization or luminescence process. In case of cooperative sensitization (Fig. 4e), two sensitizer ions (ion 1 and ion 2) absorbed photons and then together transfer this energy to activator ion (ion 3) which

promotes ion 3 to an excited state ( $E_3$ ). However, in case of cooperative luminescence, two excited ions (ion 1 and ion 2) absorbed photon and cooperate in producing emission (Fig. 4f). The photon avalanche is shown in Fig. 4g. This process requires minimum excitation power called threshold value. Above the threshold value, the luminescence intensity increases by the order of magnitude. Basically, the photon avalanche is a looping process that associated with processes of excited state absorption (ESA) for excitation light and efficient cross relaxation (CR) that produce feedback as shown in Fig. 4g. Initially non resonant weak ground state absorption populates the level  $E_1$  of ion 2 and the looping process starts with the ESA process to elevate ion 2 at the level  $E_1$  to the emitting level  $E_2$ . An efficient CR process of  $E_2$  (ion 2) + G (ion 1)  $\rightarrow$   $E_1$  (ion 2) +  $E_1$  (ion 1) between ion 1 and ion 2 is then accomplished. Finally, ion 1 transfers its energy to ion 2 to populate its level  $E_1$ , creating a complete loop. The resulting effect of the looping process is, that a single ion 2 at metastable  $E_1$  state produces two ion 2's at this state. When the looping process follows, two ion 2's at the  $E_1$  state will produce four ions and further four will produce eight ions, generating an avalanche effect for populating ion 2 in its  $E_1$  state, and thus the photo avalanche (PA) UC from the emitting level of  $E_2$ . It is easy to recognize PA because it generally requires a pump threshold and a long time (in seconds) to build up. Furthermore, the dependence of UC photoluminescence on the pump power becomes extremely strong around the threshold pumping power.<sup>45</sup>

75

Cite this: DOI: 10.1039/c0xx00000x

www.rsc.org/xxxxxx

ARTICLE TYPE

**1.2.3 Quantum cutter luminescence.** The quantum cutting is a luminescence phenomenon where one absorbed photon is converted into two or more photons. This phenomenon is also known as quantum splitting or photon cascade emission. As moreover, the energy of a vacuum ultraviolet (VUV) photon is more than twice that of a visible photon, it is theoretically possible to achieve two visible photons emissions for every incident photon.<sup>75</sup> The quantum cutting materials have quantum efficiency more than 100% that provides a new directions for development of solid state lighting, advanced display systems and strong security applications etc.<sup>76</sup> Quantum cutting phenomenon was theoretically predicated by Dexter.<sup>77</sup> There are three possible mechanisms for quantum cutting process: (a) quantum cutting using host lattice states, (b) quantum cutting on single ions and (c) quantum cutting on ion pairs.

The process (a) involves the absorption of photons with energy at least twice the band gap of the host materials. Briefly, this excited electron-hole pair generates two electron-hole pairs, each with energy approximately equal to the band-gap energy, via Auger-interaction.<sup>78</sup> Process (b) requires the well-separated energy levels of ions or atoms that can be used to generate more than one visible photon out of one UV photon. In this mechanism, two conditions that must be fulfilled are: (i) the energy gap between adjacent levels must be large enough to prevent multi-phonon relaxation and (ii) the branching ratio of visible emission must be high.<sup>75</sup> There are a number of reports available which described in detail the quantum cutting process using single ion. Sommerdijk et al. first observed the quantum cutting effect in Pr<sup>3+</sup>-doped YF<sub>3</sub>.<sup>79-80</sup> The quantum cutting phenomenon also observed in many oxide host lattices using Pr<sup>3+</sup> ion as dopant.<sup>81-83</sup> The Pr<sup>3+</sup> ion doped fluorides and several oxides are widely explored for quantum cutting with single ion doping due to their energy position of the 4f-5d states with respect to the <sup>1</sup>S<sub>0</sub> state and suitably large 4f-5d energy separation.<sup>75</sup> The energy level scheme of Pr<sup>3+</sup> favours quantum cutting (QC) by cascade emission is shown in Fig. 5. However, the quantum cutting phenomenon in other RE ions such as Tm<sup>3+</sup>, Gd<sup>3+</sup> and Er<sup>3+</sup> ions is also reported in the literature.<sup>84-88</sup>

In recent years, quantum cutting on ion pairs (two or three ions) has gained much attention as compared to other quantum cutters. In process (c), one of the ions in the pair has the ability to show the quantum cutting phenomenon by interaction with the other ion in the pair and a part of the energy is transferred to this later ion as shown in Fig. 6. There are also many reports available that show quantum cutting phenomenon using ion pairs.<sup>78</sup> The energy level scheme for ions pair based quantum cutter phenomenon for NaLaF<sub>4</sub>:Pr<sup>3+</sup>, Yb<sup>3+</sup> phosphor is shown in Fig. 6.<sup>89</sup>

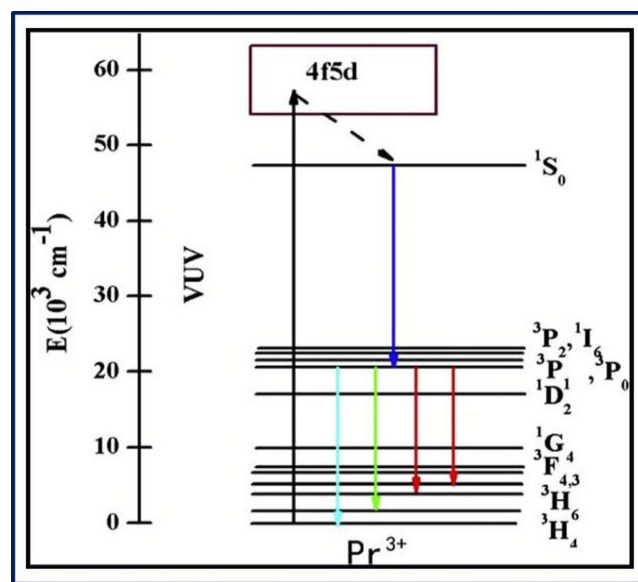


**Fig. 5** Energy level diagram of Pr<sup>3+</sup> ions that shows the concept of quantum cutting phenomenon with VUV excitation.<sup>75</sup> Reproduced with permission from ref. 75 Copyright 2009, Elsevier,

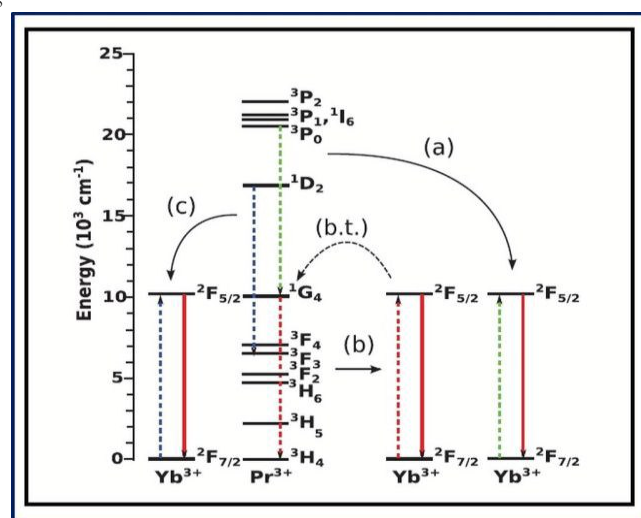


**Fig. 6** Quantum-cutting with Pr<sup>3+</sup> and Yb<sup>3+</sup> (a)–(c) are three possible mechanisms of energy transfer from Pr<sup>3+</sup> toward Yb<sup>3+</sup> and (b. t.) is the back-transfer mechanism from Yb<sup>3+</sup> to Pr<sup>3+</sup>.<sup>89</sup> Reproduced with permission from ref. 89 Copyright 2013, AIP publishing LLC.

Further, Table 2 summarizes the energy of principle 4f-4f transitions of lanthanide ions associated with DC, UC and QC luminescence processes.

5

Ln	Transitions	Emission wavelength (nm)	Energy (cm <sup>-1</sup> )	Intensity	Remarks
Pr	$^3P_2 \rightarrow ^3H_4$	440	22727	Weak	QC
	$^3P_1 \rightarrow ^3H_4$	470	21277	Weak	QC
	$^3P_1 \rightarrow ^1G_4$	872	11468	Medium	QC
	$^3P_0 \rightarrow ^3H_4$	480	20833	Strong	UC and QC
	$^3P_0 \rightarrow ^3H_5$	545	18349	Weak	UC and QC
	$^3P_0 \rightarrow ^3H_6$	606	16502	Medium	UC and QC
	$^3P_0 \rightarrow ^3F_2$	640	15625	Weak	UC and QC
	$^1D_2 \rightarrow ^3F_4$	1037	9643	Medium	QC
Nd	$^4D_{3/2} \rightarrow ^4I_{9/2}$	395	28169	Weak	UC and QC
	$^2P_{3/2} \rightarrow ^4I_{9/2}$	388	26316	Weak	UC and QC
	$^2P_{3/2} \rightarrow ^4I_{11/2}$	410	24390	Strong	UC and QC
	$^2P_{3/2} \rightarrow ^4I_{13/2}$	452	22124	Strong	UC and QC
	$^4G_{7/2} \rightarrow ^4I_{9/2}$	545	18394	Weak to strong	UC and QC
	$^4G_{7/2} \rightarrow ^4I_{11/2}$	587	17036	Weak to strong	UC and QC
	$^4G_{7/2} \rightarrow ^4I_{13/2}$	655	15267	Weak to strong	UC and QC
	$^4F_{3/2} \rightarrow ^4I_{9/2}$	886	11287	Weak to strong	QC and DS
	$^4F_{3/2} \rightarrow ^4I_{11/2}$	1064	9399	Weak to strong	QC and DS
	$^4F_{3/2} \rightarrow ^4I_{13/2}$	1340	7463	Weak to strong	QC and DS

Sm	$^4G_{5/2} \rightarrow ^6H_{5/2}$	564	17730	Medium	DS
	$^4G_{5/2} \rightarrow ^6H_{7/2}$	601	16639	Strong	DS
	$^4G_{5/2} \rightarrow ^6H_{9/2}$	644	15528	Medium	DS
Eu	$^5D_0 \rightarrow ^7F_{0, 1, 2, 3, 4}$	570-720	13889-17544	Strong	UC and DS
Tb	$^5D_4 \rightarrow ^7F_{6, 5, 4, 3}$	480-650	15385-20833	Strong	UC, QC and DS
Dy	$^4F_{9/2} \rightarrow ^6H_{15/2}$	486	20576	Medium	QC and DS
	$^4F_{9/2} \rightarrow ^6H_{13/2}$	575	17391	Strong	QC and DS
	$^4F_{9/2} \rightarrow ^6H_{11/2}$	664	15060	Weak	QC and DS
Ho	$^5S_2, ^5F_4 \rightarrow ^5I_8$	540	18519	Strong	UC and QC
	$^5S_2, ^5F_4 \rightarrow ^5I_7$	749	13351	Weak	UC and QC
	$^5S_2, ^5F_4 \rightarrow ^5I_6$	1012	9881	Weak	QC
	$^5F_5 \rightarrow ^5I_8$	644	15528	Medium	UC and QC
	$^5F_5 \rightarrow ^5I_7$	966	10352	Weak	QC
	$^5I_6 \rightarrow ^5I_8$	1180	8475	Strong	QC

Er	$^4G_{11/2} \rightarrow ^4I_{15/2}$	380	26316	Weak	UC and QC
	$^2P_{3/2} \rightarrow ^4I_{13/2}$	408	24510	Weak	UC
	$^2P_{3/2} \rightarrow ^4I_{11/2}$	480	20833	Weak	UC
	$^2H_{11/2} \rightarrow ^4I_{15/2}$	525	19048	Weak	UC and QC
	$^4S_{3/2} \rightarrow ^4I_{15/2}$	545	18349	Strong	UC and QC
	$^4S_{3/2} \rightarrow ^4I_{13/2}$	850	11765	Weak	UC and QC
	$^4F_{9/2} \rightarrow ^4I_{15/2}$	665	15038	Strong	UC and QC
	$^4I_{9/2} \rightarrow ^4I_{15/2}$	800	12500	Strong	UC and QC
	$^4I_{11/2} \rightarrow ^4I_{15/2}$	980	10204	Strong	UC and QC
	$^4I_{13/2} \rightarrow ^4I_{15/2}$	1540	6494	Strong	QC
Tm	$^1D_2 \rightarrow ^3H_4$	360	27778	Medium	UC and QC
	$^1D_2 \rightarrow ^3F_4$	450	22222	Medium	UC and QC
	$^1G_4 \rightarrow ^3H_6$	475	21053	Strong	UC and QC
	$^1G_4 \rightarrow ^3H_4$	650	15385	Strong	UC and QC
	$^1G_4 \rightarrow ^3H_5$	786	12723	Weak	UC and QC
	$^3H_4 \rightarrow ^3H_6$	800	12500	Strong	UC and QC
	$^3F_4 \rightarrow ^3H_6$	1800	5556	Weak	QC
Yb	$^2F_{5/2} \rightarrow ^2F_{7/2}$	980	10204	Strong	UC, QC and DS

**Table 2** Summary of principle transitions in the emission spectra of common lanthanide ions utilized in upconversion (UC), quantum-cutting (QC), and down-shifting (DS) luminescence processes.<sup>35</sup> Reproduced with permission ref. 35, 2013, Royal Society of Chemistry.

5

10

15

### 1.3 Luminescent quantum dots

Quantum dots are defined as the spherical nanoparticles having physical dimensions smaller than the exciton Bohr radius confining its excitons in all three spatial directions.<sup>90-92</sup> Quantum dots have gained tremendous attention in research due to their number of distinguished properties such as (i) high quantum yield (QY) and long fluorescence lifetime,<sup>93-95</sup> (ii) simultaneous excitation of multiple QDs by a single light source,<sup>96</sup> (iii) narrow, symmetrical<sup>97</sup> and (iv) broad spectral windows spanning from the ultraviolet to infrared region.<sup>98</sup> An electron-hole pair is generated when quantum dots are photo excited with particular wavelength and their recombination causes the emission of light. Particularly, an exciton is electrostatically bounded electron-hole pair and is generated in semiconductor as a result of excitation of an electron from valence to conduction band upon the absorption of a photon with energy equal or greater than the band gap. Conceptually, the exciton Bohr radius represents the average distance between the photo generated electron and hole. When the size of the particle approaches that of the exciton (for example, the exciton Bohr radius for CdSe is about 6 nm), the optical and electrical

properties of the material become dependent on its physical dimensions, due to quantum confinement effects.<sup>99</sup> Under these conditions, the band structure of the semiconductor changes into discrete energy levels as shown in Fig. 7 and the energy difference between the highest occupied level and the lowest unoccupied level widens as the particle size decreases. Furthermore, the quantum confinement is also described by simple model particle in box approximation in which the electron motion is restricted in all three dimensions by impenetrable walls. Klimov suggested a model for semiconductor based spherical QD with radius R, which predicts that a size dependent contribution to the energy gap is simply proportional to  $1/R^2$ , implying that the gap increases as the QD size decreases. Moreover, because of the quantum confinement continuous energy bands of a bulk material split into discrete, atomic like energy levels that results in discrete absorption spectrum of QDs. This discrete absorption spectrum of QDs is entirely different from the continuous absorption spectrum of a bulk semiconductor as shown in Fig. 8.<sup>100</sup> In other words, smaller the particle size more is the blue shift in their luminescence as shown in Fig. 9.

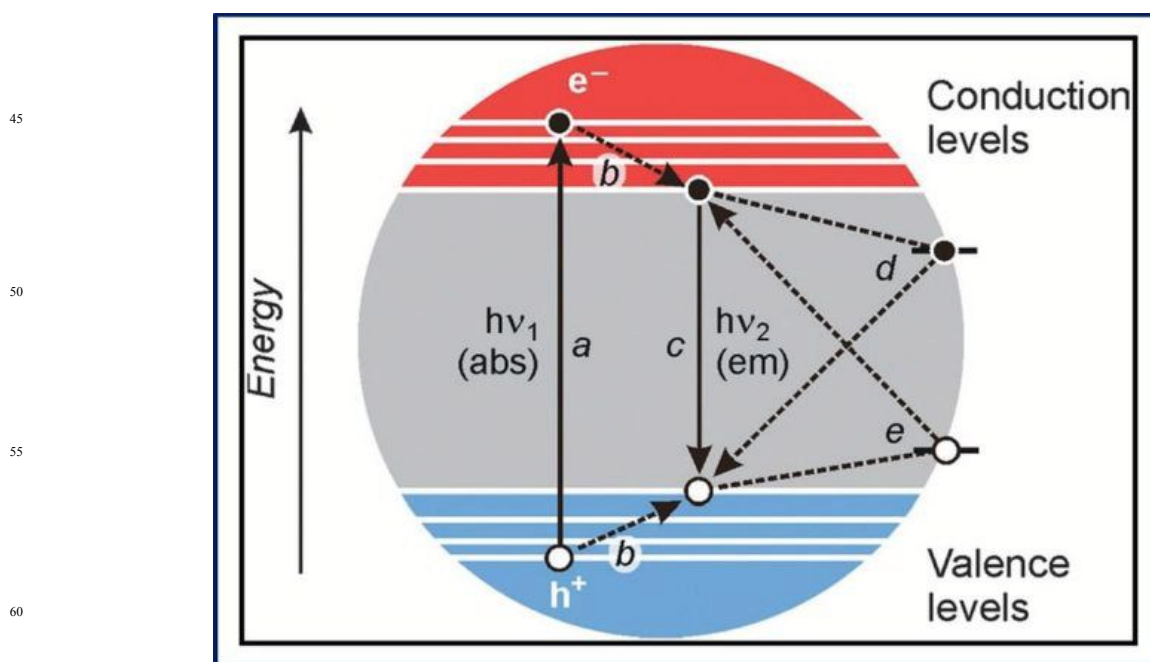


**Fig.7** Schematic representation of important optical and electronic processes in a semiconductor nanocrystal. Solid and dashed lines represent radiative and nonradiative processes, respectively. Legend of the processes: a, optical excitation; b, thermal relaxation of the excited electron and hole; c, radiative exciton recombination (luminescence); d, nonradiative exciton recombination mediated by an oxidising surface state (electron trap); e, nonradiative exciton recombination mediated by a reducing surface state (hole trap).<sup>99</sup> Reproduced with permission from ref. 99 Copyright 2015, Royal Society of Chemistry.

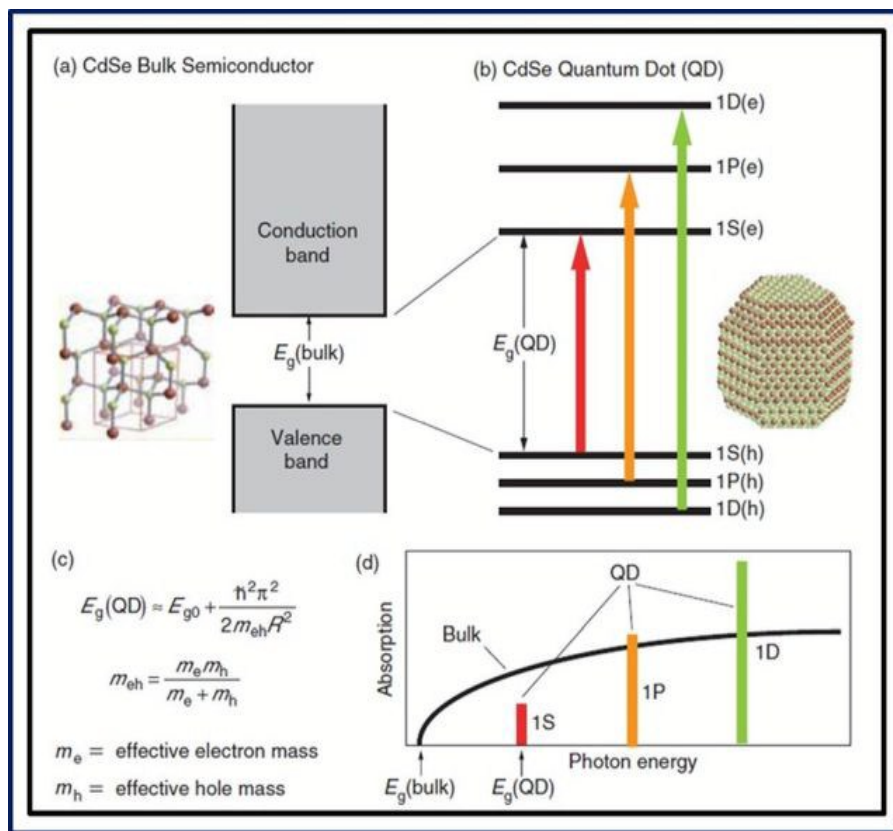


**Fig. 8** (a) A bulk semiconductor such as CdSe has continuous conduction and valence energy bands separated by a “fixed” energy gap,  $E_g(\text{bulk})$ . Electrons normally occupy all states up to the edge of the valence band, whereas states in the conduction band are empty. (b) A QD is characterized by discrete atomic-like states with energies that are determined by the QD radius  $R$ . These well-separated QD states can be labeled with atomic-like notations, such as 1S, 1P, and 1D. (c) The expression for the size dependence separation between the lowest electron and hole QD states- $E_g(\text{QD})$ , the QD energy gap-was obtained with the spherical “quantum box” model. (d) This schematic represents the continuous absorption spectrum of a bulk semiconductor (black line) compared with a discrete absorption spectrum of a QD (colored bars).<sup>100</sup> Reproduced with permission from ref. 100, Copyright 2003, Los Alamos Science.

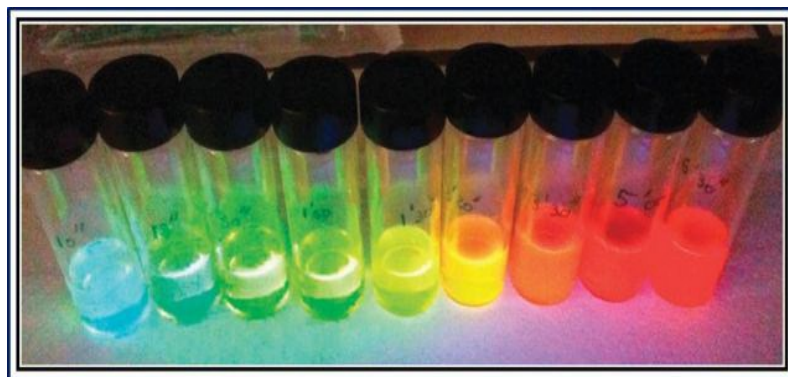


**Fig. 9** Photograph of chloroform solutions of CdSe-ZnS QDs of different sizes (smaller to larger from left to right) under UV excitation.<sup>99</sup> Reproduced with permission from ref. 99 Copyright 2015, Royal Society of Chemistry.

Cite this: DOI: 10.1039/c0xx00000x

www.rsc.org/xxxxxx

## ARTICLE TYPE

Therefore, the electronic and optical properties of quantum dots depend upon their size due to quantum effect. Hence, quantum dots with different size exhibit different fluorescence colors. Fig.10 demonstrates the change in emission of quantum dots with change in their size and the range of emission wavelength of semiconductor quantum dots.<sup>98</sup> There are extensive studies on II–VI (e.g. CdSe, CdTe, CdS, ZnSe), III–V (e.g. InP, InAs), and

IV–VI (e.g. PbSe) group and their alloys with a confined size on the nanoscale for various applications published in the literature. Every quantum dot has its own limits for the tuning of emission color with respect to its size which is demonstrated in Fig. 10. There are several reports available which elaborate the relationship between the size, shape and electronic properties of QD.<sup>101</sup>

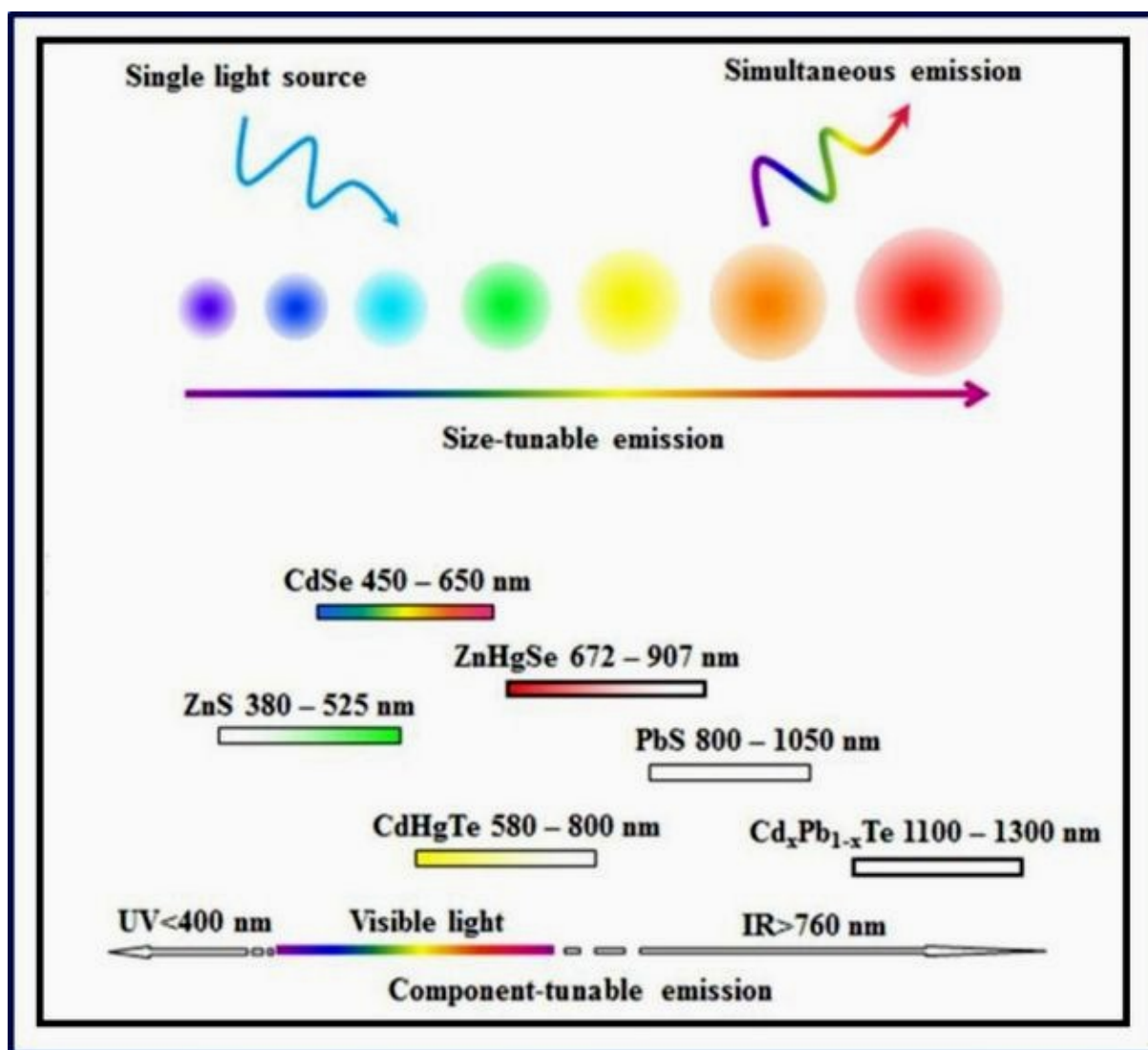


**Fig. 10** Size-tunable fluorescence emission and simultaneous excitation of multiple QDs by a single light source and the QDs with different components show broad spectral windows spanning from the ultraviolet to infrared region.<sup>98</sup> Reproduced with permission from ref. 98 Copyright 2015, American Chemical Society.

Recently, another kind of quantum dots derived from carbon which are known as carbon quantum dots (CQD) or carbon dots (CD), including the popular graphene quantum dots (GQD) have been investigated immensely.<sup>92, 102-105</sup> Unlike the semiconductor quantum dots with band gap absorptions, the carbon quantum dots have broad optical absorption due to  $\pi$ -plasmon that covers a broad UV/vis spectral range, extending into the near-IR. The photoluminescence emissions of these quantum dots is associated with defects related to structure and surface or edge sites.<sup>92, 106</sup> The carbon quantum dots were first reported by Xu et al. in 2004.<sup>107</sup> However, Sun et al specified the name '*carbon quantum dots*' for fluorescent carbon nanoparticles in 2006.<sup>108</sup>

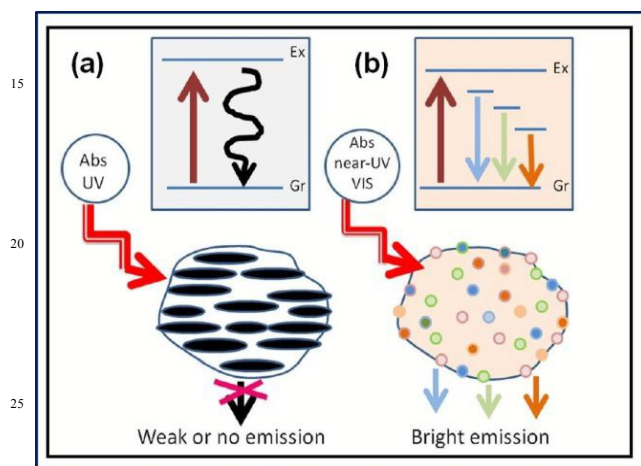


**Fig. 11** Schematic diagram of (a) CQDs with strong absorption in the UV region and weak emissions and (b) CQDs with weak absorption in the near UV-vis region but have a strong multicolour emissions in the visible region.<sup>109</sup> Reproduced with permission from ref. 109 Copyright 2013, IOP publishing.

The fluorescence emission mechanism of GQDs/CQD can be explained in two ways: (i) fluorescence emission due to bandgap transitions caused by conjugated  $\pi$ -domains and (ii) fluorescence emission origins associated with surface defects in GQDs. In the first mechanism, the bandgap transitions originate from conjugated  $\pi$ -domains. These  $\pi$ -domains are sequestered by generating  $sp^2$  hybridised islands rich in  $\pi$ -electrons through the reduction of graphene oxides.<sup>110, 111</sup> GQDs are synthesized in a way that there are no  $\pi$ -connections between the  $sp^2$  islands in graphitic lattice, because any  $\pi$ -connections between the  $sp^2$  islands would lead to interisland quenching of desired fluorescence emissions.<sup>112, 113</sup>

For such kind of bandgap transitions, single-layer graphene sheets have to be used to prevent interlayer quenching between two layers.<sup>114</sup> The single-layer graphene sheets are used as precursors for electronically slicing them into isolated  $\pi$ -conjugated domains, which is similar to large aromatic molecules with extended  $\pi$ -conjugation of specific electronic energy bandgap for optical absorption and fluorescence emissions in GQDs.<sup>115</sup> Such electronic transitions show strong absorption in the ultraviolet (UV) region, but weak or no fluorescence emissions as shown in

Fig.11a. Hence, the strong absorption is possible due to light absorption by a large amount of high density  $\pi$ -electrons in the  $sp^2$  hybridized islands, which form excitonic states while the weak emissions are probably a result of quenching via radiation less relaxations to the ground state during exciton migration to energy traps.<sup>109</sup> The second class of the fluorescence mechanism originates from surface-related defect sites. Generally, such surface sites have non-perfect  $sp^2$  domains that act as surface energy traps. Both,  $sp^2$  and  $sp^3$  hybridized carbon atoms and other functionalised surfacedefects<sup>116, 117</sup> like carbonyl-related localised electronic states<sup>114-118</sup> present in CQDs/GQDs contribute to their multicolour emissions that are intense in the blue and green regions of the visible light spectrum. These surface defects behave like aromatic molecules that are individually incorporated into solid hosts that exhibit multicolour emissions due to the existence of multiple surface defects with different excitation and emission properties.<sup>106-115</sup> Robertson and O'Reilly suggested that the optical properties of carbon nanomaterials which contain both  $sp^2$  and  $sp^3$  bonds are determined by the  $\pi$ -states of the  $sp^2$  sites.<sup>119</sup> Therefore, the bright surface defect-derived fluorescence of CQDs/GQDs is due to the recombination of electron-hole pairs in the strongly localized  $\pi$  and  $\pi^*$  electronic levels of the  $sp^2$  sites. These sites lie between the bandgap of the  $\sigma$  and  $\sigma^*$  states of the  $sp^3$  matrix,<sup>120-121</sup> which leads to strong visible emissions. Such electronic transitions exhibit weak absorption in the near ultraviolet-visible (UV-vis) region and strong emissions in the visible region as shown in Fig. 11b. Moreover, upon surface passivation or functionalization, the surface defects become more stable to facilitate more effective radiative recombination of surface-confined electrons and holes, hence achieving brighter fluorescence emissions.<sup>115</sup> Similar to semiconductor quantum dots, the emission spectra of CQDs/GQDs can also be tuned without any surface modification. But, due to low stability of defects, the quantum yield of CQDs/GQDs is very low. Therefore, the surface modification of these quantum dots with polymers leads to stable defects and strong emission. The emission colour of CQDs can be tuned by surface modification (passivation) as shown in Fig. 12.

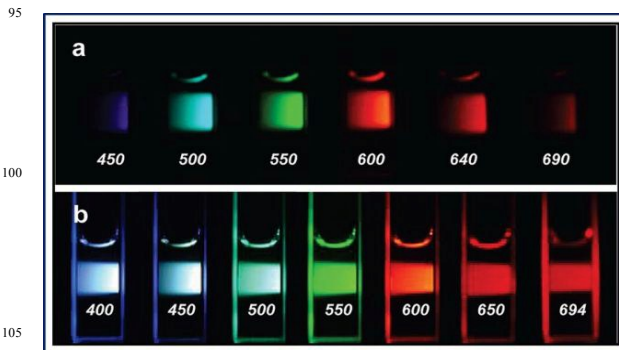


**Fig. 12** Aqueous solution of the PEG1500N-attached carbon dots (a) excited at 400 nm and photographed through band-pass filters of different wavelengths as indicated, and (b) excited at the indicated wavelengths and photographed directly.<sup>108</sup> Reproduced with permission from ref. 108 Copyright 2006, American Chemical Society.

Cite this: DOI: 10.1039/c0xx00000x

www.rsc.org/xxxxxx

## ARTICLE TYPE

### 1.4 Luminescent nanoscale metal-organic frameworks

The metal-organic frameworks (MOFs) are a new class of inorganic-organic hybrid materials synthesized from metal ions or metal cluster and organic ligands.<sup>122-126</sup> The metal-organic frameworks are also known as coordination polymers (CPs) or coordination networks. Because metal-organic frameworks have both inorganic and organic components, therefore these materials are very promising as multifunctional materials. Based on the geometries of the organic ligands/linkers and coordination modes of the inorganic metal ions or clusters of metal ions, their structures can be designed according to desired properties.<sup>124,127-129</sup> As a consequence, they show promise for an impressive number of applications in luminescent barcode security, gas storage, drug-delivery, diagnostics, sensing, catalysis, ion exchange or separation, magnetism, optics, etc.<sup>130-136</sup> However, metal-organic materials in the form of traditional bulk crystalline materials do not always fulfil all the specific needs for these applications. Depending upon the desired application, these materials are required not only to be fabricated as bulk crystalline solids, but also to be miniaturized at the nanometre length scale and immobilized at specific locations on surfaces.<sup>136</sup> For example, in order fabricate luminescent security ink, the nanoscale MOFs are more suitable because it is easier to disperse them uniformly with high stability into the ink medium as compared to bulk MOFs. In above applications, the additional advantage of nanoscale MOFs is that they have higher surface areas than their macroscopic counterpart thereby reducing the amount of luminescent MOFs required for ink fabrication. A similar situation occurs with some of its physical properties. It is well known that unique physical properties emerge prominently when at least one dimension of a material is reduced to the nanometre scale. Thus, nanoscale metal-organic materials are also expected to hold highly desirable size-dependent optical, electrical and magnetic properties.<sup>136</sup> The MOFs show tuneable luminescence behaviour covering a wide range of spectrum from UV to NIR. In MOFs, both organic ligands and inorganic metal ions or clusters can provide the platform to produce luminescence. Further, luminescence due to charge transfer between metal ion and ligand is also observed in MOFs. Moreover, introduction of guest molecule or ions can also induce luminescence.<sup>137</sup> Summary of luminescent MOFs is shown in Table 3.

In recent years, the studies on luminescent MOFs are mainly focused on investigating the fundamental synthesis, mechanism of luminescence, upconverting MOFs and emerging luminescent properties of MOFs with better tenability for luminescent security applications as well as in light-emitting and display devices. In addition to this, the permanent porosity with some luminescent MOFs has enabled their reversible storage with release of guest substrates and provided the hosts for their differential

recognitions with sensing species.<sup>137,138</sup> The Fig. 13 clearly depicts the various modes of luminescence generation as explained belows:

- 1.4.1 Linker/ligand based luminescence in MOFs
- 1.4.2 Lanthanide based luminescence in MOFs
- 1.4.3 Charge transfer luminescence in MOFs
- 1.4.4 Guest-Induced Luminescence in MOFs

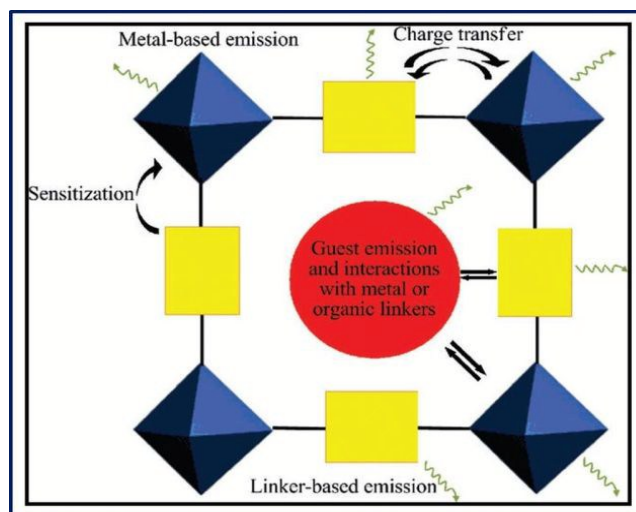


**Fig. 13** Representation of emission possibilities in a porous MOF, wherein metal clusters (blue octahedra) are linked by organic linkers (yellow rectangles) with an incorporated guest (red circle).<sup>138</sup> Reproduced with permission from ref. 138 Copyright 2009, Royal Society of Chemistry.

**1.4.1 Linker/ligand based luminescence in MOFs.** In this process of luminescence generation, the incident radiation is absorbed by typically conjugated organic compounds known as linkers. After that, the linkers transfer the charge with coordinated metal ions or clusters. But in some cases the direct emission from the organic linkers is also possible. The schematic diagram for this photo-physical process is shown in Fig. 14. The fluorescence emission in organic molecule (linker/ligand) is due to radiative decay from singlet state  $S_1$  to the ground singlet state  $S_0$ . The phosphorescence in organic molecule (linker/ligand) is due to the radiative transition from triplet state  $T_1$  to  $S_0$  and this emission has a lifetime in the range of several microseconds to seconds.<sup>137</sup>

The MOFs with  $\pi$ -conjugated organic ligands or linkers show ligand based luminescence. Various type of organic linkers can be used for MOF synthesis like rigid backbones substituted with di- or multi-carboxylate groups for metal coordination.<sup>137,138</sup> Generally, the fluorescence emission from organic ligands is due to transition from the lowest excited singlet state to the singlet ground state i.e. transitions are  $\pi \rightarrow \pi^*$  or  $n \rightarrow \pi^*$ .

Metal	MOFs	Emission wavelength (nm)
<b>Lanthanide-Based MOFs</b>		
La	[La(pmtz)(TzC)(H <sub>2</sub> O) <sub>3</sub> ](H <sub>2</sub> O)	530
Ce	[Ce <sub>2</sub> (pydc) <sub>2</sub> (μ <sub>4</sub> -SO <sub>4</sub> )-5H <sub>2</sub> O]·2H <sub>2</sub> O	357, 480
Nd	Nd <sub>2</sub> (1,4-NDC) <sub>3</sub> (DMF) <sub>4</sub> ·H <sub>2</sub> O	391.6, 449.5
	Nd(tta) <sub>3</sub> (μ-bpm)·MeOH	440, 910, 1007
Sm	[Sm(pta)(H <sub>2</sub> O) <sub>5</sub> ] <sub>3</sub> ·4H <sub>2</sub> O	558, 592, 639
	Sm <sub>2</sub> (ATPA) <sub>3</sub> (DMF) <sub>2</sub> (H <sub>2</sub> O) <sub>2</sub>	450, 561, 597, 644
Eu	Eu <sub>2</sub> (1,4-BDC) <sub>3</sub> (DMF) <sub>2</sub> (H <sub>2</sub> O) <sub>2</sub>	596, 616
	[Eu(pta)(H <sub>2</sub> O) <sub>5</sub> ] <sub>4</sub> ·4H <sub>2</sub> O	589, 613, 695
Gd	[Gd <sub>2</sub> (Hpimda) <sub>2</sub> (μ <sub>4</sub> -C <sub>2</sub> O <sub>4</sub> ) <sub>4</sub> ·4H <sub>2</sub> O]·2H <sub>2</sub> O	319, 476
Tb	[Tb(pta)(H <sub>2</sub> O) <sub>5</sub> ] <sub>4</sub> ·4H <sub>2</sub> O	491, 546, 584, 623
	K <sub>5</sub> [Tb <sub>5</sub> (IDC) <sub>4</sub> (ox) <sub>4</sub> ]	489, 545, 589, 619
Dy	Dy(1,4-BDC) <sub>3</sub> (H <sub>2</sub> O) <sub>4</sub>	481, 575
	[Dy <sub>4</sub> (BPT) <sub>4</sub> (DMF) <sub>2</sub> (H <sub>2</sub> O) <sub>8</sub> ] <sub>4</sub> ·(DMF) <sub>5</sub> ·(H <sub>2</sub> O) <sub>3</sub>	480, 573, 662
Ho	Ho <sub>3</sub> (1,4-BDC) <sub>4,5</sub> (DMF) <sub>2</sub> (H <sub>2</sub> O) <sub>3</sub> ·(DMF)(C <sub>2</sub> H <sub>5</sub> OH) <sub>0.5</sub> (H <sub>2</sub> O) <sub>0.5</sub>	~375, ~430
Er	[Er(pta)(H <sub>2</sub> O) <sub>3</sub> ] <sub>4</sub> ·4H <sub>2</sub> O	1538
	Er <sub>3</sub> (1,4-BDC) <sub>4,5</sub> (DMF) <sub>2</sub> (H <sub>2</sub> O) <sub>3</sub> ·(DMF)(C <sub>2</sub> H <sub>5</sub> OH) <sub>0.5</sub> (H <sub>2</sub> O) <sub>0.5</sub>	~380, ~430
Yb	[Yb(pta)(H <sub>2</sub> O) <sub>3</sub> ] <sub>4</sub> ·4H <sub>2</sub> O	980
	Yb(BPT)(H <sub>2</sub> O)·(DMF) <sub>1.5</sub> (H <sub>2</sub> O) <sub>1.25</sub>	980
<b>Transition-Metal-Based MOFs</b>		
Zn	[Zn <sub>4</sub> O(NTB) <sub>2</sub> ] <sub>2</sub> ·3DEF·EtOH	433
	Zn <sub>3</sub> (4,40-stilbene dicarboxylic acid) <sub>3</sub> (DMF) <sub>2</sub>	396, 420, 441
Cd	Cd(BDC-NH <sub>2</sub> )(bpy)·4H <sub>2</sub> O·2.5DMF	435
	[Cd(dtba)(bpp)] <sub>3n</sub>	434, 482
Ag	[Ag <sub>8</sub> (L) <sub>4</sub> ](NO <sub>3</sub> ) <sub>8</sub> ·4H <sub>2</sub> O, L = bis(3,5-bis((1H-imidazol-1-yl)-methyl)-2,4,6-trimethylphenyl)methane	495
Cu	Cu <sub>6</sub> (5,6-diphenyl-1,2,4-triazine-3-thiol) <sub>6</sub> ·(H <sub>2</sub> O)(DMSO)	660
	Cu <sub>3</sub> (L) <sub>2</sub> ·3H <sub>2</sub> O, L = 2,6-dicarboxy-4-hydroxypyridine	398, 478
Co	Co(L)(2,2'-bipy), L = dibenzothiophene-5,5'-dioxide-3,7-dicarboxylate	409
Mn	Mn(Hbide)	726
Fe	[FeL <sub>2</sub> Cl <sub>2</sub> ] <sub>3</sub> CH <sub>3</sub> CN, L = N <sub>0</sub> ,N <sub>0</sub> -bis[1-(pyridin-3-yl)methylidene]benzil dihydrazone	353
<b>Heterometal-Organic Frameworks</b>		
Pr-Cu	Pr(pydc) <sub>2</sub> Cu <sub>3</sub> (bipy) <sub>3</sub> ·m(H <sub>2</sub> O)	488, 532

Nd-Cd	[NdCd(imdc)(SO <sub>4</sub> )(H <sub>2</sub> O) <sub>3</sub> ].0.5H <sub>2</sub> O	430
Nd-Cu	Nd(pydc) <sub>3</sub> Cu <sub>3</sub> (bipy) <sub>3</sub> .5(H <sub>2</sub> O)	895, 1062, 1345
Sm-Ag	[SmAg(PDA) <sub>2</sub> (H <sub>2</sub> O) <sub>3</sub> ].3H <sub>2</sub> O	563, 601, 644
Sm-Cu	Sm(pydc) <sub>3</sub> Cu <sub>3</sub> (bipy) <sub>3</sub> .4(H <sub>2</sub> O)	563, 603, 645
Eu-Fe	[Eu(PDA) <sub>3</sub> Fe <sub>1.5</sub> (H <sub>2</sub> O) <sub>3</sub> ].1.5H <sub>2</sub> O	613
Eu-Ag	[EuAg(PDA) <sub>2</sub> (H <sub>2</sub> O) <sub>3</sub> ].3H <sub>2</sub> O	581, 593, 617, 651, 695
Gd-Cu	Gd(pydc) <sub>3</sub> Cu <sub>3</sub> (bipy) <sub>3</sub> .4(H <sub>2</sub> O)	488, 532
Gd-Mn	[(Gd <sub>2</sub> L)Mn(H <sub>2</sub> O) <sub>6</sub> ].0.5(H <sub>2</sub> O), L = 3,30-(4-Amino-4H-1,2,4-triazole-3,5-diyl)dibenzoic acid	428
Tb-Mn	[Tb(PDA) <sub>3</sub> Mn <sub>1.5</sub> (H <sub>2</sub> O) <sub>3</sub> ].3.25H <sub>2</sub> O	~490, ~550
Tb_Cu	Tb(pydc) <sub>3</sub> Cu <sub>3</sub> (bipy) <sub>3</sub> .4(H <sub>2</sub> O)	492, 544, 583, 622
Dy-Ag	[DyAg(PDA) <sub>2</sub> (H <sub>2</sub> O) <sub>3</sub> ].3H <sub>2</sub> O	483, 573
Dy-Cd	[DyCd(imdc)(SO <sub>4</sub> )(H <sub>2</sub> O) <sub>3</sub> ].0.5H <sub>2</sub> O	478, 573, 657
Ho-Ag	HoAg <sub>5</sub> (1,2-BDC) <sub>4</sub>	995, 1400-1600
Er-Ag	ErAg <sub>5</sub> (1,2-BDC) <sub>4</sub>	1450-1650
Yb-Cu	Yb(pydc) <sub>3</sub> Cu <sub>3</sub> (bipy) <sub>3</sub> .4(H <sub>2</sub> O)	980
Eu-Tb	Eu <sub>1-x</sub> Tb <sub>x</sub> (BTC)(H <sub>2</sub> O)	540, 589, 615
	[(Eu, Tb)(C <sub>6</sub> H <sub>8</sub> O <sub>4</sub> ) <sub>3</sub> (H <sub>2</sub> O) <sub>2</sub> ].(C <sub>10</sub> H <sub>8</sub> N <sub>2</sub> )	545, 595, 615
Er-Yb	Er <sub>x</sub> Yb <sub>1-x</sub> -PVDC-1	980, 1530
Cu-Ag	CuAg <sub>2</sub> (L) <sub>2</sub> , L = 2,6-dicarboxy-4-hydroxypyridine	515
<b>Main Group Metal-Organic Frameworks</b>		
In	In <sub>2</sub> (OH) <sub>2</sub> (TBAPy)	471
Bi	Bi <sub>3</sub> (μ <sub>3</sub> -O) <sub>2</sub> (pydc) <sub>2</sub> (Hpydc)(H <sub>2</sub> O) <sub>2</sub>	430, 460, 480, 556
Pb	Pb(pydc)(H <sub>2</sub> O)	441, 470, 520, 563
Mg	Mg(DHT)(DMF) <sub>2</sub>	508 (in DMSO)

**Table 3** Summary of luminescent MOFs.<sup>137</sup> Reproduced with permission from ref.137. Copyright 2012, American Chemical Society.

Moreover, the other organic linkers/ligands play a key role to stabilize the MOFs. Therefore, the non-radiative decay rate emission is reduced; as a result there is increase in luminescence intensity, quantum yield and lifetime. Furthermore, the solid state, molecular interactions make the molecules close together, which enables charge transfer among the organic ligands/ linkers, resulting in shift of spectra, broadening of the emission and loss

of fine structure. In addition, the size and nature of metal ions, the orientation and arrangement of linkers and the coordination environment within MOF can significantly affect the fluorescence properties of the organic linkers because these factors will induce their different intramolecular or intermolecular interactions among organic linkers.<sup>137,138</sup>

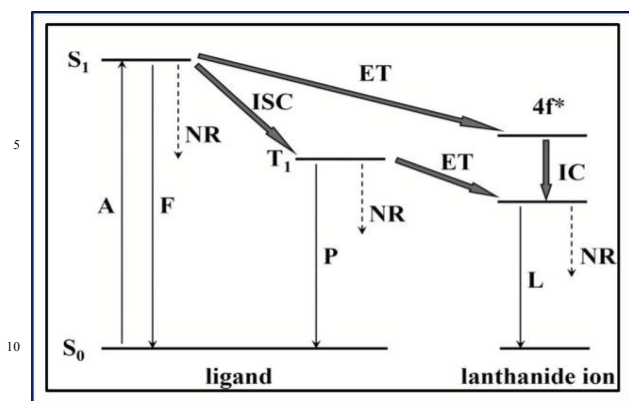


**Fig. 14** Schematic representation of energy absorption, migration, emission, and processes in MOFs. Abbreviations: A = absorption; F = fluorescence; P = phosphorescence; L = lanthanide-centered luminescence; ISC = intersystem crossing; ET = energy transfer; IC = internal conversion; S = singlet; T = triplet. Plain arrows indicate radiative transitions; dotted arrows indicate nonradiative transitions.<sup>137</sup> Reproduced with permission from ref. 137 Copyright 2012, American Chemical Society.

**1.4.2 Lanthanide based luminescence in MOFs.** Lanthanide metal ion based luminescence is associated with lanthanide complexes and rare earth metals that are sensitized by a ligand-to-metal charge transfer -type process. All  $\text{Ln}^{3+}$  ions except  $\text{La}^{3+}$  and  $\text{Lu}^{3+}$  may generate luminescent f-f emissions from a broad range covering UV to NIR.<sup>139,140</sup> The  $\text{Eu}^{3+}$ ,  $\text{Tb}^{3+}$ ,  $\text{Sm}^{3+}$  and  $\text{Tm}^{3+}$  emit red, green, orange and blue colour, respectively, while the  $\text{Yb}^{3+}$ ,  $\text{Nd}^{3+}$ , and  $\text{Er}^{3+}$  demonstrate the well established NIR emissions. The transitions metals emit intense and sharp emission bands originating from f-f transitions. However, the lanthanide ions have weak absorption due to the forbidden f-f transitions. This problem may be overcome by coupling them with the species that can absorb and transfer energy; known as sensitization or can create antenna effect.<sup>139,140</sup> The antenna effect occurs in three steps: (i) absorption of photon energy by organic ligands, present around the lanthanide ions, (ii) transfer of absorbed energy from organic ligand to lanthanide ions and (iii) emission from the lanthanide ions as shown Fig. 14. The antenna effect also observed in MOFs containing actinides metal ions.<sup>141</sup>

**1.4.3 Charge transfer luminescence in MOFs.** In this process, luminescence is generated by an allowed transition from the charge-transfer excited state to the ground state. There are two type of charge transfer in MOFs: (i) Ligand-to-metal charge transfer (LMCT) or Metal-to-ligand charge transfer (MLCT). LMCT involves the electronic transition from an organic linker-localized orbital to a metal-centered orbital, while MLCT corresponds to the electronic transition from a metal-centered orbital to an organic linker-localized orbital. Basically, the charge

transfer luminescence is observed in  $d^{10}$  metal based MOFs such as,  $\text{MOFCu}_3(\text{C}_7\text{H}_2\text{NO}_5)_2 \cdot 33\text{H}_2\text{O}$  ( $\text{C}_7\text{H}_2\text{NO}_5 = 4\text{-hydroxypyridine-2,6-dicarboxylate}$ ) exhibits blue emission peaking at 398 and 478 nm upon excitation at 333 nm, whereas  $\text{CuAg}_2(\text{C}_7\text{H}_2\text{NO}_5)_2$  and the free organic linker 4-hydroxypyridine-2,6-dicarboxylic acid exhibits green emission at 515 and 526 nm upon excitation at 358 and 365 nm.<sup>142</sup> However, in some case LMCT or MLCT luminescence and ligand based luminescence may exist together. For example in case of the zinc MOF  $\text{Zn}_2(\text{ATA})_3(\text{ATA})_{2/2}$ , there is a weak blue emission at 485 nm at excitation of 320 nm while a strong luminescence at 392 nm is generated for ligand-based emission.<sup>143</sup>

**1.4.4 Guest-induced luminescence in MOFs.** Most of the MOFs have porous structure and the pore size could be in the range of several angstroms to several nanometers. Because of this porosity, the MOFs can act as host lattice for organic molecules, fluorescent dye and lanthanides ions. For example, the series of lanthanides MOFs  $\text{Ln}^{3+}@\text{bio-MOF-1}$  ( $\text{Ln}^{3+} = \text{Tb}^{3+}, \text{Sm}^{3+}, \text{Eu}^{3+}$ , or  $\text{Yb}^{3+}$ ) was synthesized by An et al. using MOFs bio-MOF-1. The lanthanides doped MOFs show different colours depending upon doping ion at excitation of 365nm as shown in Fig. 15.<sup>144</sup>

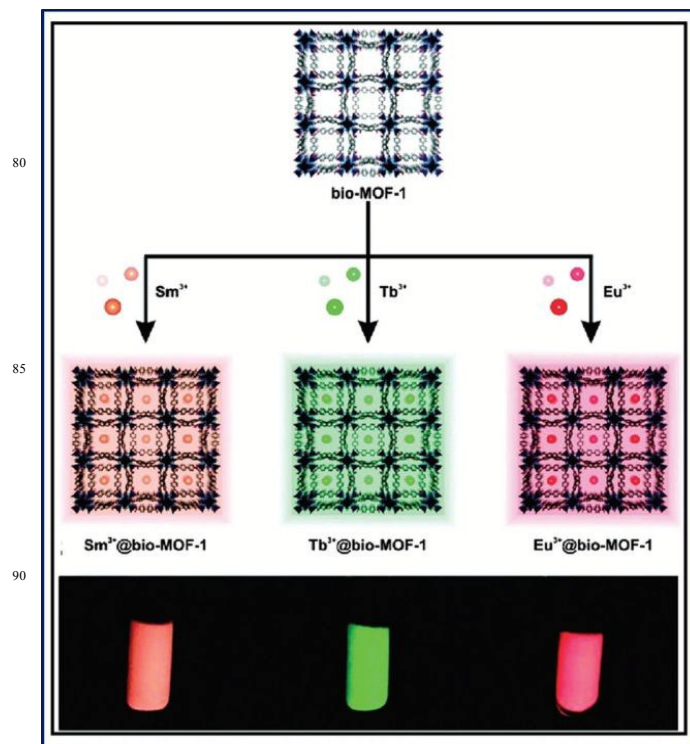
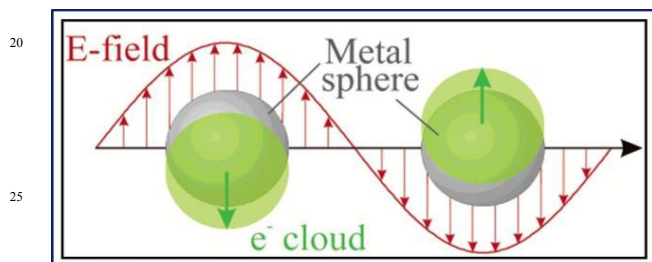


**Fig. 15** Luminescence of lanthanide ions doped in bio-MOF-1.<sup>144</sup> Reproduced with permission from ref.144. Copyright 2011, American Chemical Society.

### 1.5 Plasmonic nanomaterials

Plasmon is defined as the quantum of coherent oscillations of conduction electrons in metals in response to incident light. These oscillations can strongly be restricted to a metal-dielectric interface (surface plasmons). Such collective oscillation of conduction electrons is also known as localized surface plasmons resonance (LSPR). Conceptually, the localized surface plasmonic is observed in metal particles whose size is smaller than the wavelength of incident light.<sup>145-148</sup> When the metal nanoparticle interacts with incident light, the electron cloud (free electron cloud) undergoes a displacement from its original position relative to nuclei. As a result the restoring forces arise due to the Coulomb interaction between the electrons and nuclei that results in collective oscillations of the electron cloud relative to nuclei. The oscillation frequency is determined by four factors: the density of electrons, the effective electron mass, the shape and the size of the charge distribution. The schematic for these plasmonic oscillations for a spherical particle is illustrated in Fig.16.<sup>149</sup>



In other words, plasmonic nanomaterials are the particles whose **Fig. 16** Schematic of plasmon oscillation for a sphere, showing the displacement of the conduction electron charge cloud relative to the nuclei.<sup>149</sup> Reproduced with permission from ref. 149. Copyright 2003, American Chemical Society.

electron density can be coupled with electromagnetic radiation of wavelengths which are far larger than the particle itself. Due to the nature of dielectric-metal interface between the medium and the particles; unlike in a pure metal where there is maximum limit on the wavelength that can be effectively coupled based on material size.<sup>150</sup> Furthermore, plasmonic nanostructures have exceptional properties such the large electromagnetic field enhancements, high photothermal conversion efficiencies, and rich spectral responses. Therefore, plasmonic nanostructures are versatile class of nanomaterials which have enormous potential for variety of applications.<sup>151-158</sup> Thus, a new research field emerges, which is known as 'nanoplasmonics' and that has received worldwide attention from vast scientific community including chemistry, materials, optics, engineering, and biomedicine. A summary of the various subfields within nanoplasmonics is schematically indicated in Fig.17. Although the noble metals gold and silver are most commonly used for studies as plasmonic nanomaterials, but, now a days plasmonic nanostructure also include copper, aluminum, highly doped oxides and chalcogenides and graphene. The plasmon tuning range of aluminium is higher as compared to gold and silver as shown in Fig. 18a. However, most of the investigations have been reported on the plasmonic behavior of noble metals due to their visible-near infrared tunable plasmonic, high chemical stability and huge chemical methods for synthesis of their growth with controlled size and shape.

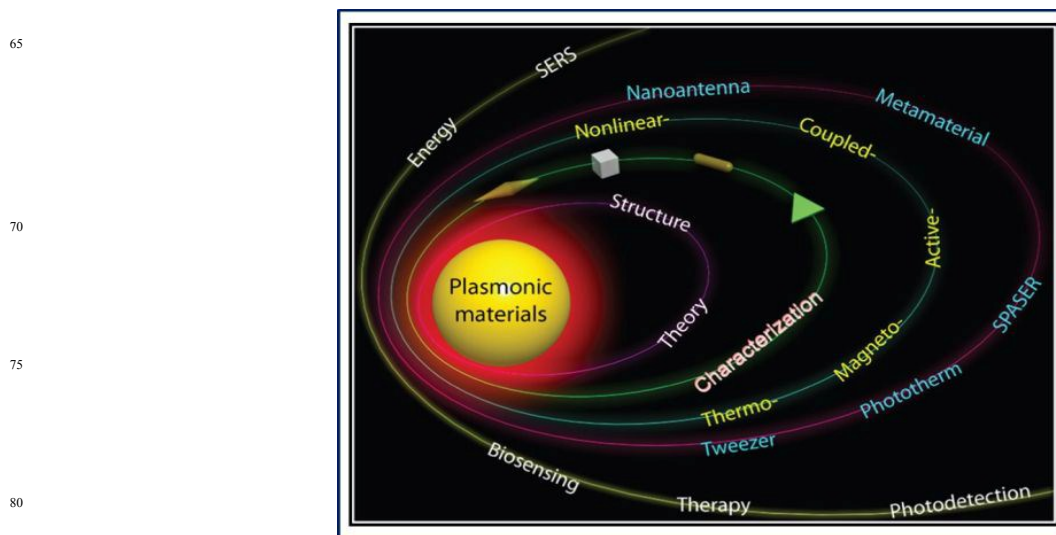


**Fig. 17** Schematic representation of various subfields that are currently studied within the field of nanoplasmonics. From the inner to outer sides are (1) the fundamentals, including the materials, theoretical background, characterization, and fabrication, (2) the properties of hybrid plasmonic nanostructures, (3) the applications in optics and optoelectronics, and (4) the applications closely related to our daily life.<sup>145</sup> Reproduced with permission from ref. 145. Copyright 2014, Royal Society of Chemistry.

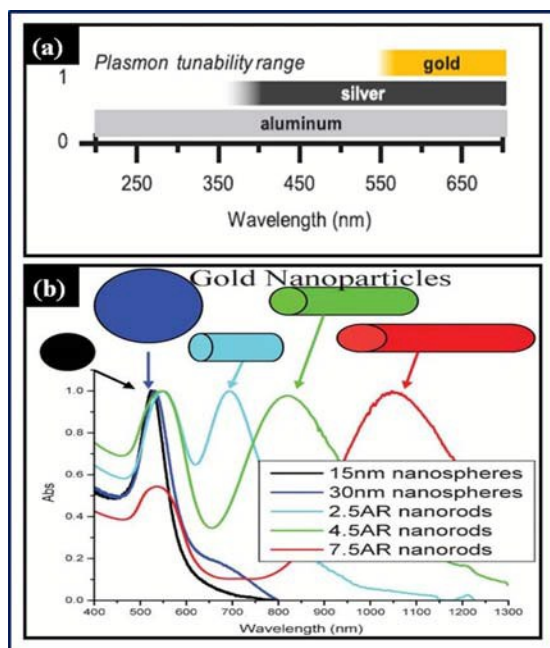


**Fig. 18** (a) Plasmon tuning ranges of Au, Ag compared with Al<sup>159</sup> and (b) Gold nanoparticles absorption of various size and shape.<sup>150</sup> (a) Reproduced with permission from ref.159 Copyright 2014, American Chemical Society. (b) Reproduced with permission from ref. 150 Copyright 2006, Royal Society of Chemistry.

It is interesting to note that the optical properties of metallic nanoparticles change slightly with the increase in the size as observed for different samples of gold nano spheres as shown in Fig. 18 b. However, when anisotropy is added to the nanoparticles; such as growth of nanorods, the optical properties of the nanoparticles change significantly.

After brief discussions on fundamentals concepts about various kinds of luminescent nanomaterials (lanthanide based, quantum dot, MOFs and plasmonic nano materials) and their mechanisms for producing luminescence, we have described in details about the different methodology to synthesize these luminescent nanomaterials and their characterizations in following sections:

## 2. Methodology for synthesis and characterization of luminescent nanomaterials

### 2.1 Lanthanide doped luminescent nanomaterials

The luminescent properties of lanthanides nanomaterials are highly dependent on their structure, size shape and host lattice etc. as reported in literature. Therefore, the method of synthesis of luminescent nanomaterials plays a seminal role in determining their desired optical properties. In the past decades, numerous efforts have been devoted to develop the different facile strategies for the synthesis of luminescent nanomaterials with tuneable size, shape and morphology. However, soft chemical routes are widely used for the synthesis of luminescent nanomaterials have several advantages over conventional methods such as solid state reaction

in terms of following aspects: (i) soft chemical routes are easy and effective ways to introduce ligands on the surface of products for preventing them from agglomeration when they are dispersed in polar or non-polar solvents. (ii) shape and size of nanoparticles can be altered by synthesis conditions such as raw materials, acidity, solvent, concentration, additive, temperature and reaction time. (iii) soft chemical routes provide synthesis of luminescent nanoparticles on large scale at low temperature using simple apparatus at economical cost. For, these notable reasons soft chemical routes have been adapted as a most favourable and versatile method for shape controlled synthesis of luminescent nanomaterials. In this section, we explored the different chemical methods for synthesis of lanthanide doped luminescent nanomaterials and their characterizations with different techniques.<sup>34</sup> Various kinds of soft chemical methods are discussed below:

**2.1.1 Hydrothermal/Solvothermal method.** The solvothermal method has been widely used for the synthesis of luminescent nanoparticles. In brief, solvothermal synthesis is based on high pressure and mild temperature reaction between solids in liquid precursors. Normally, it is carried out in a Teflon-lined autoclave, which consists of an inner Teflon liner, an outer stainless steel shell and a cap. When heated to a certain temperature, reactants and solvents sealed in the autoclave are subjected to high pressure environment, which can increase the solubility and reactivity of almost all solid reactants.<sup>34</sup> Consequently, the solvothermal method aids to increase the rate of reactions which cannot or hardly occurs at atmospheric pressure conditions. Furthermore, the reaction temperature is often above the critical point of the solvent, whereas the temperature of the usual solvent based routes is restricted by its boiling point. These favourable features make the solvothermal method highly suitable and efficient for designing and preparing high-quality nanoparticles. Hence, various types of precursors and solvents can be used for nanoparticles synthesis except for the ones that can decompose and release vast amount of gas that may cause an explosion. Normally, a solvothermal system used for preparing rare-earth (RE) materials consists of precursor, solvent, and organic additive. The RE precursors are usually simple nitrates or chlorides. HF, NH<sub>4</sub>F, NaF, and NaBF<sub>4</sub> are the commonly used fluoride source. Na<sub>3</sub>PO<sub>4</sub>/ (NH<sub>4</sub>)<sub>2</sub>HPO<sub>4</sub>/(NH<sub>4</sub>)H<sub>2</sub>PO<sub>4</sub>, Na<sub>3</sub>VO<sub>4</sub>/(NH<sub>4</sub>)<sub>3</sub>VO<sub>4</sub>, Na<sub>2</sub>MoO<sub>4</sub>/(NH<sub>4</sub>)<sub>2</sub>MoO<sub>4</sub>, Na<sub>2</sub>WO<sub>4</sub>, and HBO<sub>3</sub> are good reactants to provide acid radical ions for the formation of RE phosphate, vanadate, molybdate, tungstate, and boate, respectively. The solvent mainly includes water, ethanol, and ethylene glycol (EG). As the physicochemical properties of the solvent can significantly influence reactivity, solubility and diffusion behaviour of the reagents and different solvents can influence and control their morphology and size. For instance, ethanol, with low RE<sup>3+</sup> and F<sup>-</sup> solubility, and EG, with high viscosity and tuneable diffusion rate of ions, both have been proved to be effective solvents to slow down the nucleation and growth rate of nanoparticles.<sup>34</sup> Water is a clean and green solvent for chemical synthesis and when it is used as solvent in solvothermal synthesis, the popular hydrothermal method is formed.

Hydrothermal synthesis provides a number of other desirable advantages such as low cost, nontoxic solvent and potential for high yield production. However, using water as solvent is avoided due to its boiling point (100° C) limitations. Besides, a large number of reports have demonstrated that, in the solvothermal method, the most efficient and straight forward strategy for fine-tuning the shape and size of a targeted material is to introduce organic additives, including hydrophilic and hydrophobic ones. On one hand, the coordination effect between the hydrophilic ligands and metal ions will affect the actual concentration of free ions, thereby influencing the concentration of monomer and growth kinetics, on the other hand, the selective adsorption of ligands on different surfaces of crystallites favours a controlled morphology. The organic surfactant/ additives such as oleic acid (OA), polyethylenimine (PEI), EDTA, and cetyltrimethylammonium bromide (CTAB) are used to control

the size and shape as well as the surface modification of nanomaterials.<sup>31,160-164</sup> Additionally, the pH value of final precursor's solution is an important parameter in hydrothermal process. The crystalline phase or morphology of nanomaterials is highly depended on pH value. The J. Sun and co-workers have demonstrated that the morphology of nanophosphor depends upon the pH value of the solution as shown in Fig. 19.<sup>165</sup>

**2.1.1.1 Characterization of hydrothermally/solvothermally synthesized nanomaterials.** The structure, surface morphology and microstructural characterizations of hydrothermally /solvothermally synthesized nanomaterials are shown in Fig. 20. It is clearly evident from the Fig. 20 that the highly crystalline nanomaterials of various morphologies can be synthesized by hydrothermal or solvothermal method.

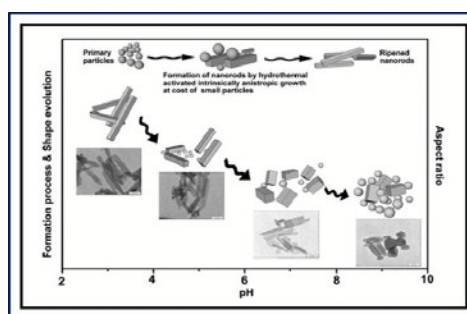


**Fig. 19** The schematic of the  $\text{Ca}_9\text{Eu}(\text{PO}_4)_7$  formation process and shape evolution mechanism produced by hydrothermal crystallization under conditions of different pH.<sup>165</sup> Reproduced with permission from ref. 165 Copyright 2015, Royal Society of Chemistry.

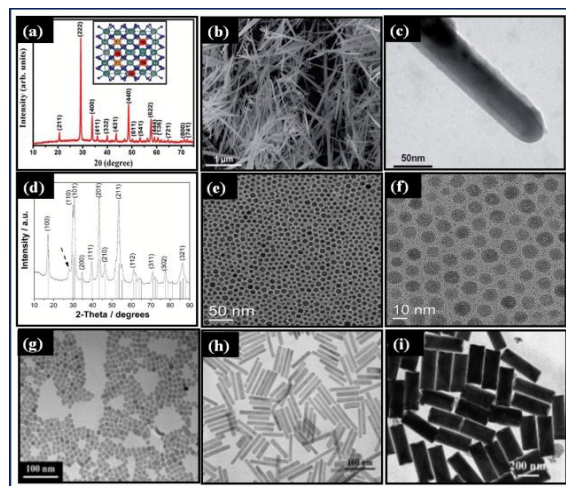


**Fig. 20** Various lanthanide doped nanomaterials synthesised by hydrothermal. (a-c) XRD, SEM and TEM of  $\text{Y}_2\text{O}_3:\text{Er}$ ,  $\text{Yb}$  nanorods,<sup>12</sup> inset of (a) exhibits crystal structure of  $\text{Y}_2\text{O}_3:\text{Er}$ ,  $\text{Yb}$  nanorods, (d-f) XRD, TEM and high resolution TEM of  $\text{NaYF}_4:\text{Yb},\text{Er}$  nanocrystals,<sup>166</sup> (g-i) XRD, TEM and high resolution TEM of  $\text{NaYF}_4:\text{Eu}$  nanocrystals.<sup>167</sup> (a-c). Reproduced with permission from ref. 12 Copyright 2014, Royal Society of Chemistry. (d-f). Reproduced with permission from ref. 166 Copyright 2006, WILEY-VCH Verlag GmbH & Co. (g-i) Reproduced with permission from ref. 167 Copyright 2007, American Chemical Society.

Cite this: DOI: 10.1039/c0xx00000x

www.rsc.org/xxxxxx

ARTICLE TYPE

**2.1.2 Sol-gel method.** The sol-gel is well known method for the synthesis of lanthanide based nanomaterials which basically involves the conversion of solutions into colloidal sol and then colloidal sol to gel. Further heating at high temperature is essential to accomplish the formation of pure phase multi-component nanoparticles with high crystallinity. Important steps involved in the sol-gel process are; hydrolysis, condensation, gelation, ageing, drying and densification.<sup>168-170</sup> The synthesis of lanthanide nanomaterials using emulsion based sol-gel process named as sol-emulsion-gel is also reported by P. N. Prasad's group.<sup>171,172</sup> The schematic for sol-gel methods is demonstrated in Fig. 21.

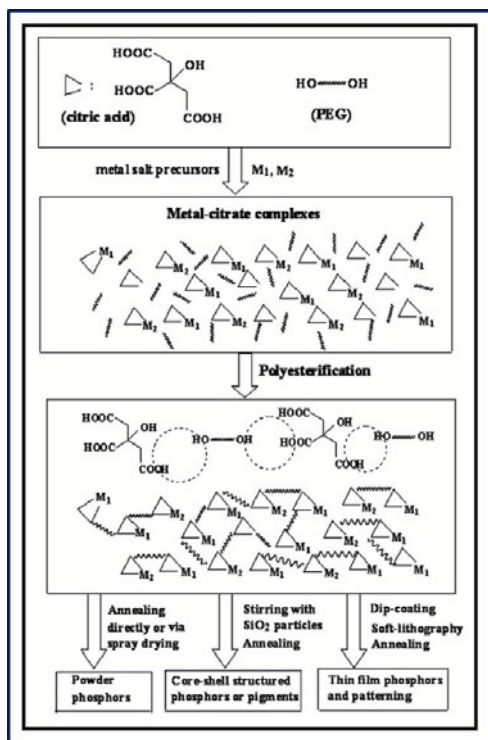


**Fig. 21** Basic principle of Pechini-Type Sol-Gel for the synthesis of phosphor.<sup>168</sup> Reproduced with permission from ref. 168 Copyright 2007, American Chemical Society.

In this method, initially, the metal precursors such as metal nitrates, metal chlorides, acetates etc. are dissolved in aqueous solutions, thereafter, the chelating agent such as citric acid or salicylic acid is used to form stable metal complexes. Furthermore, polyhydroxy alcohol such as polyethylene glycol (PEG) or ethylene glycol (EG) is used as cross-linking agent to

from homogeneous polymeric resin at molecular scale. The polymeric resin gel reduces the segregation of particular metal ions and confirms the homogeneity of the composition. Furthermore, the gel is sintered at high temperature to eradicate the organic additives and form final product with pure phase and good crystallinity.<sup>173</sup>

### 2.1.2.1 Characterization of sol-gel synthesized nanomaterials.

The structure, surface morphology and microstructural characterizations of sol-gel synthesized nanomaterials are shown in Fig. 22. It can easily be seen from the Fig. 22 that the synthesized nanomaterials are of high crystallinity.

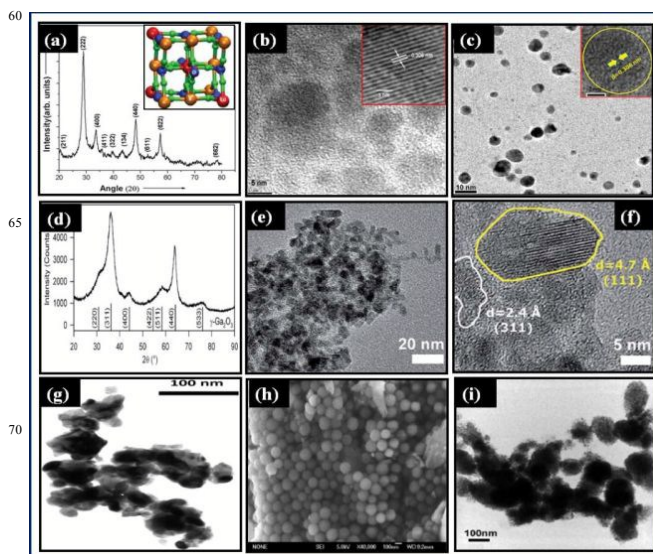


**Fig. 22** Various lanthanide doped nanomaterials synthesised by sol-gel method. (a-c) XRD, crystal structure of  $\text{Y}_2\text{O}_3:\text{Eu}$  (inset of (a)), TEM and high resolution TEM of  $\text{Y}_2\text{O}_3:\text{Eu}$  nanoparticles.<sup>15</sup> (d-f) XRD, TEM and HRTEM of  $\gamma\text{-Ga}_2\text{O}_3$  nanoparticles,<sup>174</sup> (g) TEM image of  $\text{LaOF}:\text{Eu}^{3+}$  Nanocrystals,<sup>176</sup> and (h & i) SEM and TEM image of  $\text{LaPO}_4:\text{Eu}^{3+}, \text{Li}^+$  Nanophosphors.<sup>177</sup> (a & b) Reproduced with permission from ref.15, Copyright 2010 IOP Publishing. (c) Reproduced with permission from ref. 174, Copyright 2012, WILEY-VCH Verlag GmbH & Co. (d-f) Reproduced with permission from 175, Copyright 2015 Royal Society of Chemistry. (g) Reproduced with permission from 176, Copyright 2011, American Chemical Society. (h & i) Reproduced with permission from 177, Copyright 2008, American Chemical Society.

Cite this: DOI: 10.1039/c0xx00000x

www.rsc.org/xxxxxx

## ARTICLE TYPE

**2.1.3 Thermal decomposition method.** Thermal decomposition is another method which is widely used for the synthesis of luminescent nanomaterials. The process involves the decomposition of organometallic compounds taken as precursors which decompose at an elevated temperature in high boiling point organic solvents. The organic precursors used in thermal decomposition are usually organic acid salts of rare earths such as trifluoroacetate, oleate, acetylacetonate and acetate etc. Commonly used organic solvent are oleic acid (OA), oleylamine (OM), tri-n-octylphosphine oxide (TOPO) and 1-octadecene (ODE). However, 1-octadecene (ODE) is most commonly used as solvent in thermal decomposition due to its high boiling point (315°C). Besides above, surfactants are also used in thermal decomposition method. The surfactant caps the surface of nanoparticles which make them highly dispersive in organic solvents and also prevent aggregation of nanoparticles. In addition to this, surfactant also plays another important role of controlling the growth of nanoparticles. Oleic acid (OA) and oleylamine (OM) containing organic group and a long chain of hydrocarbon acts both as an organic solvent and as a surfactant.<sup>31,34</sup> It is reported that high-quality nanomaterials with a narrow size distribution, good crystallinity and exceptional

optical properties can be synthesized by carefully optimizing the variables such as the nature of the solvents, concentration of metal precursors, reaction temperature and reaction time.<sup>31</sup> In recent few year many efforts have been attempted to study the effect of experimental conditions such as concentration of precursors, choice of solvent, choice of surfactant, reaction temperature and reaction time on size distribution, crystallinity and optical properties of nanomaterials. Yan et al. successfully synthesised the triangular nanoplates of LaF<sub>3</sub> by thermal decomposition using metal trifluoroacetate (La(CF<sub>3</sub>COO)<sub>3</sub>) as precursor, oleic acid as surfactant and octadecene as solvent.<sup>178</sup> There are many other reports on the synthesis of lanthanide doped nanomaterials using thermal decomposition with different host lattices such as LiYF<sub>4</sub>, NaYF<sub>4</sub>, NaGdF<sub>4</sub>, NaLuF<sub>4</sub>, BaYF<sub>5</sub>, KY<sub>3</sub>F<sub>10</sub>, BaGdF<sub>5</sub>, CaF<sub>2</sub>, SrF<sub>2</sub>, BaF<sub>2</sub>, YOF, LuOF, LaOF, and GdOF.<sup>178-205</sup>

**2.1.3.1 Characterization of thermal decomposition synthesized nanomaterials.** The microstructural analysis of nanomaterials synthesized by thermal decomposition method is shown in Fig. 23.

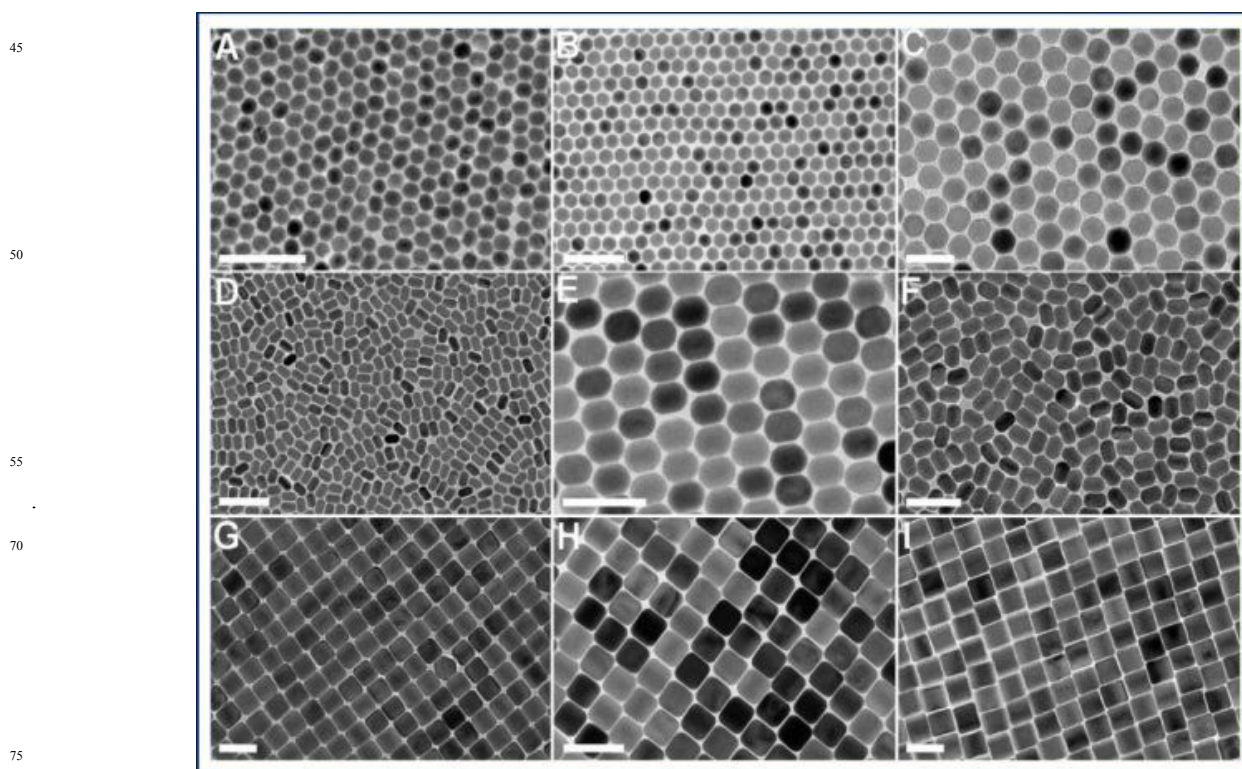


**Fig. 23** TEM images of the  $\beta$ -NaYF<sub>4</sub>-based upconversion nanoparticles synthesized by thermal decomposition. All scale bars represent 100 nm.<sup>205</sup> Reproduced with permission from ref. 205, Copyright 2010, National Academy of Science, USA.

80

**2.1.4 Coprecipitation method.** The coprecipitation method is one of the oldest and most useful methods for the synthesis of lanthanide based nanomaterials. The coprecipitation method has several advantages over the thermal decomposition method such as mild reaction condition, low cost set-up, simple protocol and short reaction time. Van et al synthesized rare earth doped  $\text{LaF}_4$ :  $\text{Ln}^{3+}$  ( $\text{Ln}^{3+} = \text{Eu}, \text{Er}, \text{Nd}$  and  $\text{Ho}$ ) nanoparticle using coprecipitation method.<sup>206</sup> The ammonium di-n-octadecylthiophosphate was used as a surfactant which controls the growth of nanoparticles, prevents nanoparticles from agglomeration and also provides the stability in organic solvent. Further, Yi and co-workers implemented this method for the synthesis of  $\text{NaYF}_4$ :Yb/Er nanoparticles assisted by ethylenediaminetetraacetic acid (EDTA).<sup>207</sup> In their study, the size of nanoparticles was varied from 37 nm to 166 nm by tailoring the molar ratio of EDTA and  $\text{Ln}^{3+}$  ion. Zhang et al synthesized rare earth doped hexagonal  $\text{NaYF}_4$ :Yb/Er (or Tm) nanoparticles using OA as capping agent and ODE as solvent.<sup>208</sup>

There are many other reports on the synthesis of lanthanide based nanomaterials with different host lattices such as  $\text{Ln}^{3+}$ -doped  $\text{LiYF}_4$ ,  $\text{NaYF}_4$ ,  $\text{NaGdF}_4$ ,  $\text{NaTbF}_4$ ,  $\text{NaLuF}_4$ ,  $\text{KGdF}_4$ ,  $\text{NaScF}_4$ ,  $\text{CaF}_2$ , and  $\text{LaF}_3$ .<sup>209-221</sup> However, size and shape of the nanomaterials synthesized by this method can be controlled by tailoring the reaction conditions. But, these nanomaterials exhibit a weak luminescence intensity that can be enhanced by sintering at high temperature which carbonises the capping agent and reduces the hydrophilicity of nanoparticles. Consequently, some suitable surface modifications are further needed prior to using these nanoparticles for luminescent security ink application. Nevertheless, the coprecipitation method has important industrial applications due to low cost, high yield, environment benignancy and synthetic suitability.

**2.1.4.1 Characterization of coprecipitation method synthesized nanomaterials.** The microstructural investigation of nanomaterials synthesized by coprecipitation method is shown in Fig. 24.

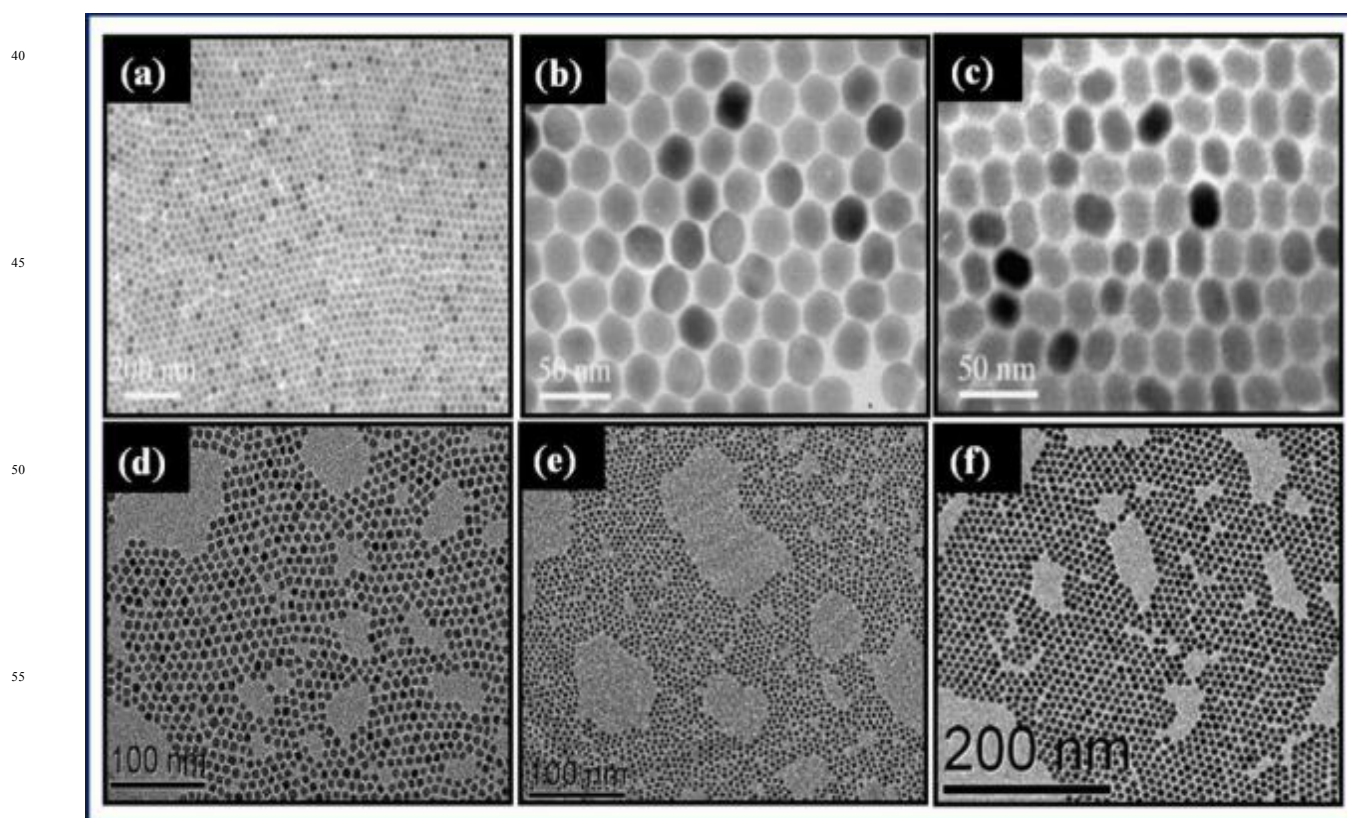


**Fig. 24** (a–c) TEM images of lanthanide-doped  $\beta\text{-NaYF}_4$ ,<sup>209</sup> (d&e) ultrasmall  $\text{CaF}_2$ <sup>31</sup> and (f)  $\text{NaGdF}_4$  core-only NPs.<sup>31</sup> All nanomaterials are synthesised by coprecipitation method. (a–c) Reproduced with permission from ref. 209, Copyright 2008, WILEY-VCH Verlag GmbH & Co. (d–f) Reproduced with permission from ref. 31, Copyright 2013, Royal Society of Chemistry.

70

65

75

## 2.2 Synthesis of quantum dots (QDs)

The synthesis of quantum dots has gained immense interest worldwide due to their wide range of applications. Several methods are reported in literature that can be employed for the synthesis of quantum dots. However, the reproducibility with controlled size and band gap engineering of QDs is also an interesting and challenging topic of research. The various methods for the synthesis of QDs can be classified into two categories – “top-down” and “bottom-up”.

**2.2.1 Synthesis of semiconductor quantum dots (SQDs).** Top-down technique involves the breaking of bulk/large structure into small structure with dimensions in nanometer range. In case of semiconductor quantum dots, top-down techniques includes the molecular beam epitaxy (MBE), reactive ion etching (RIE), ion implantation, e-beam lithography and X-ray lithography techniques for the synthesis of QDs. Scherer and co-workers fabricated the QDs using reactive ion etching technique. In their study, the synthesis of QDs with size ~40 nm was reported. Tsutsui et al. also fabricated the ZnTe quantum dots in a mixture of CH<sub>4</sub> and H<sub>2</sub> using reactive ion etching technique. Bottom-up is another technique, where fundamental building blocks such as molecules or atoms interact with each other and form nanostructures. There are several bottom-up techniques for the synthesis of QDs that can be divided into two types: wet chemical methods and vapour phase methods. The wet chemical methods include the microemulsion, sol-gel, competitive reaction chemistry, hot-solution decomposition and electrochemistry. While the vapour phase methods include molecular beam epitaxy (MBE), sputtering, liquid metal ion sources and aggregation of gaseous monomers. However, most of the luminescent semiconductor QDs are synthesized by using wet chemical methods. In wet chemical methods, the size of quantum dots can be controlled by optimizing the growth parameters. Qu et al. synthesized the CdSe QDs having size in the range of 6-9 nm using wet chemical method. Murray and co-workers synthesized high-quality CdE (E = S, Se, Te) semiconductor QDs using the process based on the pyrolysis of organometallic reagents assisted by their injection into a hot coordinating solvent. In another interesting report, Qu and co-workers synthesized high quality CdSe nanocrystals in a very broad size range from ~1.5 nm to above 25nm using different wet chemical routes. Li et al. synthesized CdTe nanocrystals in the aqueous phase by microwave irradiation with controllable temperature. In general, the MBE has been mainly used to self-assemble QDs from III-V and II-VI semiconductors. Xin and co-workers synthesized CdSe QDs having diameters of 40 ± 5 nm using MBE technique. Further, Liu and co-workers reported synthesis of CdSe SQDs using commercial diesel as the reaction solvent and oleic acid as ligand. The wet chemical methods have important advantages that the size, shape of QDs can be controlled by simply varying the factors like temperature, electrostatic double layer thickness, stabilizers or micelle formation, concentrations of precursors, ratios of anionic to cationic species and solvent.

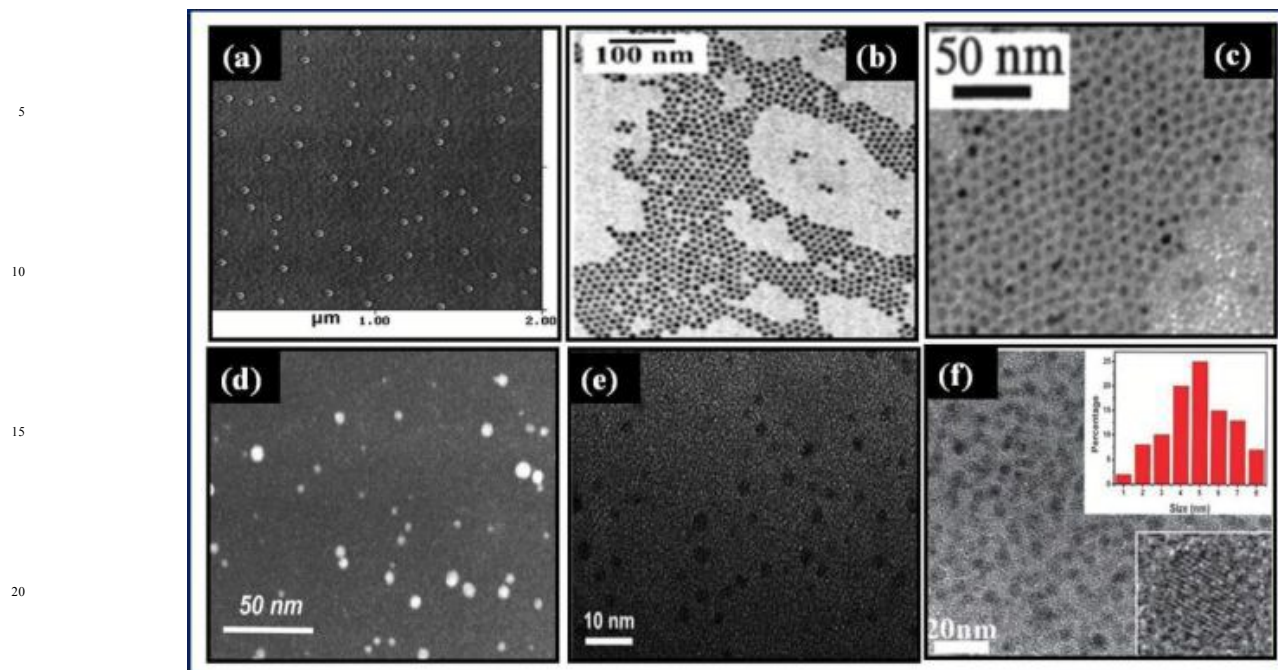
**2.2.2 Synthesis of carbon quantum dots (CQDs).** Top-down

methods involves the breaking down of the larger carbon structures like nanodiamonds, graphite, carbon nanotubes, carbon soot, activated carbon, graphite oxide and reduced graphene oxide. Most common methods like arc discharge, laser ablation and electrochemical oxidation are used to break down the large carbon lattice. Xu and co-workers reported the synthesis of fluorescent CQDs from carbon soot in 2004. Sun et al. synthesized the CQDs by laser ablation of a carbon target in the presence of water vapors with argon as carrier gas. The fluorescence was not detected in the as-synthesized sample. Consequently, to make sample fluorescent, as-synthesized sample was further treated with acid for oxidation followed by surface passivation. The electrochemical synthesis of CQDs was reported by Zhou et al. They performed electrochemical synthesis in an electrochemical cell containing degassed acetonitrile solution with 0.1 M tetrabutylammonium perchlorate (TBAP) as the supporting electrolyte. The chemical vapor deposition (CVD) grown MWCNTs on a carbon paper was also inserted into the cell. The electrochemical process converts MWCNTs into highly efficient luminescent CQDs, which can easily be dispersed in various solvents. In another report, Ming et al. reported electrochemical synthesis of CQDs using graphite as carbon source which decreases the cost of precursor materials and increases the scale of production. Further, J.M. Tour's group has reported a facile approach for large scale synthesis of GQDs at an economical cost from various types of coal. The bottom-up techniques involves the synthesis of CQDs from molecular precursors such as citrate, carbohydrates and polymer-silica nanocomposites. Usually, combustion/thermal treatments and supported synthetic and microwave synthetic methods are used for the synthesis of CQD in bottom-up approach. Liu and co-workers reported synthesis of CQD based on the use of modified silica spheres as carriers and resols as carbon precursors. Bourlinos et al. reported the synthesis of CQDs by thermal decomposition method using ammonium citrate salts or 4-aminoantipyrines precursors. In an interesting report, Zhu and co-workers synthesised CQD from a solution of poly(ethylene glycol) (PEG) and saccharide by heating in a 500W microwave oven. However, the cost is one of the major parameter for the large scale production of CQDs. In recent years, a large number of efforts have been devoted to develop green synthesis of CQDs. Further, Li and co-workers reported the synthesis of fluorescent CQDs by using simple and green route. They synthesized the fluorescent CQDs from ethanol by a one-step sodium hydroxide-assisted electrochemical process. The synthesized CQDs have high water solubility, better stability and good sensitivity to pH. Furthermore, there are many reports available on the synthesis of fluorescent CQDs using inexpensive and biocompatible precursors such as ethanol, citrate, glucosamine, ascorbic acid, saccharides, candle soot, orange juice, strawberry juice, sugar cane juice, chicken eggs, chitosan, organogel and gelatin.

**2.2.3 Characterization of SQDs and CQDs.** The Fig. 25 demonstrates the microstructural analysis of QDs synthesized by various methods.

Cite this: DOI: 10.1039/c0xx00000x

www.rsc.org/xxxxxx

**ARTICLE TYPE**

**Fig. 25** Various QDs synthesized by different vapour phase and wet chemical methods. (a) AFM image of self-organized CdSe dots,<sup>231</sup> (b) TEM image of CdSe QD,<sup>227</sup> (c) TEM image of wurtzite CdSe QD,<sup>229</sup> (d) STEM images of carbon dots surface-passivated with PEG<sub>1500N</sub>,<sup>108</sup> (e) HRTEM image of carbon dots surface-passivated with PEG<sub>1500N</sub>.<sup>242</sup> (f) TEM image of fluorescent CQDs, the inset shows the particle size distribution and HRTEM of fluorescent CQDs.<sup>244</sup> (a) Reproduced with permission from ref. 231, Copyright 1996, American Institute of Physics. (b) Reproduced with permission from ref. 227, Copyright 2002, American Chemical Society. (c) Reproduced with permission from ref. 229, Copyright 2001, American Chemical Society. (d) Reproduced with permission from ref. 108, Copyright 2006, American Chemical Society. (e) Reproduced with permission from ref. 242 Copyright 2009, WILEY-VCH Verlag GmbH & Co. (f) Reproduced with permission from ref. 244 Copyright 2011, Royal Society of Chemistry.

### 2.3 Metal-organic-frameworks (MOFs)

Metal-organic frameworks (MOFs) are the most attractive, fascinating and novel class of porous nanomaterials. Their miniaturization into the nano MOFs is expected to serve myriad applications.<sup>262</sup> Consequently; enormous efforts have been devoted to synthesize MOFs by different methods. Extensive reports have been published till date regarding the synthesis of MOFs.<sup>263,264</sup> In past years, a number of methods have been adopted for the synthesis of MOFs having various crystal size or shape depending upon their suitability for further applications. The various methods for the synthesis of MOFs are summarized in Fig 26. Different strategies have been adopted for the synthesis of luminescent nanoscale MOFs. Generally, in simple diffusion technique, the solution containing metal salts is slowly diffused into organic linker. This method is tedious and time consuming with low yield. Hydrothermal syntheses of MOFs have been feasible to those reaction systems in which organic linkers may be partially soluble in water at higher temperature. However,

there are many other methods reported for the synthesis of MOFs such as mechanochemical solid-state grinding and liquid-assisted grinding, emulsions or templates based synthesis, sonochemical, microwave-assisted and spray-drying synthesis.<sup>263,264</sup> Lu and his team synthesized the lanthanide based nanoscale luminescent MOFs (MOF-253).<sup>265</sup> They synthesized lanthanide ion (Eu, Tb and Sm) containing MOF-253 which emits in the visible range. The emission intensity of MOFs is directly proportional to the amount of lanthanide ion in MOFs. The emission colour of nanoMOFs was also tailored by varying the ratio of Eu/Tb. In another interesting report Carne-Sanchez et al. synthesized nanoMOFs using spray-drying method. This spray-drying method facilitates the construction of a multi-component MOFs superstructures and the encapsulation of guest species within these superstructures.<sup>262</sup> The spray-drying method is a versatile method and by using this method the nanoMOFs can be prepared easily and rapidly with controlled size and shape as shown in Fig. 27.<sup>262</sup>

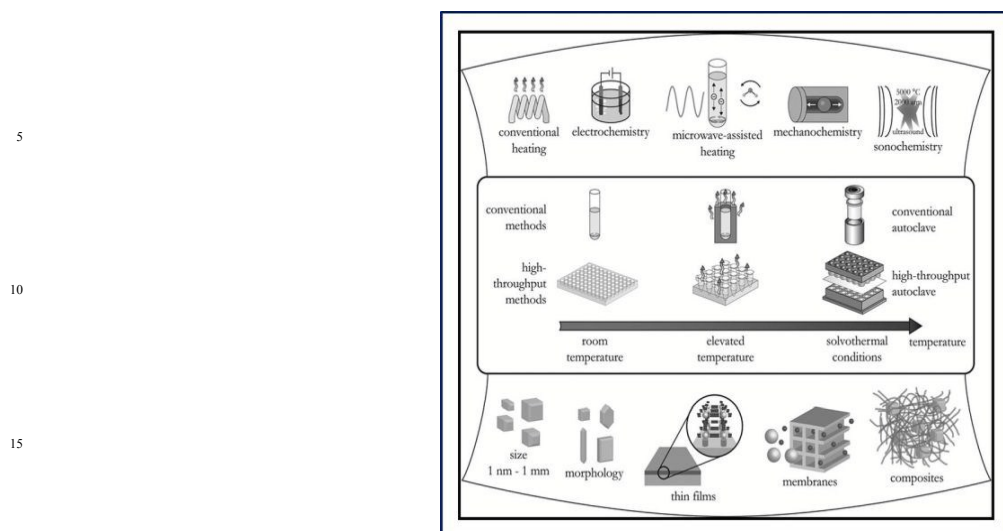


**Fig. 26** Overview of synthesis methods, possible reaction temperatures and final reaction products in MOF synthesis.<sup>263</sup> Reproduced with permission from ref. 263 Copyright 2012, American Chemical Society.

**2.3.1 Characterization of MOFs.** Series of MOFs synthesized by spray-drying method and these MOFs are characterized by using superstructures and discrete nanoMOFs crystals synthesized by XRD, SEM, and TEM techniques as shown in Fig. 27.

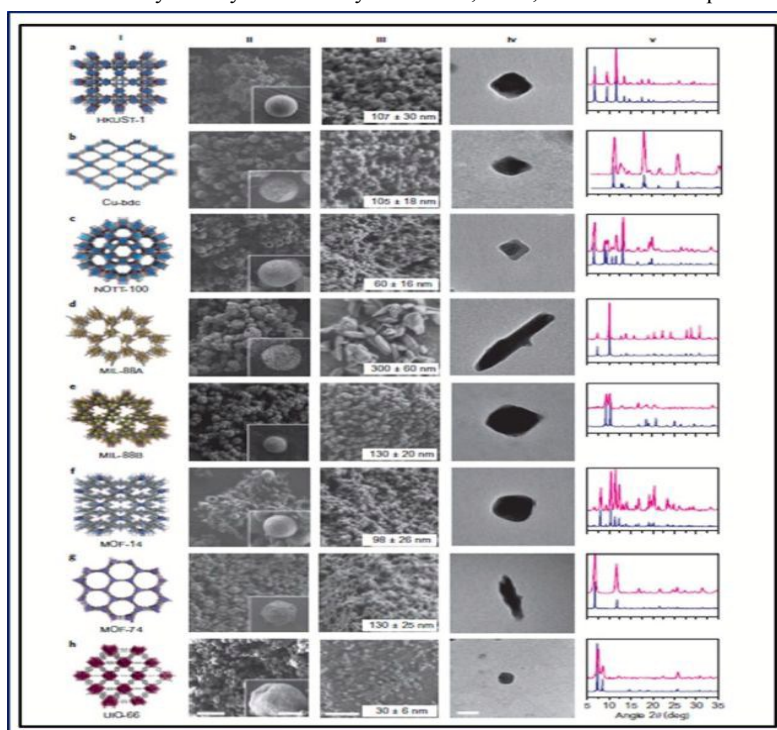


**Fig. 27** Series of MOFs superstructures and discrete nanoMOFs crystals synthesized by spray-drying. Synthesized MOFs: a, HKUST-1 (for comparison), b, Cu-bdc, c, NOTT-100, d, MIL-88A, e, MIL-88B, f, MOF-14, g, Zn-MOF-74, h, UiO-66. FESEM (ii, ii inset, iii) and TEM (iv) images of the synthesized MOF superstructures and discrete nanoMOF crystals, and the corresponding experimental (pink) and simulated (blue) XRPD patterns (v, for comparison), are shown for each MOF. Scale bars: 10 μm (ii), 2 μm (inset to ii), 500 nm (iii), 90 nm (iv).<sup>262</sup> Reproduced with permission from ref. 262 Copyright 2013, Nature publishing group.

50

55

## 2.4 Synthesis of plasmonic nanomaterials

The Nobel metal (Au and Ag) nanoparticles usually exhibit the size and shape dependent plasmonic properties. Plasmonic nanoparticles with different shape and size can be synthesized by using four different routes:<sup>266-274</sup>

### 2.4.1 One-pot-one-step synthesis of plasmonic nanoparticles

#### 2.4.2 Synthesis of plasmonic nanoparticles via seeded growth

10 Synthesis

#### 2.4.3 Synthesis of plasmonic nanoparticles via reshaping/etching synthesis

15 2.4.4 Templated assisted synthesis of plasmonic nanoparticles

#### 2.4.1 One-pot-one-step synthesis of plasmonic nanoparticles.

This method is easiest of all for the synthesis of metal nanoparticles. By using this method the morphology of nanoparticles (for examples; stars, rods, plates, and prisms) can be controlled by changing the reaction conditions like temperature, solvent and additives etc. The most commonly used reducing agent and capping agent for the nanoparticles is polyvinylpyrrolidone (PVP). It can potentially modify the nucleation, growth, and shape of nanoparticles because of its proficiency to interact with metal ions and surfaces as well as the preferable attachment to distinct crystal facets of certain metals (e.g., silver).<sup>272,275-280</sup> Furthermore, the choice of solvent is also a very important factor for the synthesis of plasmonic nanoparticles. The nanoparticles can also be tuned to any desired shape by changing the solvent. Kedia and co-worker reported the effect of solvent on the synthesis of gold nanoparticles. They tuned the morphology of gold nanoparticles from spherical to star shaped by changing the solvent.<sup>281</sup> This study reveals that apart from capping agent, the interaction between capping agent-solvent-metal ion also affects the final structure of nanoparticles. In another report, Angelome et al. discussed the effect of temperature on the synthesis of plasmonic nanoparticles. In their study, they showed that the wavelength of LSPR in gold nanoparticles can be tuned from 600 nm to 1400 nm by simply varying the reaction temperature (between 30 and 10 °C) and the reagent concentrations.<sup>282</sup> Zhang et al. demonstrated the synthesis of silver nano prisms using hydrogen peroxide (H<sub>2</sub>O<sub>2</sub>). The hydrogen peroxide facilitates the formation of planar-twinned defects which are a prerequisite for the formation of nanoprisms.<sup>283</sup>

**2.4.2 Synthesis of plasmonic nanoparticles via seeded growth synthesis.** This method includes two reaction steps. The first step reaction involves the formation of nuclei whereas, in second reaction step, the seed formed in the first step is added to growth solution. Further, the nanoparticles with different morphologies can be synthesized under different growth conditions. Langille et al. synthesized gold nanoparticle by seeded growth method and in their report, they showed the effect of halides ion on the growth of gold nanoparticles. Gold nanoparticles with different shapes

can be synthesized by kinetic control, surface passivation, or by a combination of both, either in the absence or presence of the silver ions as shown in Fig.28.<sup>284</sup> Ye et al. synthesized gold nanorods having different aspect ratios by introducing aromatic additives into well established seeded synthesis method with better control on monodispersity of gold nanorods.<sup>285</sup>

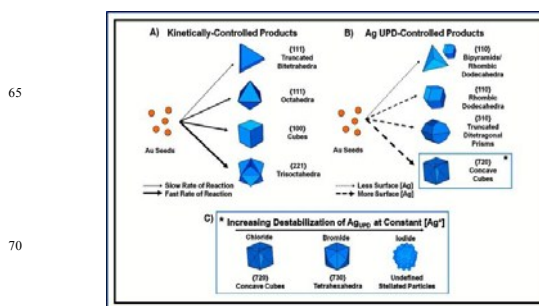


**Fig. 28** Scheme illustrating how halides and silver ions can be used to direct the growth of gold seeds down different growth pathways to yield different shaped products namely: (A) kinetically controlled products in the absence of silver ions; (B) Ag under potential deposition (UPD) controlled products where the interactions of silver with the particle surface dictate the product shape; (C) effect of varying the stability of the Ag UPD layer with high concentrations of chloride, bromide, or iodide in the growth solution, yielding concave cubes, tetrahedra and stellated particles, respectively.<sup>284</sup> Reproduced with permission from ref. 284 Copyright 2012, American Chemical Society.

#### 2.4.3 Synthesis of plasmonic nanoparticles via reshaping/etching synthesis.

Reshaping of particles is indirectly used during many synthetic procedures. Post synthesis ageing and transformation of nanoparticles is often an undesired process as it results in limiting the lifetime and usability of a specific particle type. But the mechanisms for these processes need to be understood in order to enhance their stability. In addition, it is also possible to deliberately use them in order to obtain novel nanostructures.<sup>272</sup> Ng et al. demonstrated that the reshaping of gold nanorods by simple thermal route.<sup>286</sup> The longitudinal plasmonic resonance of gold nanorods was tuned from 800 to 560 nm using reshaping of nanorods. The author synthesized gold nanorods with aspect ratio 3:3 and then heated these nanorods at various temperatures. In another study, Damn et al. studied the reshaping of silver by the ageing of aqueous suspensions of rod at 25°C for different time-interval.<sup>287</sup> Further, Min and his team purposed combination of a top-down (etching) and a bottom-up (growth) for the synthesis of gold-platinum nanoparticles. Initially, platinum was deposited at different positions of gold nanospheres, cubes, and octahedra synthesized via the polyol process. Then, gold nanohexapods or empty platinum shells (depending on the initial structure) was obtained by adding cyanide solution due etches the gold surface.<sup>288</sup>

Nanoscale Accepted Manuscript

#### 2.4.4 Templated assisted synthesis of plasmonic nanoparticles.

This method employs prefabricated structure (known as template) to collect multiple, discrete nano-objects into a larger, well-defined, ordered architecture. The templated growth of nanomaterials is carried out via physical deposition of metal in specific geometry or via chemically directing growth to occur at a specific locations or crystallographic direction. The templated based growth offers to fabricate collective or discrete nano-object into large, well defined and ordered structures.<sup>274</sup> Bridges and his co-workers synthesized gold nanotubes of different thickness using anodized aluminum as template via electrochemical synthesis.<sup>289</sup> The morphology of structure and thickness of core depend upon the nature of solvent/electrolyte. The thickness of gold nanotubes was varying through polymer core hydrophobicity. Nykypanchuk et al. reported the DNA-guided crystallization of colloidal nanoparticles.<sup>290</sup>

#### 2.4.5 Characterizations of plasmonic nanomaterials.

The surface morphologies and microstructural characterizations of gold and silver plasmonic nanoparticles synthesized by one-pot-one-step and via seeded growth methods are shown in Fig.29. The Fig. 30 represents the surface morphologies and microstructural micrographs of gold and silver nanomaterials synthesized by reshaping/etching and templated methods.

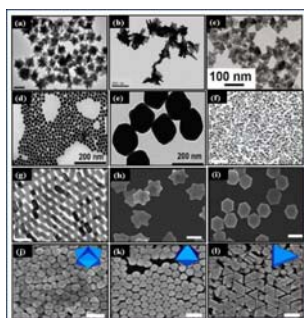


**Fig. 29** Gold and silver nanoparticles synthesized via the one-pot-one-step synthesis or the seeded growth methods. (a) TEM image of gold nanoparticles, scale bar = 100nm,<sup>281</sup> (b) TEM image of gold nanoparticles,<sup>282</sup>(c) TEM image of silver nanoparticles,<sup>283</sup> (d)& (e) TEM images of gold nanoparticles,<sup>291</sup>(f)TEM image of gold nanoparticles, scale bar = 200nm,<sup>285</sup>(g) TEM image of gold nanoparticles, scale bar = 50nm<sup>285</sup>(h) & (i) SEM images of gold nanoparticles, scale bar = 200nm<sup>292</sup>(j-l) SEM images of gold nanoparticles, scale bar = 200nm<sup>284</sup>(a) Reproduced with permission from ref. 281, Copyright 2012, American Chemical Society. (b) Reproduced with permission from ref. 282 Copyright 2012, American Chemical Society. (c) Reproduced with permission from ref. 283. Copyright 2011, American Chemical Society. (d) & (e) Reproduced with permission from ref. 291. Copyright 2011, American Chemical Society. (f) & (g) Reproduced with permission from ref. 285, Copyright 2012, American Chemical Society. (h) & (i) Reproduced with permission from ref. 292, Copyright 2012, WILEY-VCH Verlag GmbH & Co. (j-l) Reproduced with permission from ref. 284, Copyright 2012, American Chemical Society.

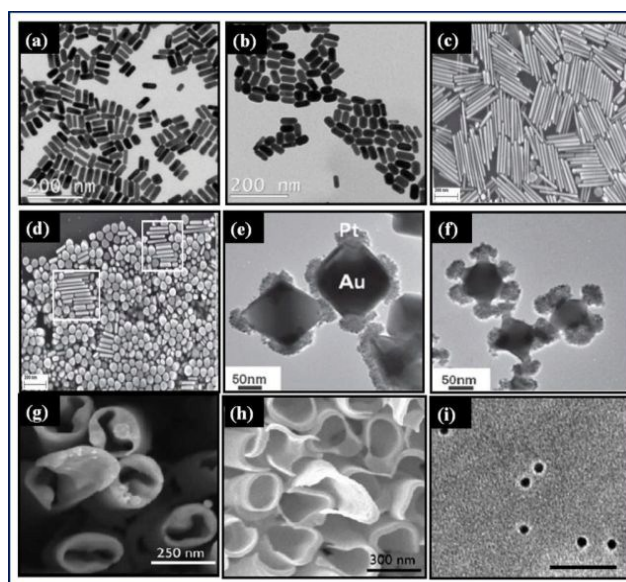


**Fig.30** Plasmonic nanomaterials synthesized by reshaping/etching and templated methods. (a) & (b) TEM images of gold nanorods,<sup>286</sup> (c) & (d) SEM images of silver nanorods and nanoparticle,<sup>287</sup> (e) & (f) TEM images of gold nanoparticle,<sup>288</sup> (g) & (h) SEM images of gold nanotubes,<sup>289</sup>(i) TEM images of gold nanoparticle, scale bar = 50 nm<sup>293</sup>(a) & (b) Reproduced with permission from ref. 286. Copyright 2012, IOP publishing. (c) & (d) Reproduced with permission from ref. 287. Copyright 2011, WILEY-VCH Verlag GmbH & Co. (e) & (f) Reproduced with permission from ref. 288 Copyright 2011 Royal Society of Chemistry. (g) & (h) Reproduced with permission from ref. 289 Copyright 2013 Royal Society of Chemistry. (i) Reproduced with permission from ref. 293 Copyright 2010 WILEY-VCH Verlag GmbH & Co.

After detailed discussions on different types of synthesis routes for various kinds of luminescent nanomaterials (lanthanide based, quantum dot, MOFs and plasmonic nano materials), we have thoroughly discussed about the different methods for fabrication and design of security inks and strategies employed for various types of security code printing techniques in following sections:

### 3. Fabrication and designing of luminescent security ink

The fabrication and designing strategies of luminescent security ink play a key role for their commercial use in anti-counterfeiting applications. The major challenge in this area is to fabricate the luminescent ink having high stability, ease of availability of ink medium at low cost, good dispersion of luminescent nanomaterials in ink medium, high luminescent intensity of ink, convenience of printing and sticky nature of ink medium on different surfaces (viscosity around 3000  $\mu\text{P}$  and better surface tension). Furthermore, it also important to understand the chemistry of luminescent security ink formation (whether the ink is hydrophobic or hydrophilic in nature) prior to its potential use in printing of security codes/ bars on different types of surfaces.

There are certain criteria to fabricate and design the luminescent security ink with desired properties as discussed below:

### 3.1 Choice of the luminescent ink medium

The appropriate choice of ink medium is an important part for fabrication of luminescent ink in which the luminescent nanomaterials can be dispersed homogeneously and consequently form colloidal suspensions without forming any cluster or settling down at bottom. Besides the above, the viscosity of medium used for ink fabrication is also an important factor because it provides essential sticky nature to ink suitable for printing on different type of surfaces. In addition to this, the boiling point of medium used for ink fabrication is also a key factor. The volatile medium (such as toluene) exhibits the 'coffee-ring effect', which concentrates the medium along the rim of a drop as shown in Fig. 31a.<sup>294</sup> Furthermore, the faster evaporation at the edges leads to flow of ink medium towards the drop edge. This issue can be minimized by adding a solvent having high boiling point. Blumenthal et al. have reported various solvents such as Xylene, cyclohexanone and methyl benzoate for the minimization of coffee-ring effect. They used methyl benzoate because of its ability to dissolve polymethyl methacrylate (PMMA) and is easy to mix with toluene. In their study, they observed that toluene and methyl benzoate mixed together in volume ratio of 90:10 eliminated the 'coffee ring effect' as shown in Fig. 31 b.<sup>294</sup> Apart from PMMA, many other mediums such as polyvinyl alcohol (PVA), aqueous solution of sodium hexametaphosphate (SHMP), polyvinyl chloride (PVC) gold medium can be used for ink fabrication.<sup>12,15,294</sup>

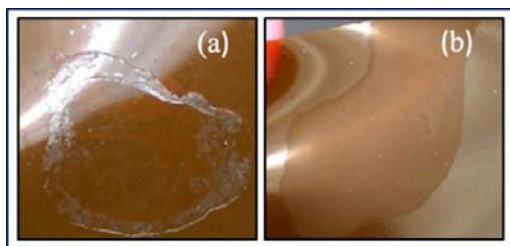


**Fig. 31** (a) Drop test of PMMA dissolved in toluene and deposited on Kapton; image shows 'coffee ring effect' in which the polymer is excessively deposited at edges of the drop due to the high evaporation rate. (b) Drop test of PMMA dissolved in toluene and methyl benzoate mixture at 90:10 with 1 wt% upconversion nanoparticles deposited on Kapton.<sup>294</sup> Reproduced with permission of ref. 294, Copyright 2012, IOP publishing.

### 3.2 Various types of luminescent ink formulation

This section briefly describes the formation of different types of luminescent security inks based on various types of luminescent nanomaterials such as lanthanide based luminescent nanomaterials (downconversion, upconversion and dual mode), luminescent quantum dots, luminescent MOFs and plasmonic nanomaterials as described below:

#### 3.2.1 Lanthanide nanomaterials based luminescent security ink

#### 3.2.2 Quantum dot based luminescent security ink

#### 3.2.3 MOFs based luminescent security ink

#### 3.2.4 Plasmonics nanomaterials based luminescent security ink

**3.2.1 Lanthanide nanomaterials based luminescent security ink.** In recent years the lanthanide based luminescent nanomaterials have gained huge attention due to their remarkable optical properties and wide range of applications in many potential areas such as luminescent security ink, optical displays, sensors, optoelectronics, laser cooling, bio-imaging and security applications etc. There are several potential advantages to use lanthanide based luminescent security inks for anti-counterfeiting applications as compared to standard fluorescent inks, which normally produce visible emission when subjected to UV excitation. Furthermore, the lanthanide based luminescent inks exhibit both downconversion and upconversion processes in a single host lattice which makes them intrinsically more difficult to duplicate as compared to the standard fluorescent dyes. Additionally, another advantage of lanthanide based inks over the commercially used fluorescent dyes is that former have sharper transitions without photobleaching. Moreover, lanthanide based inks can be formulated to produce the correct color rendering index only under specific excitation power densities, making them even more difficult to duplicate the authentic read conditions.

This section of review article will be mainly focused on fabrication and design of lanthanides based luminescent security ink including downconversion/downshift, upconversion and dual-mode lanthanide based luminescent security inks.

#### 3.2.1.1 Downconversion nanomaterials based luminescent security ink.

In our earlier reports on luminescent security ink, we have demonstrated the strategy for the fabrication of downconversion security inks based on  $Y_2O_3:Eu^{3+}$  nanoparticles. Initially, sodium hexametaphosphate (SHMP) was dissolved in de-ionized (DI) water at molar concentration of 5%. After that, 500 mg of  $Y_2O_3:Eu^{3+}$  nanoparticles were added to 30 ml of SHMP solution with continuous stirring for 15 min. Further, 5 ml ethanol was added to the mixture and kept under an ultrasonic bath for about an hour. Finally, the capped nanoparticles particulates were collected using an ultracentrifuge. 0.2 mg  $cm^{-3}$  of this was re-dispersed in fresh DI water at room temperature to make an aqueous-stable and highly transparent luminescent ink.<sup>15</sup>

#### 3.2.1.2 Upconversion nanomaterials based luminescent security ink.

Blumenthal and co-workers suggested an approach to fabricate the upconversion security ink using toluene as ink medium.<sup>295</sup> The 2 wt% of upconversion nanoparticles of  $NaYF_4:Er,Yb$  were dispersed in toluene and 1 wt% poly methyl methacrylate (PMMA) was added to the dispersion along with enough methyl benzoate. Further, direct-write and screen printing technique was used to print with the fabricated ink. Meruga et al. also demonstrated a method for the fabrication of green and blue security inks based on upconversion nanoparticles of  $NaYF_4:Er,Yb$  and  $NaYF_4:Tm,Yb$  respectively for printing QR codes.<sup>11h</sup> For ink formation the upconversion nanophosphor and PMMA beads were added to a solution of 90:10 v: v toluene and methyl benzoate. Thereafter, solution was vigorously stirred followed by sonication to form uniform dispersion and complete

Cite this: DOI: 10.1039/c0xx00000x

www.rsc.org/xxxxxx

ARTICLE TYPE

dissolution of polymer and dispersion of nanoparticles. You and co-workers reported both hydrophobic and hydrophilic inks based on upconversion nanoparticles of  $\beta$ -NaYF<sub>4</sub>:Er,Yb.<sup>295</sup> For fabricating hydrophobic ink having optimum viscosity and surface tension; upconversion nanoparticles were added to a solution containing cyclohexane and glycerol trioleate in volume ratio of 90 : 10 to 70 : 30.<sup>295</sup> while for hydrophilic ink; upconversion nanoparticles were added to a solution containing ethanol (10%) and glycerol in volume ratio of 85 : 15 to 65 : 35. Further, to control the surface tension, sodium dodecyl sulfate (SDS) was added to hydrophilic ink at a concentration of 3mgL<sup>-1</sup>.

**3.2.1.3 Dual-mode luminescent nanomaterials based security ink.** In our earlier report, we presented a strategy to fabricate the invisible dual mode security ink using a commercially available PVC gold medium. In typical ink fabrication process; 200 mg of dual mode nanoparticles were dispersed in 50 ml of PVC gold medium and ultra-sonicated at 45 kHz to form good dispersion. Further, the fabricated ink was used successfully for printing different security codes and images by screen printing technique.<sup>12</sup>

**3.2.2 Quantum dots based luminescent security ink.** Lu et al. reported multicolor rewritable fluorescent system using branched polyethyleneimine (BPEI)- CdTe quantum dots.<sup>296</sup> In a typical synthesis, 0.01 mM red emitting QDs, 1% BPEI solution and polydimethylsiloxane (PDMS) masks were used to reversibly write and erase fluorescent patterns on a glass slide. Initially, the slide was immersed in the BPEI solution followed by washing and drying. Then the PDMS mask having a designed pattern was placed on the substrate and exposed to QDs solution for selectively anchoring CdTe nanocrystals via electrostatic force to form a pattern with red emission, which was imaged under a 460 nm irradiation. The fluorescent pattern was easily erased with a drop of BPEI solution to decompose the surface-attached one layer of QDs. After washing and drying, the film is ready for the next writing.<sup>296</sup>

**3.2.3 MOFs based luminescent security ink.** Luz et al. also demonstrated strategy to fabricate the MOFs based luminescent ink for the inkjet printing. In their study, they discussed about the aqueous solution based red, green and NIR-MOF inks.<sup>297</sup> Basically in this process aqueous solution of MOFs was dispersed in color cartridge to print the security codes for anti-counterfeiting applications. In summary, Luz et al. have demonstrated a facile, low-cost, and time efficient strategy for the positioning of photoluminescent Ln-MOFs on flexible substrates (paper and plastic foils). Literature reports suggest that the small volume of ink allows for the quick drying of the ink solvent; furthermore, rapid crystal nucleation permits the production of patterned photoluminescent Ln-MOFs without the multiple "printing drying" cycles.<sup>297</sup>

**3.2.4 Plasmonics nanomaterials based luminescent security ink.** Campos-Cuerva et al. demonstrated the strategy to print metallic nanoparticles as authentication tags on different types of paper using screen printing technique.<sup>298</sup> The metal nanoparticle based ink was fabricated using water based or oil-based varnishes. In order to accomplish this, 80 ml of water based or oil based varnish was added to gold (20 ml gold nanorods 3.7 mg ml<sup>-1</sup>) or silver (20 ml of silver nanoparticles 6.7 mg ml<sup>-1</sup>) suspensions in ether water or acetone. Further, a mesh with specific design was used for screening printing.<sup>298</sup>

#### 4. Various types of printing techniques

The three main techniques of printing objects, patterns and security codes for anti-counterfeiting are briefly described in following sections:

##### 4.1 Screen printing techniques

##### 4.2 Aerosol Jet printing technique

##### 4.3 Inkjet printing techniques

#### 4.1 Screen printing techniques

Screen printing is a printing technique whereby ink is transferred on a substrate using a mesh except in areas made impermeable to the ink by a blocking stencil. A squeegee is moved across the screen to fill the open mesh apertures with ink. A reverse stroke then causes the screen to touch the substrate momentarily along a line of contact. This causes the ink to wet the substrate and be pulled out of the mesh apertures as the screen springs back after the blade has passed. In our earlier publications, we have introduced this strategy to print security codes and images by using the fabricated ink through screen printing technique. The step by step process for screen printing is shown in Fig. 32. Campos-Cuerva et al. demonstrated the strategy to print plasmonic nanoparticles based inks on different types of paper using screen printing, as already discussed in previous section.<sup>298</sup>

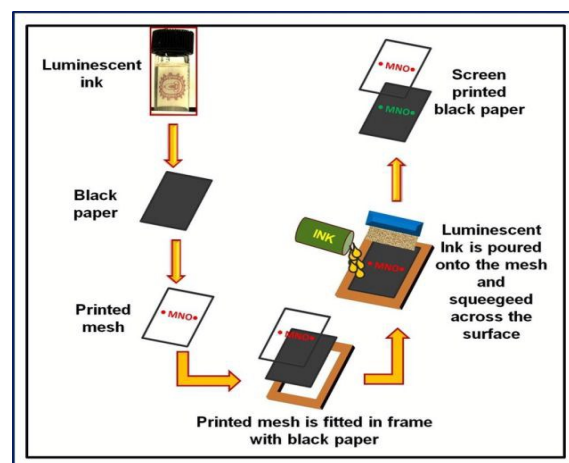


**Fig. 32** Schematic diagram for screen printing process.<sup>12</sup> Reproduced with permission of ref. 12, Copyright 2014, Royal Society of chemistry.

Cite this: DOI: 10.1039/c0xx00000x

www.rsc.org/xxxxxx

## ARTICLE TYPE

**4.2 Aerosol Jet printing techniques**

The aerosol jet printing process employs aerodynamic focusing for the high-resolution deposition of colloidal suspensions and/or chemical precursor solutions. An aerosol stream of the deposition material is focused, deposited and patterned onto a planar or 3D substrate.<sup>299</sup> The basic system consists of two key components:

- (i) A module for atomizing liquid raw materials.
- (ii) The other module for focusing the aerosol and depositing the droplets.

Meruga et al. demonstrated a method for the fabrication of green and blue upconversion nanoparticles based inks and their usability for printing QR codes on paper using aerosol jet

printing.<sup>11h</sup> The protocol for the printing of QR codes employing aerosol Jet printer is demonstrated in Fig. 33. Initially, the QR code was designed using QR code generator and stored in an Auto-CAD file for transferred to the aerosol jet printer. Thereafter, the QR code was printed on paper using aerosol Jet printer. The parameters used for printing were sheath 125 ccm, atomizer 30 ccm, atomizer power 35 V, a nozzle size of 250  $\mu\text{m}$  and deposition speed of 5  $\text{mm s}^{-1}$ . In another study, Meruga et al. followed similar approach for fabrication and printing of red-green-blue upconversion nanoparticles based luminescent inks.<sup>300</sup>

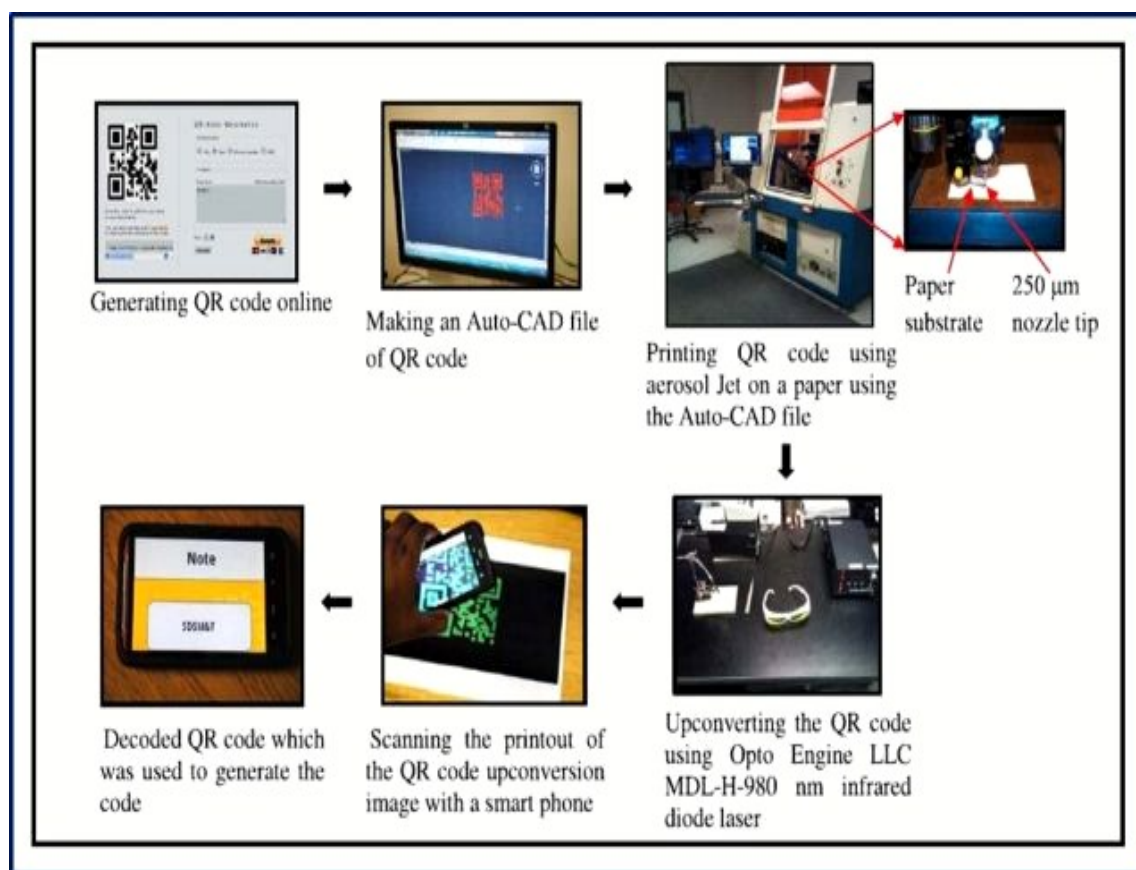


**Fig. 33** Protocol for the printing of QR code using aerosol Jet printer.<sup>11h</sup> Reproduced with permission of ref.11h, Copyright 2012, IOP publishing.

Nanoscale Accepted Manuscript

### 4.3 Inkjet printing techniques

The inkjet printing process involves the ejection of a fixed amount of ink in a chamber, from a nozzle through a sudden, quasi-adiabatic reduction of the chamber volume via piezoelectric action.<sup>301</sup> A chamber filled with liquid is contracted in response to application of an external voltage. This sudden reduction sets up a shockwave in the liquid, which causes a liquid drop to eject from the nozzle. This process has been analyzed at some extent and elaborated in recent review papers.<sup>302,303</sup> The ejected drop falls under action of gravity and air resistance until it impinges on the substrate, spreads under momentum acquired in the motion, and surface tension aided flow along the surface.<sup>304</sup> The drop then dries through solvent evaporation,<sup>305</sup> as shown in Fig. 34. Recent studies<sup>306</sup> show that drop spreading and the final printed shape strongly depend on the viscosity, which in turn is a function of the molar mass of the polymer. More interestingly, the aforementioned group also found a printing height dependence of the final dried-drop diameter, which was a function of the

polymer concentration. The usability of ink jet printers for printing security codes can be credited to its attractive features like.<sup>295</sup>

- (i) The possibility for purely additive operation, in which the corresponding inks are deposited only where they are needed.
- (ii) The flexibility in the choice of structure designs for producing complicated security patterns, where changes can be implemented right away using software-based printer-control systems as shown in Fig.35
- (iii) Its compatibility to use with large-area substrates.
- (iv) The potential for high spatial resolution (depending on the DPI) and mass production.<sup>295</sup>

You et al. introduced a digital and flexible inkjet printing technique for the printing of security patterns with high resolution and high luminescence.<sup>295</sup> The schematic diagram for inkjet printing using upconversion inks is shown in Fig. 35.

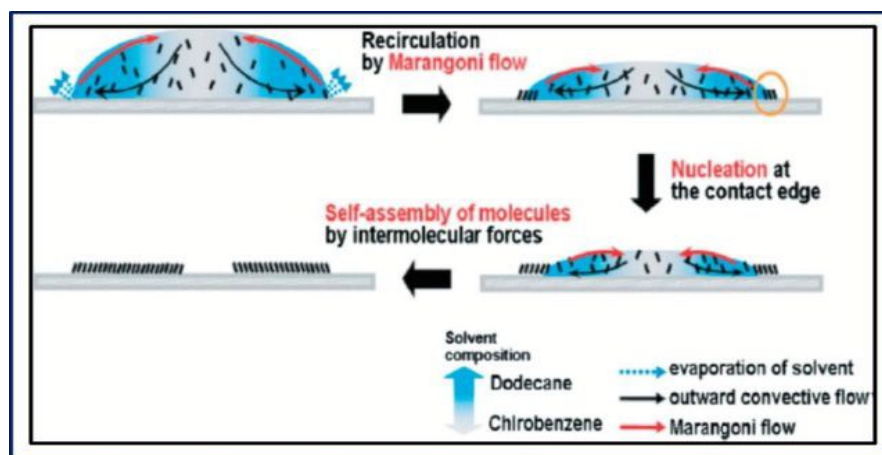


**Fig.34** The process of drop drying after deposition with inkjet printing.<sup>305</sup> Reproduced with permission from 305 Copyright 2008, Wiley.

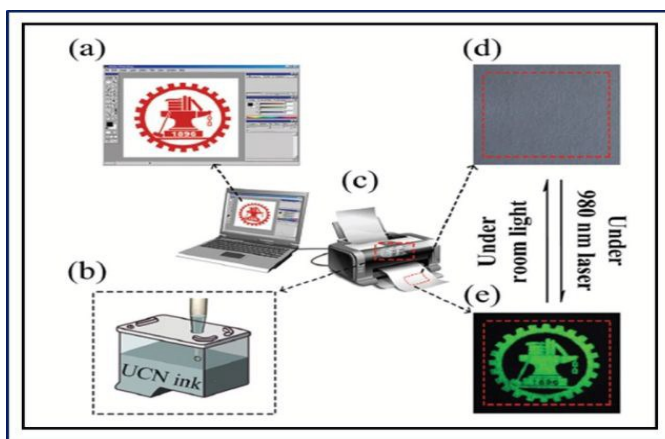


**Fig.35** Schematic diagram of inkjet printing.<sup>295</sup> Reproduced with permission 295, Copyright 2015, Royal Society of chemistry.

**4.3.1 Inkjet properties.** Inkjet printing technique requires the attention pertaining to several important features, which are discussed in details below:

**4.3.1.1 Ink properties.** Ink properties such as dynamic viscosity and surface tension etc. play a vital role for effectiveness of inkjet printing. The flow of liquid drops on the substrate can affect the printing resolution considerably. The spreading of the liquid drops could be measured using the inverse Ohnesorge number,

here,  $\alpha$  is nozzle diameter,  $\gamma$  is surface tension,  $\rho$  is density of ink and  $\eta$  is the dynamic viscosity.<sup>295</sup>

You et al. optimized the inverse Ohnesorge number and hence the surface tension and dynamic viscosity for the effective inkjet printing to achieve uniform and high resolution patterns. The obtained dynamic viscosity and surface tension vary as a function of the ratio between cyclohexane and glycerol trioleate as shown in Fig. 36a & b. A similar result was claimed by them for the aqueous printing ink as shown in Fig. 36c & d.<sup>295</sup>

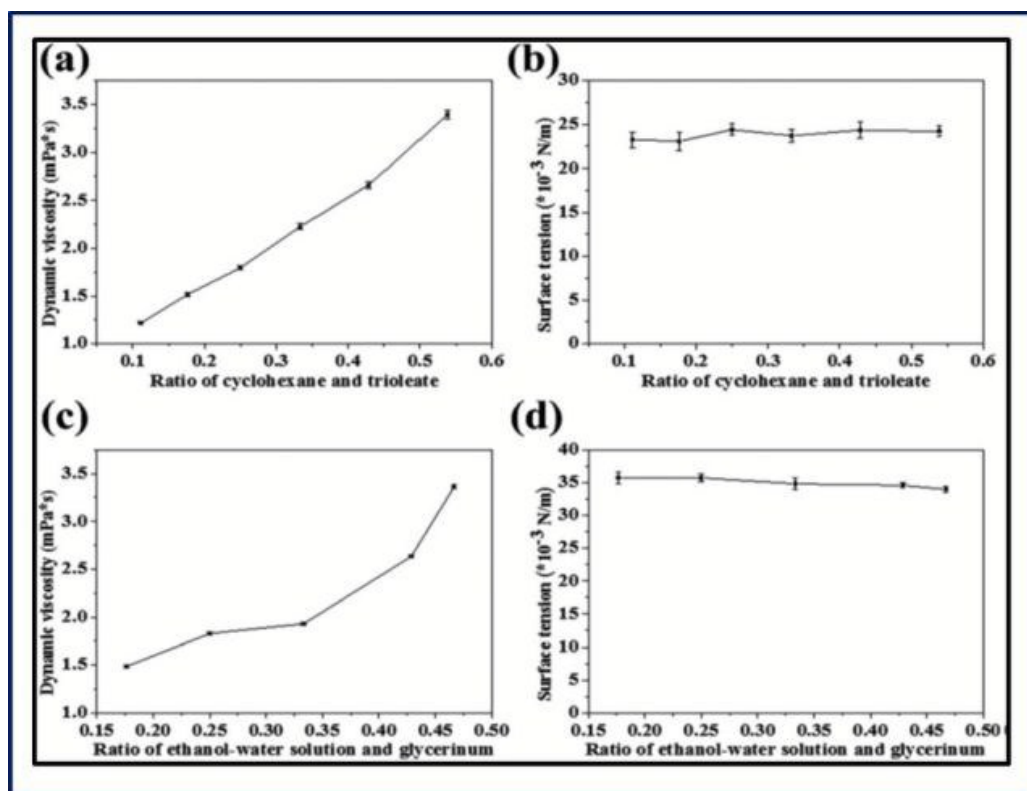
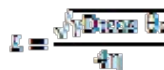


**Fig. 36** Characterization of the UCNP ink with varying ratios of components at  $25 \pm 1$  °C. (a) The dynamic viscosity of solvent based printing ink changes with the v : v cyclohexane : glycerol trioleate ratio. (b) The gas–liquid surface tension of solvent based printing ink changes with the v : v cyclohexane : glycerol trioleate ratio. (c) The dynamic viscosity of aqueous printing ink changes with the v : v ethanol–water solution(10%):glycerol ratio. (d) The gas–liquid surface tension of aqueous printing ink changes with the v : v ethanol–water solution(10%) : glycerol ratio.<sup>295</sup> Reproduced with permission 295, Copyright 2015, Royal Society of chemistry.

**4.3.1.2 Contact angle and spatial resolution.** Another important parameter for the effective inkjet printing with better resolution is the contact angle.<sup>295</sup> When a liquid droplet lands on flat surface, a partial wetting results infinite angle between the liquid and the substrate, known as the contact angle,  $\theta_c$ . This parameter affects the penetration of the ink into substrates which can be described by Washburn's equation:



where  $\gamma$  is the surface tension,  $D$  is the diameter of the capillary tube (capillary porosity between paper fibers),  $\theta_c$  is the contact angle, and  $\eta$  is the dynamic viscosity. The quality of printed patterns is mainly affected by different contact angles formed when ink drops on the substrates. You et al. optimized the contact angle and spatial resolution for both solvent based and aqueous based luminescent security inks. The optimum values of contact angles for solvent based and aqueous based luminescent security inks are  $25.7 \pm 0.8$  degrees and  $32.8 \pm 1.2$  degrees respectively as shown in Fig. 37a & b. The spatial resolution printed using solvent based and aqueous based luminescent security inks was optimized at 100–200  $\mu\text{m}$  and using solvent based ink is 400–500  $\mu\text{m}$  respectively as shown in Fig. 37c & d.<sup>295</sup>

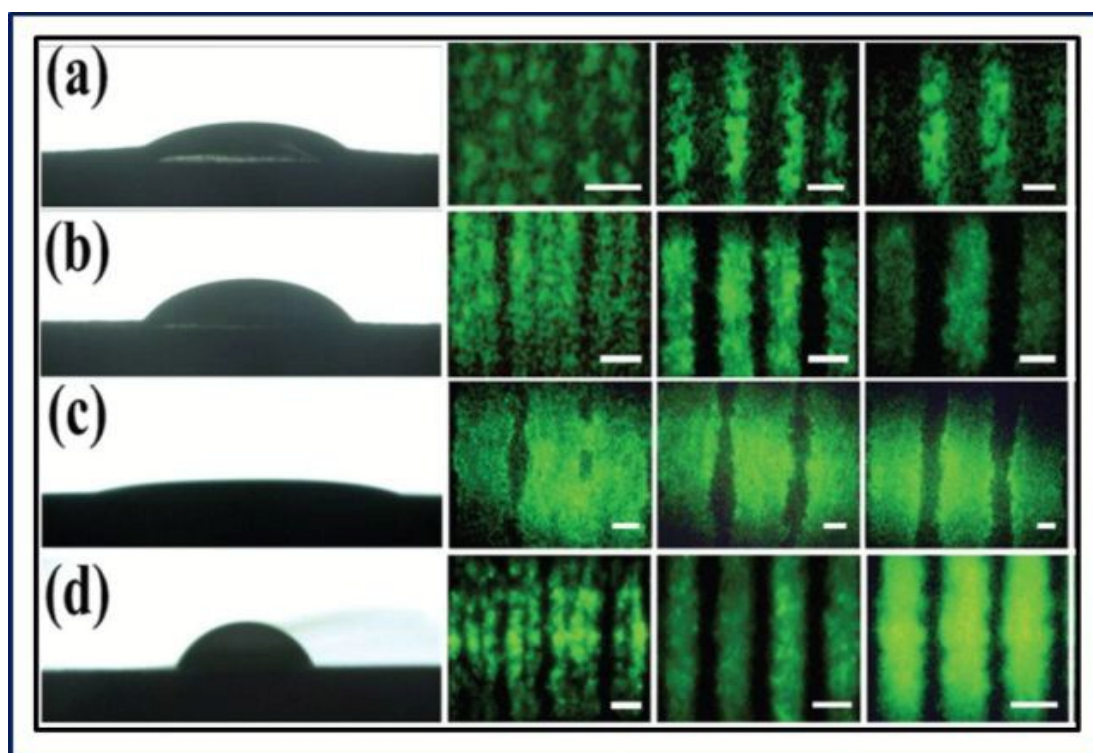


**Fig. 37** Characterization of the spatial resolution of printing a) Droplet morphology of solvent based printing ink on A4 duplicating paper and equal interval and width (from left to right, 100  $\mu\text{m}$ , 200  $\mu\text{m}$ , 300  $\mu\text{m}$ ) lines printed. (b) Droplet morphology of aqueous printing ink on A4 duplicating paper and equal interval and width (from left to right, 100  $\mu\text{m}$ , 200  $\mu\text{m}$ , 300  $\mu\text{m}$ ) lines printed. (c) Droplet morphology of solvent based printing ink on vegetable parchment and equal interval and width (from left to right, 400  $\mu\text{m}$ , 500  $\mu\text{m}$ , 600  $\mu\text{m}$ ) lines printed. (d) Droplet morphology of aqueous printing ink on vegetable parchment and equal interval and width (from left to right, 100  $\mu\text{m}$ , 200  $\mu\text{m}$ , 300  $\mu\text{m}$ ) lines printed. The scale bar of each represents 300  $\mu\text{m}$ .<sup>295</sup> Reproduced with permission 295, Copyright 2015, Royal Society of chemistry.

Cite this: DOI: 10.1039/c0xx00000x

www.rsc.org/xxxxxx

ARTICLE TYPE

**4.3.1.2 Luminescence intensity and uniformity.** Identification of printed patterns depends mainly on the luminescence uniformity which is affected by the size and distribution of droplets ejected by the nozzle. You et al. tested the variance of the luminescence intensity in a ring printing area with different UCNP concentrations varying from 0.3 mg ml<sup>-1</sup> to 7.5 mg ml<sup>-1</sup> under 980 nm excitation with a power density of ~50 mW mm<sup>-2</sup> as shown in Fig. 38a. For each concentration, they randomly tested the luminescence intensity of five points from the printing area. The corresponding luminescence spectrum of UCNPs with different concentrations under 980 nm excitation and the deviation in the luminescence intensity peaking at 538 nm are shown in Fig. 38 b & c.<sup>295</sup>

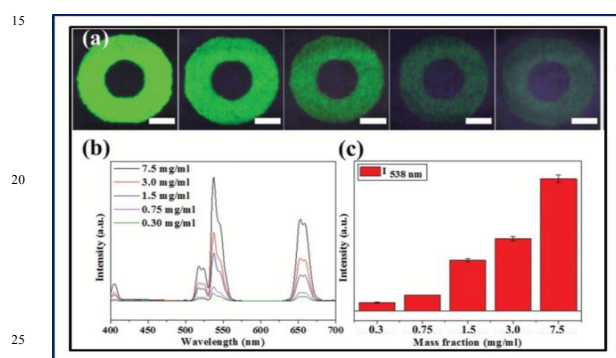


**Fig. 38.** Characterization of luminescence intensity and uniformity. (a) Luminescence changes along with the change of the UCNP concentration (from left to right 7.5 mg ml<sup>-1</sup>, 3.0 mg ml<sup>-1</sup>, 1.5 mg ml<sup>-1</sup>, 0.75 mg ml<sup>-1</sup>, 0.3 mg ml<sup>-1</sup>). Patterns are explored under a 980 nm laser, with a power density of ~50 mW mm<sup>-2</sup>. Figures are obtained using a Nikon D90 camera under f 5.8 (aperture) and 6s (shutter duration) conditions. (b) Luminescence spectrum of different mass fractions of UCNPs. (c) Variance of the luminescence intensity at 538 nm wavelength of ring printing areas with different mass fractions of UCNPs. The scale bar of each represents 2 mm.<sup>295</sup> Reproduced with permission 295, Copyright 2015, Royal Society of chemistry.

## 5. Luminescent materials for anti-counterfeiting applications

After brief discussions on the strategy for fabrication and design of security inks as well as various types of printing techniques, we have explored the details about the different luminescent materials based anti-counterfeiting applications including exploratory studies on other important luminescent inks based on electroluminescence and chemiluminescence in the following sections:

### 5.1 Lanthanide based luminescent security ink for anti-counterfeiting applications

We have described here the different types of lanthanide doped luminescent nanomaterials based security inks, and also discussed in this section about the downconversion based luminescent nanomaterials, upconversion based luminescent nanomaterials and dual mode emissions based luminescent nanomaterials used for the purpose of security ink fabrication.

#### 5.1.1 Downconversion/downshift based luminescent security ink for anti-counterfeiting applications.

Andres et al. reported the red and green emitting downconversion luminescent security inks.<sup>7</sup> These green and red emitting luminescent inks were used to print full colour image on paper by commercially available inkjet printer which is invisible under white light and emit (red, green and blue) RGB colours under UV light that acts as an excitation source. The commercially available blue ink was added in green and red emitting luminescent inks in order to achieve the production of full colour image in visible range. The colour range of the luminescent print was as wide as standard RGB displays. Fig. 39a exhibits the photographs of a set of standard images produced with the luminescent inks on the Canson paper under white light and excite under UV light 254 nm wavelength. We have also reported earlier the strategy for the synthesis and fabrication of the invisible luminescent security ink designed by using ultra-fine red emitting Y<sub>2</sub>O<sub>3</sub>:Eu<sup>3+</sup> nanophosphor (luminescent nanoparticles) for anti-counterfeiting applications.<sup>15</sup> The colloidal solution of ultra-fine nanophosphor was highly stable and emitted strong red colour (emission wavelength ~611 nm) under the excitation of 254 nm UV light. The colloidal solution of Y<sub>2</sub>O<sub>3</sub>:Eu<sup>3+</sup> nanophosphor dispersed in sodium hexametaphosphate under white light and UV light (250 nm) is illustrated in Fig. 39 b. Fig. 39 c demonstrated the bright glow of screen printed letters using colloidal solution of nanophosphor in sodium hexametaphosphate aqueous solution under UV (250 nm). Furthermore, our group recently reported the facile method for the synthesis of highly luminescent and biocompatible europium doped lanthanum orthophosphate (La<sub>0.85</sub>PO<sub>4</sub>Eu<sub>0.15</sub><sup>3+</sup>) nanorods and their applications against counterfeiting.<sup>14</sup> These nanorods emit strong red colour (emission wavelength ~610 nm) upon 394 nm excitation wavelength and form transparent as well as stable solution with commercially available PVC gold medium (hydrophobic in nature), which can be further used for screen printing to print patterns or objects on black paper. In order to explore the feasibility test of fabricated luminescent ink, two kinds of black papers were used which are named as art black paper (smooth and shining in nature) and pastel black paper (rough surface and dull shining in nature) as shown in Fig. 39d & e. These printed patterns on black papers (screen printed CSIR-NPL alphabet and rough pastel black paper

Nanoscale Accepted Manuscript

screen printed VARANASI alphabet) remains invisible in white light and emits red colour upon excitation with 254 nm wavelength of UV light as shown in Fig. 39 d-g. Therefore, these luminescent nanorods can be used in security ink fabrication for anti-counterfeiting applications for the protection of brands and valuable documents such as bank notes, diplomas and certificates.

Further, in another study, Chen et al. suggested that the (Y,Gd)VO<sub>4</sub>:Bi<sup>3+</sup>, Eu<sup>3+</sup> phosphor can be utilized for anti-counterfeiting applications.<sup>307</sup> The emission colour of (Y,Gd)VO<sub>4</sub>:Bi<sup>3+</sup>, Eu<sup>3+</sup> phosphor is sensitive to temperature and excitation wavelength. Additionally, the emission colour can be tailored from green to orange by varying Bi<sup>3+</sup> and Eu<sup>3+</sup> concentrations.

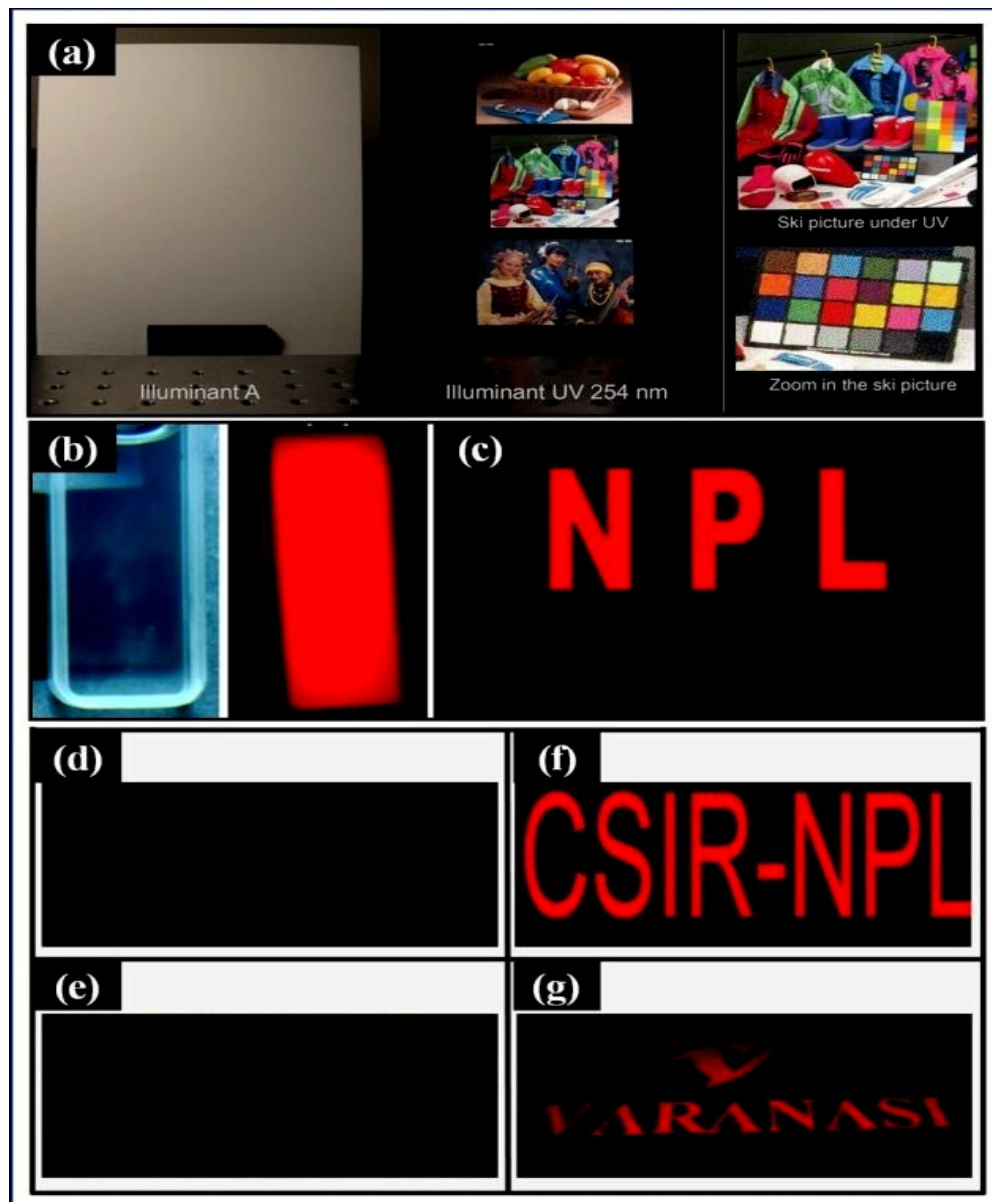


**Fig. 39**(a) exhibits the photographs of a set of standard images reproduced with the luminescent inks on the Canson paper under white light and UV excitation at 254 nm.<sup>7</sup> (b) The colloidal solution of nanophosphor in sodium hexametaphosphate under white light and UV (250 nm), (c) bright glow of screen printed letters under UV (250),<sup>15</sup> (d) & (e) shining art black paper screen printed CSIR-NPL alphabet and rough pastel black paper screen printed VARANASI alphabet in normal light. (f) & (g) the bright red luminescent alphabets upon excitation of 254 nm,<sup>14</sup> (a) Reproduced with permission of ref.7, Copyright 2014, WILEY-VCH Verlag GmbH & Co. (b & c) Reproduced with permission of ref. 15, Copyright 2010, IOP publishing. (d-g) Reproduced with permission of ref. 14, Copyright 2015, American Chemical Society.

**5.1.2 Upconversion based luminescent security ink for anti-counterfeiting applications.** Blumenthal et al. reported a strategy to fabricate a invisible luminescent security ink using upconverting nanophosphors.<sup>294</sup> The upconverting ink solution is composed of upconverting nanophosphor in toluene with oleic acid as capping agent and polymethyl methacrylate (PMMA) as the binding agent along with methyl benzoate. This upconverting ink can be utilized for printing using both direct-write printing and screen-printing techniques. These printed features are invisible in normal light, but it can be easily seen by naked eye when these printed objects are excited under light of 980 nm wavelength. Fig.40 a & b exhibit the images of the printed features under normal light and upon excitation of 980 nm. In another study, Meruga et al. demonstrated that the upconversion nanophosphor can be used for the formulation of security ink in anti-counterfeiting application.<sup>11b</sup> They have printed quick response codes (QR) using green and blue upconverting inks via an aerosol jet direct writing machine. The printed QR code using green upconverting ink is shown in Fig. 40c & d. The QR is invisible in normal light and show bright green colour under NIR excitation of 980 nm. The high level of QR code security was created by printing two different colour inks; green and blue on the substrate. The printed QR code under excitation of 980 nm wavelength is shown in Fig. 40 e. The image clearly reveals the printed upconverting QR code under excitation of 980 nm. In another study, Meruga et al. presented tri-colour QR codes using red, green and blue upconverting inks.<sup>300</sup> The QR codes are printed using an aerosol jet printer. The tri colour printed QR code shows highly resolved multi-colour image of pattern under excitation of 980 nm. Furthermore, they printed red, green and blue inks as isolated and overlapping with each other's to produce red, green, blue, cyan, magenta, yellow and white upconversion luminescence. The printed QR code under normal light and upon excitation of 980 nm is demonstrated in Fig. 40 f. Further, Wang et al. elegantly utilized the lanthanides doped upconversion luminescent nanomaterials for the detection of latent fingerprints which are invisible in normal light and emit green colour when they are excited under 980 nm NIR wavelength of light.<sup>308</sup> They had successfully demonstrated the detection of latent fingerprints on various substrates such as glass, ceramic tiles, floor leathers, marble of different surface textures, metallic materials, polymeric materials, wood materials and various papers. Fig. 40 g-j exhibits the latent fingerprints on the surface of various paper substrates, which were stained by NaYF<sub>4</sub>:Yb,Er upconversion nanoparticles (UCNPs) and then detected by NIR-induced fluorescence imaging upon excitation wavelength of 980nm. Thus, this investigation opens up new avenues for use of lanthanide doped nanomaterials in forensic science for the development or detection of latent fingerprints. Zhang et al. suggested the use of multicolor barcoding in single upconversion crystal.<sup>309</sup> In their study, they synthesized multicolour emitting upconversion microrods by facile hydrothermal methods and demonstrated their anti-counterfeiting applications. Moreover, they also reported the end-on growth of the  $\beta$ -NaYF<sub>4</sub> microrods by using  $\alpha$ -NaYF<sub>4</sub> nanoparticles as precursor material. Fig 40 g shows fluorescent image of the

multicolor emitting microrods under 980 nm excitation wavelength. The multicolor emitting upconversion microrods were found to be well dispersed in dimethyl sulphoxide solvent, which is transparent in white light and shows bright colour upon excitation of 980 nm NIR wavelength. Fig. 40 k demonstrates the magnified luminescent image of a stamped letter S which is printed with inks consist of microrods. The emission spectrum of microrods is shown in Fig. 40 i. Thus, these multi-colour emitting microrods suggest the new opportunity of fluorescent barcodes for anti-counterfeiting applications.

Further, You et al. introduced a strategy for the digital or flexible printing using upconversion nanoparticles based ink for fabrication of security pattern with high resolution and high luminescence intensity for anti-counterfeiting application.<sup>295</sup> In their study, they fabricated both hydrophobic and hydrophilic luminescent security inks using upconversion nanophosphors and used simple inkjet printing to produce anti-counterfeiting pattern. Moreover, the upconversion nanophosphor was combined with downconversion nanophosphor to produced different pattern in same area which can be seen separately upon excitation of different sources. Fluorescent image of multi-colour patterning of green upconversion nanophosphor (NaYF<sub>4</sub>:Yb,Er) and blue down conversion nanophosphor (NaYF<sub>4</sub>:Yb,Tm) are shown in Fig. 40 m and n by direct-writing with a pen on black surface. Hence, the reported technique is quite promising to use against counterfeiting due to its feasibility to produce easily and hard to duplicate.

Sangeetha et al. presented three dimensional (3D) QR codes which was formed using upconversion nanophosphor by atomic force microscopy (AFM) anoxerography.<sup>310</sup> In this study, it was observed that the fabrication of 3D pattern using assembly of NaYF<sub>4</sub> nanocrystals (NCs) depends upon surface potential of the charge patterns, the NC concentration, the polarizability of the NCs and the polarity of the dispersing solvent. The QR code with different thickness and QR code with two colour emitting upconversion nanophosphor was fabricated. The fabricated QR code can be readily imaged using photoluminescence mapping technique. Fig. 40 o & p exhibit the AFM topographical image of QR code fabricated by two different upconverting NCs. Fig.40 q reveal blue emission at 485nm upconversion PL mapping after passing the light through a 500 nm short pass filter. In Fig.40 r, the number "31" hidden with the QR code and it is revealed in green colour emission of 545 nm wavelength, when light passed through a 530 nm long pass filter as well as 650 nm short pass filter. Hence, the atomic force microscopy (AFM) nanoxerography result suggests that it can be ultimate choice for the high end protection against counterfeiting. In another interesting study, Ramos et al. suggested 3D security-ink stamps or fluorescent labels for visual identification of orthodontic adhesives, which exhibits visible luminescence upon infrared light as shown in Fig. 40 s& t.<sup>311</sup>

Another interesting result was reported by Baride et al. where they fabricated NIR to NIR upconversion security inks based on Yb<sup>3+</sup>/Tm<sup>3+</sup> doped  $\beta$ -NaYF<sub>4</sub> nanophosphor. Fig. 41 shows the printed QR codes which are invisible under ambient conditions and NIR luminescent images (800 nm) of QR codes can be easily

captured by CCD camera.<sup>312</sup>

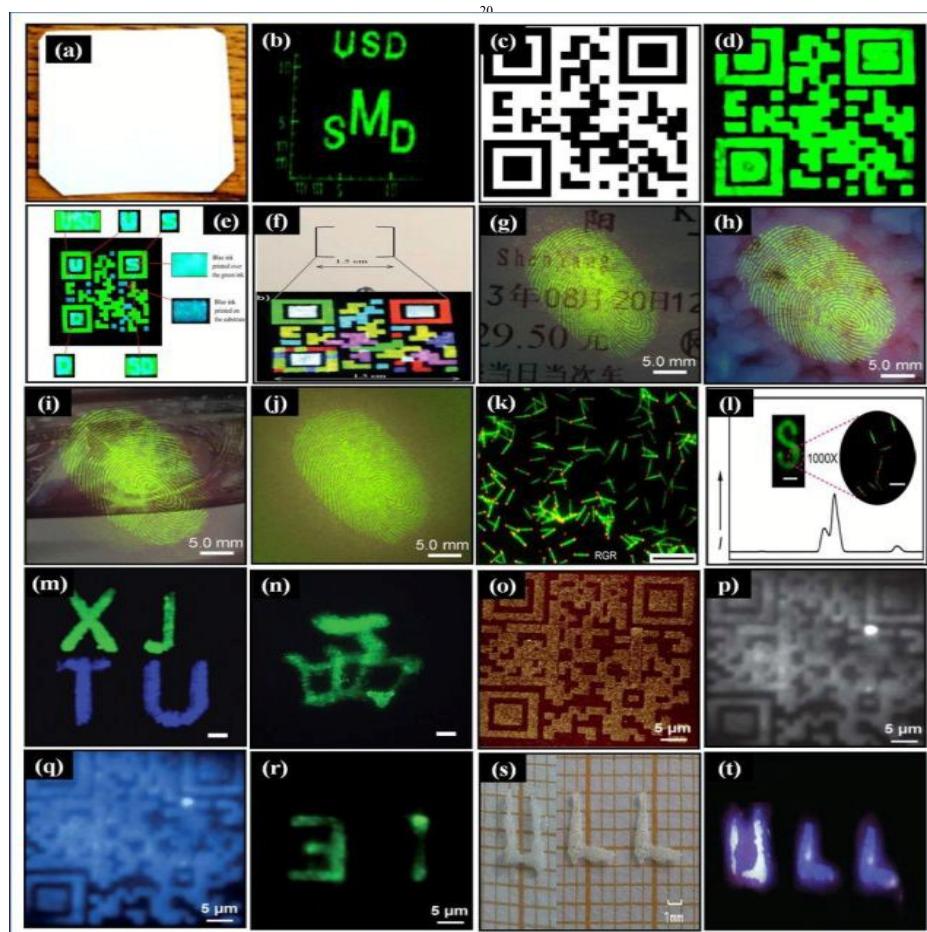


**Fig. 40** (a) & (b) Photographs of printed features in normal light and upon excitation 980 nm wavelength,<sup>294</sup> (c) & (d) the QR code printed on paper in normal light and upon excitation of 980 nm,<sup>11h</sup> (e) Upconverting image of QR code which has the literal text 'USD'; 'U', 'S', and 'D'; and 'SD' inserted in the code image with blue upconverting ink as indicated.<sup>11h</sup> (f) QR code printed using RGB upconverting ink in normal light and upon excitation 980 nm,<sup>300</sup> (g-j) fluorescent images of latent fingerprints on different surfaces (train ticket, printing paper, magazine cover, and note paper),<sup>308</sup> (k) & (l) fluorescent images of dual-mode microrods and letter S written by using dual-mode microrods,<sup>309</sup> (m) & (n) Multicolor patterning of NaYF<sub>4</sub>:Yb,Er (green) and NaYF<sub>4</sub>:Yb,Tm (blue) upconverting inks,<sup>295</sup> (o) AFM topographical image of QR code made of a binary NC assembly consisting of green and blue upconverting NCs, (p) total upconversion photoluminescence mapping of this QR code, (q) blue (485 nm) upconversion PL mapping after passing the light through a 500 nm short pass filter and (r) the number "31" hidden within the QR code is revealed in green (545 nm), only when the PL light is passed through 530 nm long pass and 650 nm short pass filters<sup>310</sup> (s&t) photograph of 3D-printed printed letters ULL in normal light and under infrared light radiation.<sup>311</sup> (a) & (b) Reproduced with permission of ref. 294, Copyright 2012, IOP publishing. (c-e) Reproduced with permission of ref. 11h Copyright 2012, IOP publishing. (f) Reproduced with permission of ref. 300, Copyright 2014, Royal Society of Chemistry. (g-j) Reproduced with permission of ref. 308 Copyright 2015, Springer. (k) & (l) Reproduced with permission of ref. 309 Copyright 2014, American Chemical Society. (m) & (n) Reproduced with permission of ref. 295, Copyright 2015, Royal Society of Chemistry. (o-r) Reproduced with permission of ref. 310 Copyright 2013, Royal Society of Chemistry. (s) & (t) Reproduced with permission of ref. 311, Copyright, 2015 Royal Society of Chemistry.

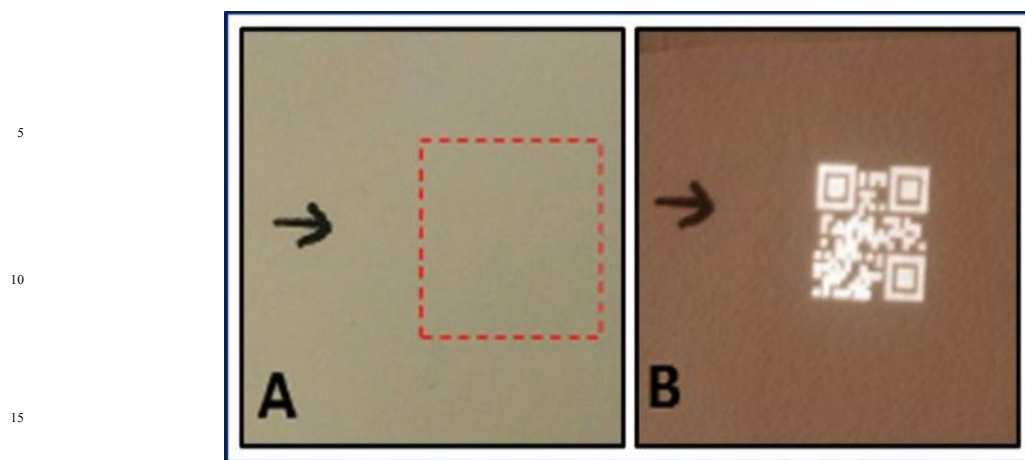


**Fig. 41**(a) & (b) codes printed with NIR-to-NIR upconversion ink under ambient conditions, with a NIR sensitive camera using 980 nm illumination.<sup>312</sup> Reproduced with permission of ref. 312 Copyright 2015, Royal Society of Chemistry.

### 5.1.3 Dual mode luminescent security ink for anti-counterfeiting applications.

Single stage coding capability for either upconversion or downconversion based security inks implies that the developed luminescent ink can be excited by a single wavelength and it subsequently emits only a single wavelength. This coding technique appears comparatively less effective in order to protect the documents. Owing to this reason, a high performance multi-stage coding with many excitations and at least two colour emissions is much awaited for a long time. To develop a phosphor having all the above desirable properties at an economical cost is a great challenge in this area which is being recently addressed in few reports. The development of multi-stage excitable ink provides the multi-stage coding capability in a single host lattice which is not only economical but is also beneficial for high end protection of documents to avoid counterfeiting. Lu et al. reported a strategy to fabricate dual mode security ink based on lanthanide doped nanocrystals. The fabricated ink was used to print anti-counterfeiting stamps.<sup>313</sup> The printed stamps (in Chinese character) exhibit bright green colour upon excitation of 980 nm and blue colour upon excitation of 365 nm as shown in Fig. 42 a. Furthermore, we have reported dual mode lanthanide nanorods for anti-counterfeiting application which are capable of emitting green colour upon excitation wavelengths 379 nm and 980 nm.<sup>12</sup> To fabricate and design dual mode ink using  $Y_2O_3:Er,Yb$  nanorods, we dispersed these nanorods into commercially available PVC gold medium. The ink can be printed on paper by screen printing technique. Fig. 42b exhibits the printed pattern under normal light and different excitation wavelengths (379 nm and 980 nm). The schematic of the proposed application of this dual mode luminescent security ink for currency protection against counterfeiting is shown in Fig. 42c. Thus, this multistage excitable invisible ink opens up new opportunities for the dual mode projection against counterfeiting. In another study, Singh et al. demonstrated a strategy to synthesize a dual mode security ink based on inorganic-organic hybrid nanostructure which produced visible emission both via UC and DC processes.<sup>314</sup> In hybrid structure, the  $Gd_2O_3:Er^{3+}/Yb^{3+}$

nanophosphor (inorganic material) contributes for upconversion process while  $Eu(DBM)_3Phen$  complex (organic materials) contributes for downconversion process. This hybrid material was dispersed in ethanol to form a stable security ink and further used for security code printing. Fig. 42 d-g exhibits ink solutions and the printed pattern in UV and NIR excitation wavelength which can be easily seen by naked eye.

### 5.2 Quantum dots based security ink for anti-counterfeiting applications

Quantum dots (QD) demonstrate the light emission which depends upon their size. Due to their extraordinary photoluminescence behavior, quantum dots can be used for fabricating security inks. Lu et al. reported a rewritable multicolour fluorescent patterns based on QDs.<sup>296</sup> In this rewritable fluorescent system, branched polyethyleneimine (BPEI) acts as both writer and remover. The process of erasing or writing the fluorescent patterns is shown in Fig. 43 a. Thus, this technique has prospective to produce multistate memory chips with highly protected and ultrahigh data storage capacity for broad applications in anti-counterfeiting.<sup>296</sup> In another report, Bao et al. fabricated fluorescent CdS QD-polymer nanocomposite patterns through inkjet printing using cadmium source loaded ink, followed by treating the patterns with hydrogen sulfide gas.<sup>315</sup> Furthermore, CdS QD-polymer composite (PC) with enhanced fluorescence are fabricated by introducing monodispersed poly(styrene-methyl methacrylate-acrylic acid) (poly(St-MMA-AA)) microspheres that serve as the PC building blocks into the inks. The fabricating process is straightforward and flexible, which would find diverse applications in patterning nanocomposites for optoelectronic devices. Fig 43 b demonstrates photograph and fluorescent images of dot-matrix-constructed CdS QD-polymer composite patterns. This CdS QD-polymer composite would have potential use in anti-counterfeiting applications.

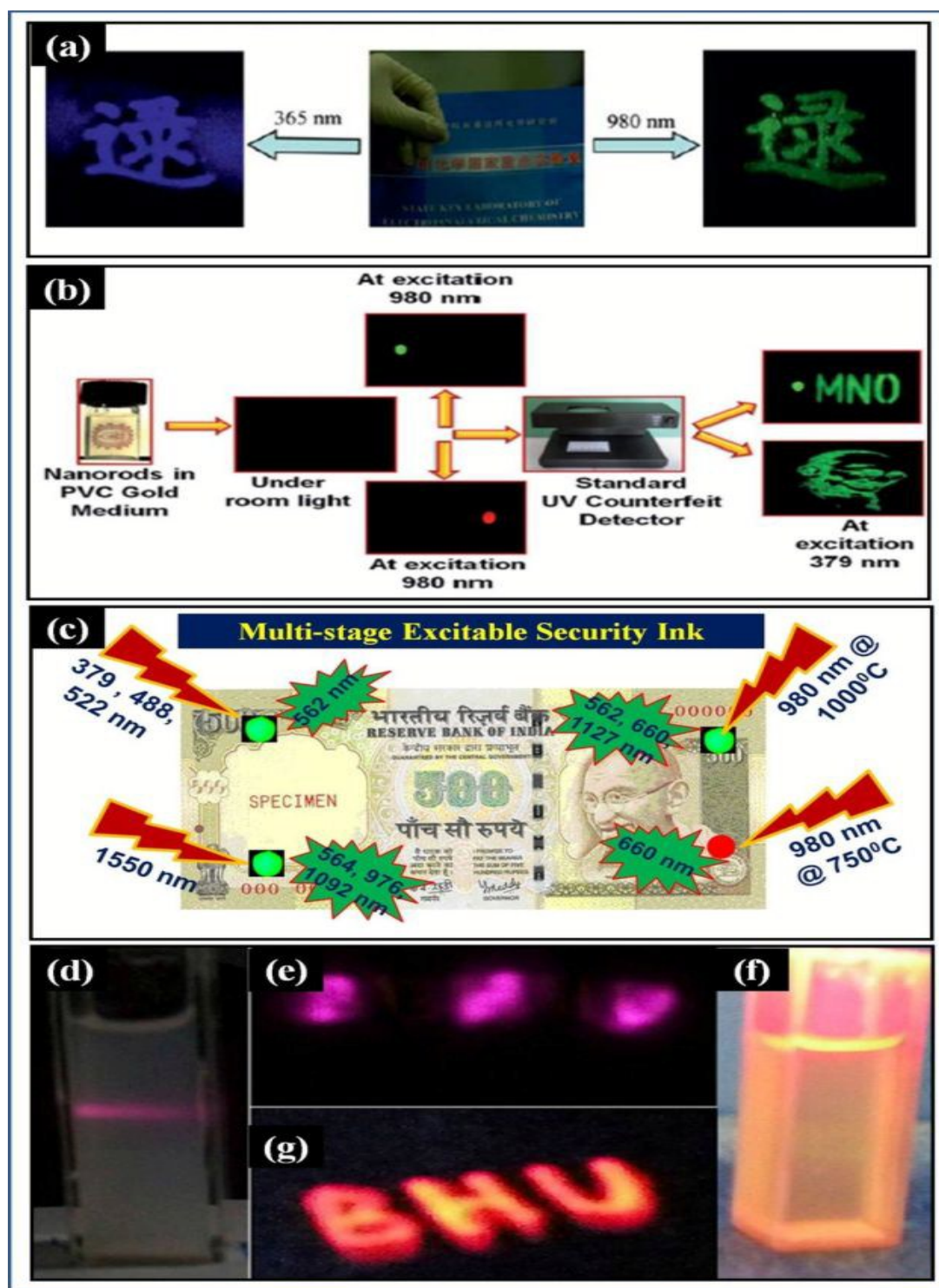


**Fig. 42** (a) Bright field (middle), UC (right) and DC (left) fluorescence images of the character stamped on the transparent film,<sup>313</sup> (b) printed pattern under normal light and under different excitation wavelength (379 nm and 980 nm),<sup>12</sup> (c) the schematic or the proposed application of up converting ink, (d-g) upconverting inks solutions and the printed pattern in UV and NIR excitation wavelength.<sup>314</sup> (a) Reproduced with permission of ref. 313, Copyright 2011, Royal Society of Chemistry. (b) Reproduced with permission of ref. 12 Copyright 2014, Royal Society of Chemistry. (d-g) Reproduced with permission of ref. 314, Copyright 2011, IOP Publishing.

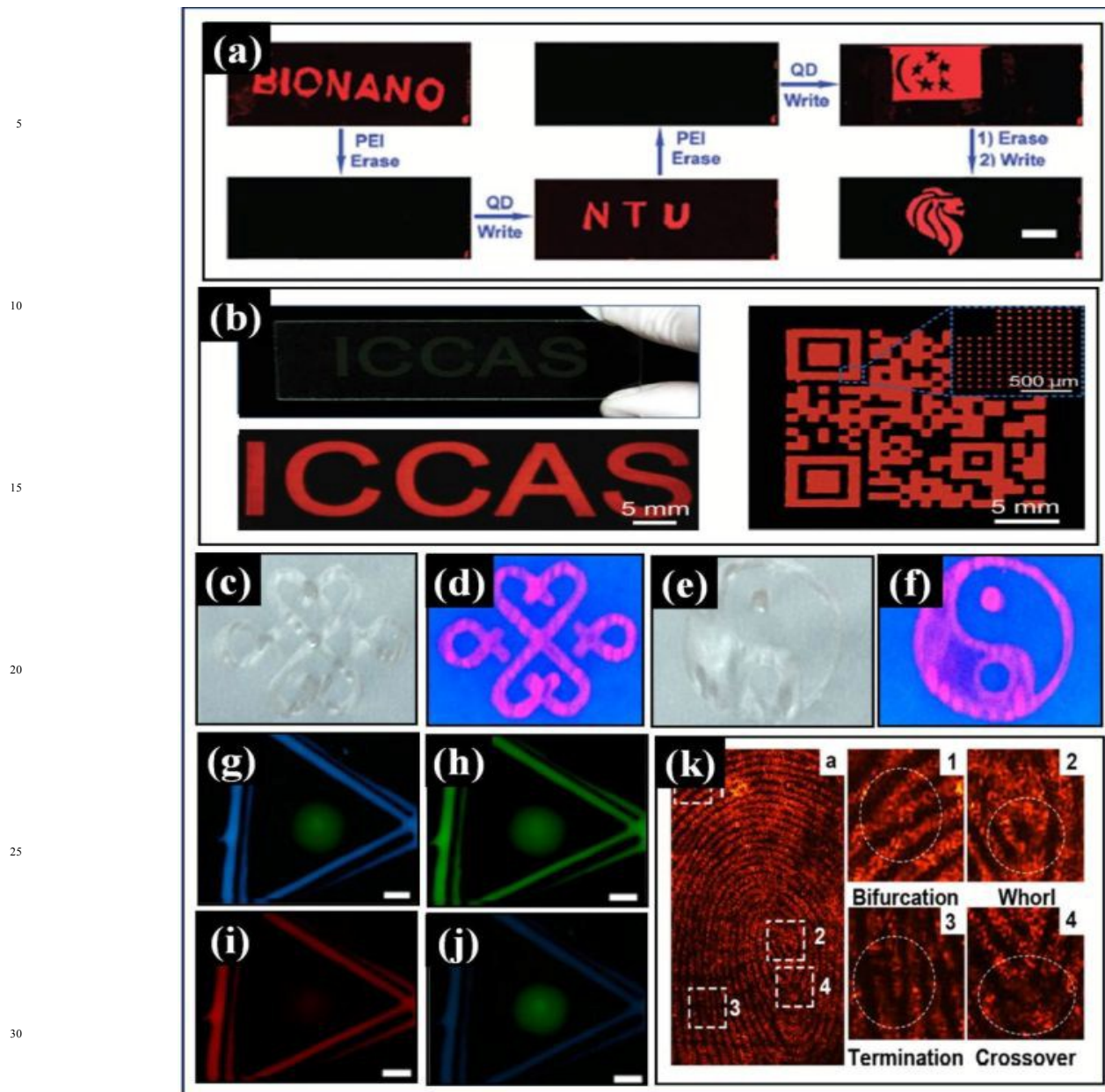


**Fig. 43** (a) Reversible writing and erasing of QD-based fluorescent patterns,<sup>296</sup> (b) photograph and fluorescent image of text pattern as well as fluorescent image 2D code pattern construct by using CdS QD-PC composite,<sup>315</sup> (c-f) anti-counterfeit labels painted with m-SiO<sub>2</sub>/CdTe/Ag NSs ink under visible light and UV light excitation,<sup>316</sup> (g-j) fluorescent images of pattern composite of silica nanodots solution (triangle) or commercially available green ink (circle) under UV light,<sup>317</sup> (k) Photothermal images of LFPs: bifurcation (1), whorl (2), termination (3), and crossover (4).<sup>318</sup> (a) Reproduced with permission of ref. 296, Copyright 2011, Royal Society of Chemistry. (b) Reproduced with permission of ref. 315, Copyright 2015, WILEY-VCH Verlag GmbH & Co. (c-f) Reproduced with permission of ref. 316, Copyright 2015, American Chemical Society. (g-i) Reproduced with permission of ref. 317, Copyright 2015, American Chemical Society. (k) Reproduced with permission of ref. 318, Copyright 2015, American Chemical Society.

In another report Gao et al. reported the fluorescent/ antibacterial multifunctional nanomaterials of m-SiO<sub>2</sub>/CdTe/Ag for anti-counterfeiting applications.<sup>316</sup> In their study, the CdTe QD were implanted into the mesoporous-SiO<sub>2</sub> nanospheres which prevents QDs from agglomeration. Additionally, Ag nanoparticles were introduced to make antibacterial composite ink. The objects painted with composite ink under normal light and UV light are

shown in Fig. 43 c-f. The m-SiO<sub>2</sub>/CdTe/Ag composite inks could offer/open new avenues to develop fluorescent/antibacterial inks for anti-counterfeiting application. Zhou et al. developed a strategy to synthesize water soluble silica QDs by ionic liquid (IL)-assisted solution route and their potential use for anti-counterfeiting applications.<sup>317</sup> The synthesized silica QDs exhibits excitation depended photoluminescence and possesses temperature

sensitive properties. Fig. 43g-j shows the fluorescent microscope images of pattern composed from silicon QDs solutions (triangle) and commercially available green fluorescent ink (circle) under UV light. In another report, Cui et al. introduced an approach for photothermal latent fingerprints (LFP) imaging method based on high photothermal conversion efficiency of  $\text{Cu}_7\text{S}_4$  nanocomposites.<sup>318</sup> In their study, they performed photothermal LFP imaging on different substrates with various background colours. In suggested photothermal imaging approach, not only well-resolved ridge patterns with good separation between furrows and ridges of the LFP is achieved but a detailed information on a fingerprint, including bifurcation, whorl, termination, and crossover, could also be recognized in high-magnification images as shown in Fig. 43 k.<sup>318</sup> Further, Wang et al. fabricated an ink based on the dual mode (down conversion and upconversion) luminescent quantum dot fluid (CDF) direct thermal decomposition method.<sup>319</sup> The ink was stable up to six months at room temperature and can be used for inkjet printing. The photographs of the inkjet printed logo on weighing paper using CDF, under normal, UV and NIR light is shown in Fig. 44a. In another approach, Wen et al. synthesized luminescent inks based on green fluorescent carbon dots (CD) by pyrolysis and microwave treatment using cotton as precursor.<sup>320</sup> The multicolor patterns using CD based ink showing favorable application in anti-counterfeiting are shown in Fig. 44b-c.

Wang et al. reported luminescent security ink based on amphiphilic fluorescent carbon dots (CDs) which were synthesized by rapid plasma-induced method using natural chicken egg as precursor materials.<sup>321</sup> The synthesized CDs were amphiphilic in nature and can be easily dissolved in water and most of the organic solvent. The fluorescent ink based on CDs can be used for both inkjet and silk-screen printing. Fig. 44d-g shows the photographs of fluorescent pattern printed using fluorescent ink based on CDs. In another study, Wang et al. reported luminescent security ink based on carbon quantum dots synthesized by pyrolysis using citric acid as precursor and imidazolium (1-aminopropyl-3-methylimidazolium bromide, [APMIm][Br]) based capping agent.<sup>322</sup> The amphiphilicity of synthesized CQDs was tuned by anion exchange and phase transfer. Further, author demonstrated that these hydrophobic CQD could be utilized for fabrication of fluorescent inks which can be used for writing on various surfaces for anti-counterfeiting application. The photographs of different letters written on various surfaces using CQD fluorescent are shown in Fig 44 h. Gao et al. introduced another strategy for the synthesis of nitrogen-doped carbon dots (N-CDs) via hydrothermal treatment.<sup>323</sup> The supernatant emits hyperfine blue emission under UV light and further can be used as fluorescent ink. Fig. 44 i demonstrates the image of printed object using supernatant as ink under UV light.

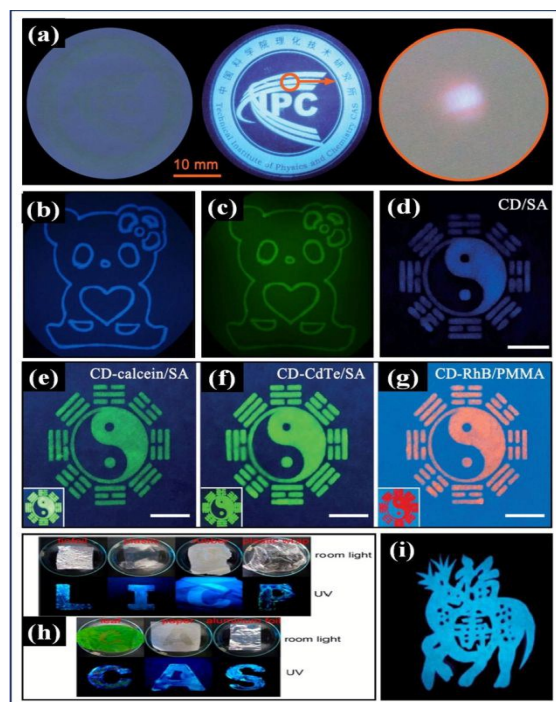


**Fig.44** (a) Photographs of the inkjet-printed logo on weighing paper using CDF under normal, UV and NIR light,<sup>319</sup> (b-c) photographs of the fluorescent patterns under UV light excitation and 470 nm excitation,<sup>320</sup> (d-g) fluorescent image of pattern using CD/SA, CD-calcein/SA, CDCdTe/ SA and CD-RhB/PMMA under UV light,<sup>321</sup> (h) The photographs of different letter written on various surface using CQD fluorescent,<sup>322</sup> (i) fluorescent image of printed object using supernatant as ink under UV light.<sup>323</sup> (a) Reproduced with permission of ref. 319, Copyright 2014, Royal Society of Chemistry. (b-c) Reproduced with permission of ref. 320, Copyright 2015, Elsevier. (d-g) Reproduced with permission of ref. 321, Copyright 2012, Wiley.(h) Reproduced with permission of ref. 322 , Copyright 2015, American Chemical Society. (i) Reproduced with permission of ref. 323, Copyright 2014, Royal Society of Chemistry.

### 5.3 Luminescent MOFs for anti-counterfeiting applications

Metal-organic frameworks (MOFs) are of great interest due to their fascinating properties and potential use in various applications. Recently, metal-organic frameworks (MOFs) have also been used for anti-counterfeiting applications.<sup>324</sup> Luz et al. reported the fabrication of luminescent inks based on Lanthanide-MOFs.<sup>297</sup> The fluorescent MOFs were printed on flexible substrates (paper and plastic foil) using inkjet printer. The author suggested that the MOFs based security inks can potentially be used as invisible security labels or encoding for anti-counterfeiting application. Fig. 45a & b demonstrate the bright red and green emitting patterns deposited by lanthanide MOF inks (R and G-MOFs) on polyethylene terephthalate (PET) substrate under UV light (254 nm). In another report, Li et al. introduced a novel approach to fabricate patterned luminescent

metal-organic-frameworks (LMOF) film by using electrochemically assisted microwave deposition technique.<sup>325</sup>

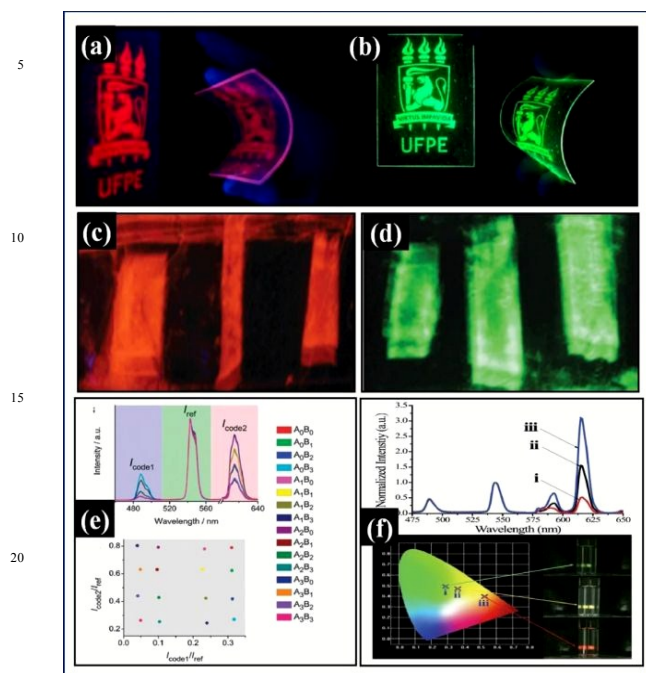


**Fig. 45** (a) & (b) fluorescent image of R and G-MOFs deposited onto transparent PET substrate under UV light (254 nm),<sup>297</sup> (c) & (d) fluorescent images of Eu-MOFs and Tb-MOFs pattern,<sup>325</sup> (e) Emission spectra of Eu<sup>3+</sup>/Tb<sup>3+</sup>@MIL-100 (In) films with various dye (FL and MB) loading combinations and two dimensional matrix of the ratiometric codes,<sup>326</sup> (f) Eu<sup>3+</sup> and Tb<sup>3+</sup> emission spectra recorded under excitation at 330 nm, normalized to the Tb<sup>3+</sup> signal, color-coded of the barcode readout in CIE chromaticity diagram and the photograph of the MOF-253-based barcoded material (dispersed in ethanol) under excitation at 330 nm, (i), (ii) and (iii) is MOF-253–Tb<sub>x</sub>Eu<sub>1-x</sub>, MOF-253–Tb<sub>0.995</sub>Eu<sub>0.005</sub> and MOF-253–Tb<sub>0.99</sub>Eu<sub>0.01</sub>.<sup>265</sup> (a) & (b) Reproduced with permission of ref. 297, Copyright 2015, American Chemical Society. (c) & (d) Reproduced with permission of ref. 325, Copyright 2016, Royal Society of Chemistry. (e) Reproduced with permission of ref. 326 Copyright 2015, Royal Society of Chemistry. (f) Reproduced with permission of ref. 265, Copyright 2014, Royal Society of Chemistry.

The electrochemical deposition technique was used to fabricate patterned lanthanide hydroxide on conducting glass. Further, microwave technique was used to convert patterned lanthanide hydroxide into MOFs. This method could be an ultimate choice to spatially locate MOFs on the surface of substrate. Therefore, these LMOFs might be used for anti-counterfeiting applications. The photograph barcodes based on LMOFs (Eu-MOFs and Tb-MOFs) are shown in Fig. 45c & d. Zhou et al. reported a facial strategy to develop a barcode system based on lanthanide photo-functionalized metal-organic-frameworks (MOFs) film that contains multiple emission bands corresponding to lanthanide ion.<sup>326</sup> The intensity of multiple emission bands can be predicted

and tuned by controlling the filtered dye loading, which gives distinct radiometric optical code. Therefore, this strategy can be used to generate barcodes using lanthanide MOFs and can be potentially used for anti-counterfeiting applications. Fig. 45e demonstrates the emission spectra of Eu<sup>3+</sup>/Tb<sup>3+</sup>@MIL-100 (In) film with various dye loading combinations and two dimensional matrix of radiometric code. Lu et al. reported a new method for luminescent barcode based on nanoscale MOFs (MOF-253).<sup>265</sup> The barcoding was realized by postsynthetic method (PSM) to introduce lanthanide ions (Eu<sup>3+</sup>, Tb<sup>3+</sup> and Sm<sup>3+</sup>). The emission intensity of each of the lanthanide ion is proportional to its amount in the MOFs, resulting in unique luminescent barcodes that depend on the lanthanide ion ratios and compositions. Therefore, luminescent barcodes depend upon the ratio of lanthanide ions used and their composition. The emission spectra of MOF-253–Tb<sub>x</sub>Eu<sub>1-x</sub> displays the characteristic transition of Eu<sup>3+</sup> ion and Tb<sup>3+</sup> ion upon excitation 330 nm as shown in Fig. 45f. Fig. 45 f also demonstrates the colour-coding of the barcode readout in CIE chromaticity diagram and the photograph of the MOF-253-based barcoded material dispersed in ethanol under excitation of 330 nm.

#### 5.4 Plasmonic nanomaterials for anti-counterfeiting applications

The plasmonic nanomaterials have a great prospective as the next generation security labels/ codes for anti-counterfeiting applications. However, there are limited reports published on the application of plasmonic nanomaterials for anti-counterfeiting applications. Zhang et al. prepared luminescent inks using glutathione-capped gold nanoclusters (GS–AuNCs), synthesized by solution-based microwave method.<sup>327</sup> The emission colour of GS–AuNCs was tuned by controlling the reaction time. The photoluminescence emission of GS–AuNCs was blue shifted when the reaction time is increased. Fig. 46a-c shows the photographs of filter paper with words, written using GS–AuNCs based luminescent inks in normal light and UV light (365 nm). Campos-Cuerva et al. reported another approach for combination of both optical and magnetic materials for the anti-counterfeiting applications.<sup>298</sup> In their study, they chose single phase spherical nanoparticles (Ag, Au and magnetite) and printed them on different papers by screen printing technique. The combinations of optical and magnetic materials provide both optical and magnetic signals from same spot that can be detected independently. The major advantage of these printed codes is that printed signals remain stable under accelerating conditions, thereby, providing a strategy for high multi-stage security inks for anti-counterfeiting applications. Fig. 46 d shows the word ‘NANOTECHNOLOGY’ in which the letters ‘NA’ have been screen printed with Ag nanoparticles, the letters ‘CH’ with gold nanorods, the letters ‘GY’ with commercial green ink, the first letters ‘NO’ have two overlapping layers, the first printed with magnetic nanoparticles and on top of it the same printing with Ag nanoparticles; the second letters ‘NO’ also contains two overlapping layers, the one underneath printed with magnetic nanoparticles and one on top printed with gold nanorods.<sup>298</sup>

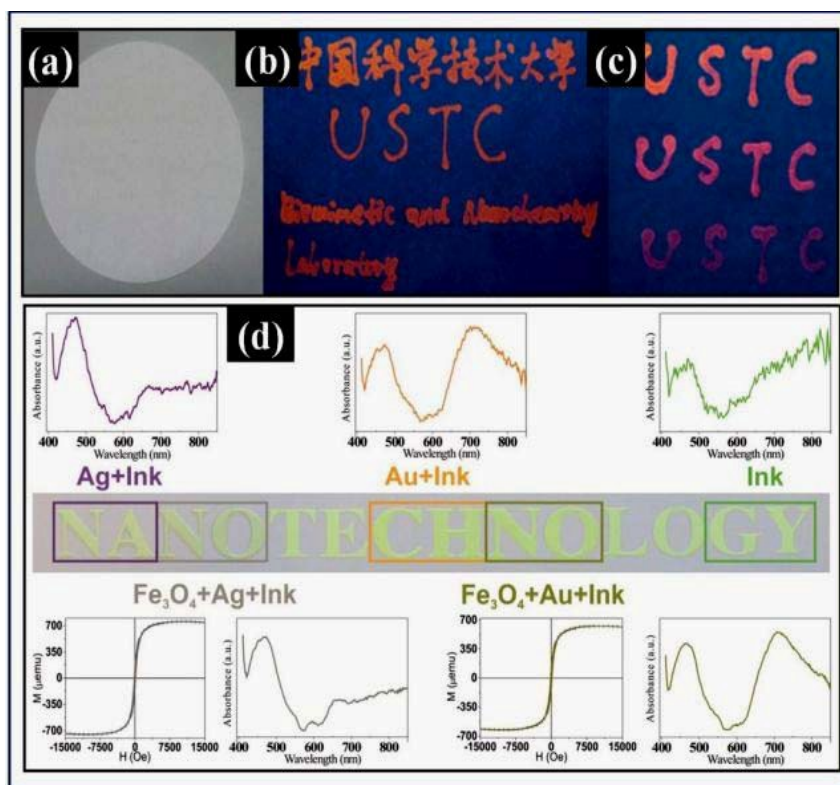


**Fig. 46** Photos of an ordinary piece of filter paper with invisible words written by using the AuNCs-3h ink (a) under room light and (b, c) under UV light (365 nm),<sup>327</sup> (d) photograph of printed letter Nanotechnology using (Ag+ink), (Au+ink), and ink,<sup>298</sup> (a-c) Reproduced with permission of ref. 327, Copyright 2015, Royal Society of Chemistry. (d) Reproduced with permission of ref. 298, Copyright 2016, IOP publishing.

### 5.5 Other anti-counterfeiting applications based on electroluminescence and chemiluminescence based security ink

Recently, electroluminescence and chemiluminescence based security inks have gained immense interest because of their use in the field of security applications. Huebner et al. reported the electroluminescent colloidal inks for flexographic roll-to-roll printing.<sup>328</sup> A wide range of colour was produced by mixing red, green and blue emitting nanoparticles in different ratios. The light emitting diodes (LEDs) were fabricated using these electroluminescent colloidal inks. Optical images of colloidal based organic light emitting devices templated into a 12.7 mm wide tiger paw insignia with varying RGB dye ratios and the corresponding electroluminescence spectra is shown in Fig 47.<sup>328</sup> Xu at al. reported another approach for the detection of protein/polypeptide residues in latent fingermarks by electrochemiluminescence.<sup>329</sup> Electrochemiluminescence (ECL) is a form of chemiluminescence where light emission is due to the electro chemical reaction. In electrochemiluminescence, the light emitting species are formed near the electrode surface which offers approach for imaging electrochemical or biosensing events. The important advantage of ECL imaging is that it does not involve any sophisticated instruments and is not equipped with explosive items. Fig. 48a shows the ECL image of a hIgG groomed fingermark treated by the single-HRP route and its

magnified images showing secondary level details are shown in Fig 48 b. The image was obtained at an applied potential of -0.7 V in a 0.1 M Tris-HCl buffer solution (pH 8.5, sodium salts) containing 0.5 mM luminol and 0.23 mM p-iodophenol. Xu at al. reported a strategy for the visualization and detection of latent fingermarks on the metal surfaces via electrochemiluminescence.<sup>330</sup> In their study, they produced a negative image of fingerprint using electrochemiluminescence. The ECL images of fingermarks on different surfaces are shown in Fig. 48c-f. In another study, Xu et al. presented two methods to visualize the latent fingermarks on the basis of spatially controlled ECL.<sup>331</sup> In one method (negative mode), the negative image of fingermarks were produced by directly exposing the electrode bearing fingermarks to solution of tris(2,2'-bipyridyl) ruthenium(II) ([Ru(bpy)<sub>3</sub>]<sup>2+</sup>) and tri-n-propylamine (TPrA). While in the other method (positive mode), electrode bearing fingerprint ridge deposit was tagged with ECL-generating luminophores. The immobilized luminophores can then react with freely diffusing co-reactants to generate ECL. There are many reports on the visualization of latent fingermarks using electrochemiluminescence.<sup>332-333</sup>

Further, summary of the luminescent nanomaterials used for the fabrication and design of luminescent security inks, method of their synthesis and different techniques employed for printing security codes is shown in Table 4.

Cite this: DOI: 10.1039/c0xx00000x

www.rsc.org/xxxxxx

ARTICLE TYPE

5

15

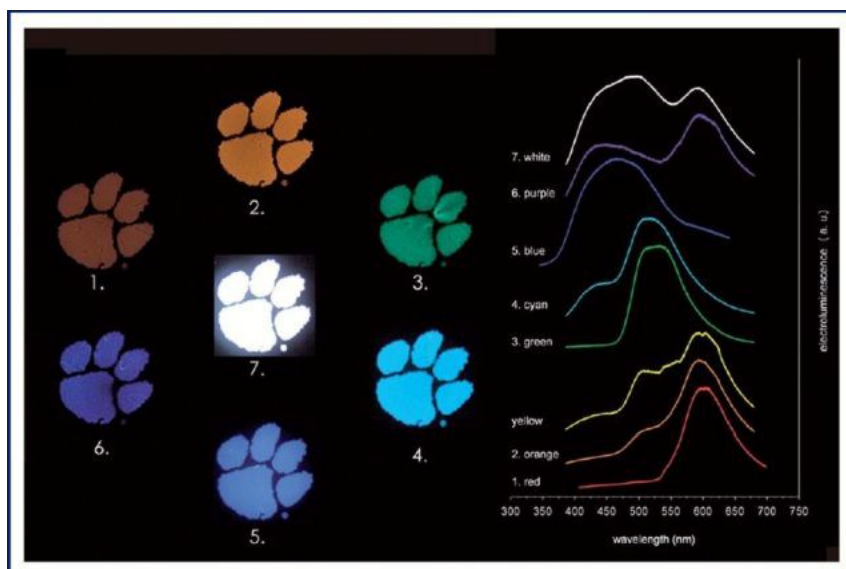


**Fig. 47** The optical images of colloidal based organic LED templated into a tiger paw insignia with varying RGB dye ratio and 20 corresponding spectra.<sup>328</sup> Reproduced with permission of ref. 328, Copyright 2008, Royal Society of Chemistry.

25

30

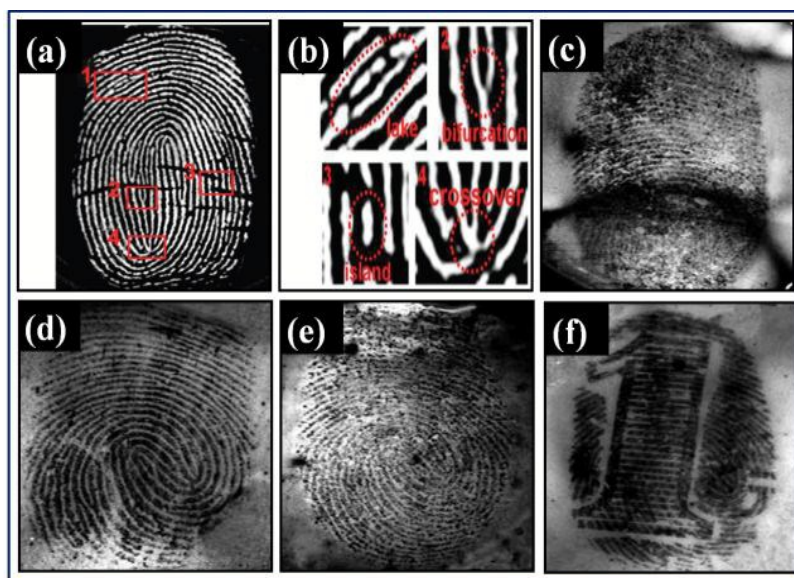


**Fig. 48** (a) ECL image of an hIgG groomed fingerprint treated by the single-HRP route. (b) Magnified images showing secondary level details including lake (1), bifurcation (2), island (3), and crossover (4), as indicated by the red rectangles in (a),<sup>329</sup> ECL images of the sebaceous fingerprints collected from different object surfaces: (c) computer screen, (d) optical disk, (e) laboratory cabinet, (f) coin.<sup>330</sup> (a) & (b) Reproduced with permission of ref. 329, Copyright 2014, Royal Society of Chemistry. (c-f) Reproduced with permission of ref. 330, Copyright 2013, Royal Society of Chemistry.

Cite this: DOI: 10.1039/c0xx00000x

www.rsc.org/xxxxxx

ARTICLE TYPE

Luminescent nanomaterials	Synthesis methods	Printing Techniques	Refs.
<i>Lanthanide based nanomaterials</i>			
LaPO:Eu	Hydrothermal	Screening printing	14
Y <sub>2</sub> O <sub>3</sub> :Eu	Sol-gel	---	15
NaYF <sub>4</sub> :Er/Yb	High-temperature coprecipitation	Direct-writing and screen printing	294
NaYF <sub>4</sub> :Er/Yb and NaYF <sub>4</sub> :Tm/Yb	High-temperature coprecipitation	Aerosol jet printing	11h
sNaYF <sub>4</sub> :Er/Yb	Hydrothermal	---	308
NaYF <sub>4</sub> :Er/Yb	Hydrothermal	---	309
β-NaYF <sub>4</sub> :Er/Yb	Thermal decomposition	Inkjet printing	295
NaYF <sub>4</sub> :Er/Yb	--	AFM nanoxergraphy	310
<i>Quantum dots</i>			
CdTe	Wet- chemical	Mask based printing	296
CdS	Wet- chemical	Inkjet printing	315
CdTe	Wet- chemical	---	316
Silica nanodots	Wet- chemical	Stamp Printing or latent fingerprints	317
Cu <sub>7</sub> S <sub>4</sub>	Wet- chemical	Latent Fingerprints	318
Carbon Quantum Dots (CQD)	Thermal decomposition	Inkjet printing	319
Carbon nanodots	Pyrolysis and microwave treatment	Simple writing by pen	320
Carbon dots	Rapid plasma-induced method	Inkjet printing	257
Carbon Quantum Dots (CQD)	Pyrolysis	---	322
<i>MOFs</i>			
Ln-MOFs (Ln= Eu <sup>3+</sup> , Tb <sup>3+</sup> , Gd <sup>3+</sup> and Eu <sup>3+</sup> )	Chemical method	Inkjet printing	297
Eu-MOF and Tb-MOF	Electrochemically-assisted microwave	Electrochemical deposition	325
MOF-253-Ln	-----	barcode	265
<i>Plasmonic nanomaterials</i>			
Gold nanostructure	Microwave method	Writing with pen	327
Gold and silver nanoparticles	Chemical method	Screen printing	298

**Table 4** Summary of the different types of luminescent nanomaterials, synthesis methods and printing techniques.

## 6. Conclusions: prospects, challenges and new directions

The widespread act of counterfeiting in all kinds of important documents including currency has become a real threat to society. This review article brings to a close view the recent trends adopted for anti-counterfeiting applications which are urgently required for scientific communities, industries, government offices and consumers to protect their important documents. This review article begins with historical background of luminescent nanomaterials, basic concepts of luminescence mechanism, their classification and then covers in detail the entire process right from the development of desired luminescent nanomaterials, ink designing and fabrication, various types of printing techniques for security codes and in the end explores the anti-counterfeiting applications. In this review, we have explored the modern strategies adopted for the synthesis of lanthanide doped luminescent nanomaterials (downconversion, upconversion and dual mode) luminescent quantum dots (semiconductor and carbon dots), luminescent metal organic frameworks and plasmonic nanostructures, their surface morphologies and

structural/microstructural characterizations. Further, we have described the choice of luminescent nanomaterials used for the formulation of different types of security inks and their properties. Moreover, we have discussed in details about the ink fabrications and designing based on lanthanide doped luminescent nanomaterials, luminescent quantum dots, luminescent metal organic frameworks and plasmonic nanomaterials. After that, we described in details about the three popular printing techniques which are; screen printing, aerosol jet printing and inkjet printing used for the printing of security codes and images. Using these fabricated security inks reported by us and other groups, we have clearly demonstrated their use in anti-counterfeiting applications by printing the security codes/bars, fingerprints and images on different surfaces and their clear detections. Additionally, we have also made some exploratory studies related to other important luminescent inks based on electroluminescence and chemiluminescence for anti-counterfeiting applications. The major outcome of this review

provides a series of solutions related to use and choice of various kinds of luminescent nanomaterials, their use in ink fabrication for high end security printing for protection against the counterfeiting of documents, banknotes, medicine and branded items etc.

Although huge progress has been made in the development of security ink based on different types of luminescent nanomaterials for anti-counterfeiting applications till date, numerous challenges and issue still remain to be resolved and there is still a long way to go to substantiate their practical application. In terms of synthesis of different types of luminescent nanomaterials and designing of ink formulation, novel synthetic methods still need to be explored to improve the short coming of the current methods. The limitations with these luminescent nanomaterials used presently are manifold. In general they are expensive, or have limited availability, higher photobleaching effect and low yield of synthesis. The major challenge in the present scenario is the full exploitation of these luminescent nanomaterials which are free of these constraints. Another important challenge in this area is to develop a medium for fabrication of luminescent ink having a higher lifetime, desired viscosity, less expensive and having ease of dispersion of luminescent material into the medium with good colloidal stability. In a nutshell, contents of the review are highly useful in current scenario due its wide coverage from the synthesis of different kinds of luminescent nanomaterials based inks to anti-counterfeiting applications.

The discussions in this review take up in details the different kinds of luminescent nanomaterials, ink fabrications and various kinds of printings techniques for security codes for anti-counterfeiting applications and they will reignite researchers and serve as stepping stone to carry out further research in this field to develop a luminescent security ink with desired properties for establishing a strong anti-counterfeiting technology.

## Acknowledgements

The authors wish to thank Dr. D. K. Aswal, Director CSIR-N.P.L., New Delhi, for his keen interest in this review article. The authors are thankful to Prof. O. N. Srivastava (Banaras Hindu University, Varanasi) and Mr. H. K. Maini (former Scientist, CSIR-NPL, New Delhi), for his encouragement. Mr. P. Kumar and Mr. S. Singh gratefully acknowledge the financial support from University Grant Commission (UGC), Government of India. The authors are grateful to the CSIR-TAPSUN program of India.

## Notes and references

<sup>a</sup> Academy of Scientific and Innovative Research (AcSIR), CSIR-National Physical Laboratory Campus, Dr K S Krishnan Road, New Delhi 110012, India

<sup>b</sup> Luminescent Materials and Devices Group, Materials Physics and Engineering Division, CSIR - National Physical Laboratory, Dr K S Krishnan Road, New Delhi, 110012, India

\* Corresponding author. Tel.: +91-11-45608284, Fax: +91-11-45609310

\*E-mail: [bipinbhu@yahoo.com](mailto:bipinbhu@yahoo.com) (B.K.G.)

1. C. Zhang and J. Lin, *Chem. Soc. Rev.*, 2012, **41**, 7938-7961.
2. C. Feldmann, T. Justel, C.R. Ronda and P.J. Schmidt, *Adv. Funct. Mater.*, 2003, **13**, 511-516.
3. G. Blasse and B.C. Grabmaier, *Luminescent Materials*, Verlag, Berlin, 1994.
4. Y. Liu, D. Tu, H. Zhu, R. Li, W. Luo and X.Y. Chen, *Adv. Mater.*, 2011, **22**, 3266-3271
5. E. L. Prime and D. H. Solomon, *Angew. Chem. Int. Ed.*, 2010, **49**, 3726-3736.
6. OECD, The Economic Impact of Counterfeiting and Piracy, OECD, Publishing, Paris, Paris, **2008**.
7. J. Andres , R. D. Hersch , J. E. Moser and A. S. Chauvin, *Adv. Funct. Mater.*, 2014, **24**, 5029-5036.
8. R. L. Van Renesse , Optical Document Security , Artech House , Boston 2004 .
9. Halftoning converts continuous tone levels to ink dot surface coverages. When the size of the halftone dots is small, the halftone is perceived by a human viewer as a continuous tone. For more information, see C. Hains, S.-G. Wang, K. Knox, in *Digital Colour Imaging Handbook* (Ed: G. Sharma), CRC Press , Boca Raton 2003 , pp. 385 – 490 .
10. a) R. D. Hersch , P. Donze and S. Chosson , *Acm. T. Graphic*, 2007 , article 75, b) W. J. Coyle and J. C. Smith , Angstrom Technologies, Inc., US Patent 7821675, 2010.
11. a) J. D. Auslander , W. Berson and Pitney Bowes, US Patent 5542971, 1996, b) B. A. Lent , G. G. Deng and J. F. Ezpeleta , The General Electric Company, Plc, WO 1997, 97/10307, c) V. Aboutanos , T. Tiller , C. Reinhard and S. Rascagnères , SICPA Holding SA, US Patent, 2010, **8**, 685,276, d) G. A. Ross , P. Pollard , C. Hunter , S. Officer and G. R. Prabhu , NRC Corporation, US Patent, 2004, **7**, **129**, 506, e) S. Officer , G. R. Prabhu , P. Pollard , C. Hunter and G. Ross , Proc. SPIE-IS&T Electronic Imaging 2004 , **5310** , 387-395, f) G. Kaur , Y. Dwivedi , A. Rai and S. B. Rai , *Spectrochim. Acta A: Mol. Biomol. Spectr.*, 2012 , **95** , 511 – 516, g) Y. Liu , K. Ai and L. Lu , *Nanoscale*, 2011, **3**, 4804 – 4810, h) J. M. Meruga , W. M. Cross , P. S. May , Q. Luu , G. A. Crawford and J. J. Kellar , *Nanotech.* 2012, **23** , 395201 .
12. P. Kumar, J. Dwivedi and B. K. Gupta, *J. Mater. Chem. C*, 2014, **2**, 10468-10475
13. B. L. Volodin, B. Kippelen, K. Meerholz, B. Javidi and N. Peyghambarian, *Nature*, 1996, **83**, 58-60.
14. M. Saraf, P. Kumar, G. Kedawat, J. Dwivedi, S. A. Vithayathil, N. Jaiswal, B. A. Kaiparettu, and B. K. Gupta, *Inorg. Chem.* 2015, **54**, 2616-2625.
15. B. K. Gupta, D. Haranath, S. Saini, V. N. Singh and V. Shanker, *Nanotechnology*, 2010, **21**, 055607.
16. S. Armstrong, O. Graydon, D. Pile and R. Won, *Nat. Photonics*, 2012, **6**, 801.
17. W. J. Kim, M. Nyk and P. N. Prasad, *Nanotechnology*, 2009, **20**, 185301.
18. J. M. Meruga, W. M. Cross, P. S. May, Q. Luu, G. A. Crawford and J. J. Kellar, *Nanotechnology*, 2012, **23**, 395201.

Cite this: DOI: 10.1039/c0xx00000x

www.rsc.org/xxxxxx

## ARTICLE TYPE

19. B. Valeur and M. N. Berberan-Santos, *J. Chem. Educ.* 2011, **88**, 731–738.
20. S. Shionoya, W. M. Yen and H. Yamamoto, *Phosphor Handbook*, CRC Press, 2006.
21. W. E. Safford, *Ann. Rep. Smithsonian Inst.* 1915, 271–298.
22. J. R. Partington, *Ann. Sci.* 1955, **11**, 1–26.
23. M. J. Muyskens, *Chem. Educ.* 2006, **83**, 765–768.
24. A. U. Acuna and F. Amat-Guerri, Early History of Solution Fluorescence: The Lignum nephriticum of Nicolas Monardes. In *Fluorescence of Supermolecules, Polymers and Nanosystems*; Springer Series on Fluorescence, Vol. 4; Berberan-Santos, M. N., Ed.; Springer Verlag: Berlin, 2008; 3–20.
25. A. U. Acuna, *J. Chem. Educ.* 2007, **84**, 231.
26. A. U. Acuna, F. Amat-Guerri, P. Morcillo, M. Liras and B. Rodriguez, *Org. Lett.* 2009, **11**, 3020–3023.
27. E. N. Harvey, A History of Luminescence from the Earliest Times until 1900; The American Philosophical Society: Philadelphia, PA, 1957.
28. G. G. Stokes, *Philos. Trans.* 1852, **142**, 463–562.
29. S. E. Braslavsky, Glossary of Terms used in Photochemistry, 3rd edition (IUPAC recommendations 2006), *Pure Appl. Chem.* 2007, **79**, 293–465.
30. F. Perrin, *Ann. Phys. (Paris, Fr.)* 1929, **12**, 169–275.
31. Y. Liu, D. Tu, H. Zhu and X. Chen, *Chem Soc Rev*, 2013, **42**, 6924–6958.
32. J. C. G. Bünzli and S. V. Eliseeva, *J. Rare Earths*, 2010, **28**, 824–842.
33. B. M. van der Ende, L. Aarts and A. Meijerink, *Phys. Chem. Chem. Phys.*, 2009, **11**, 11081–95.
34. S. Gai, C. Li, P. Yang and J. Lin, *Chem. Rev.* 2014, **114**, 2343–2389.
35. X. Huang, S. Han, W. Huang and X. Liu, *Chem. Soc. Rev.*, 2013, **42**, 173–201.
36. A. Nadort, J. Zhao and E. M. Goldys, *Nanoscale*, 2016, DOI:10.1039/C5NR08477F
37. A. K. Singh, S. K. Singh and S. B. Rai, *RSC Adv.*, 2014, **9**, 27039–27061.
38. G. Chen, H. Qiu, P. N. Prasad and X. Chen, *Chem. Rev.* 2014, **114**, 5161–5214.
39. Emory M. Chan, *Chem. Soc. Rev.*, 2015, **44**, 1653–1679.
40. M. K. Tsang, G. Bai and J. Hao, *Chem. Soc. Rev.*, 2015, **44**, 1585–1607.
41. G. Chen, H. Ågren, T. Y. Ohulchanskyy and P. N. Prasad, *Chem. Soc. Rev.*, 2015, **44**, 1680–1713.
42. B. Yoon, J. Lee, I. S. Park, S. Jeon, J. Lee and J. M. Kim, *J. Mater. Chem. C*, 2013, **1**, 2388–2403.
43. L. Prodi, E. Rampazzo, F. Rastrelli, A. Speghinic and N. Zaccheronia, *Chem. Soc. Rev.*, 2015, **44**, 4922–4952.
44. Q. Zhang, C. F. Wang, L. T. Ling and Su Chen, *J. Mater. Chem. C*, 2014, **2**, 4358–4373.
45. J. Zhou, Q. Liu, W. Feng, Y. Sun, and F. Li, *Chem. Rev.*, 2015, **115**, 395–465.
46. G. Wang, Q. Peng and Y. Li, *Acc. Chem. Res.*, 2011, **44**, 322–332.
47. F. Wang and X. Liu, *Chem. Soc. Rev.*, 2009, **38**, 976–989.
48. Y. Zhang, W. Wei, G. K. Das and T. T. Y. Tan, *J. Photochem. Photobiol. C Photochem. Rev.*, 2014, **20**, 71–96.
49. S. V. Eliseeva and J.-C. G. Bünzli, *Chem. Soc. Rev.*, 2010, **39**, 189–227.
50. X. Chen, Y. Liu and D. Tu, *Lanthanide-Doped Luminescent Nanomaterials*, Springer, 2014.
51. J. Vuojola and T. Soukka, *Methods Appl. Fluoresc.*, 2014, **2**, 012001.
52. F. Wang, D. Banerjee, Y. Liu, X. Chen and X. Liu, *Analyst*, 2010, **135**, 1839–54.
53. G. Liu, *Chem. Soc. Rev.*, 2014, **44**, 1635–1652.
54. F. Auzel, *Chem. Rev.* 2004, **104**, 139–173.
55. H. Dong, L. D. Sun and C. H. Yan, *Chem. Soc. Rev.*, 2015, **44**, 1608–1634.
56. X. Li, F. Zhang and D. Zhao, *Chem. Soc. Rev.* 2015, **44**, 1346–1378.
57. J. Chen and J. X. Zhao, *Sensors*, 2012, **12**, 2414–35.
58. D. R. Gamelin and H. U. Gu, *Acc. Chem. Res.* 2000, **33**, 235–242.
59. A. Kenyon, *Progress in Quantum Electronics.* 2002, **26**, 225–284.
60. J. C. Boyer, M. P. Manseau, J. I. Murray and F. C. J. M. van Veggel, *Langmuir* 2010, **26**, 1157–1164.
61. N. Bogdan, F. Vetrone, G. A. Ozin and J. A. Capobianco, *Nano Lett.* 2011, **11**, 835–840.
62. Y. Zhang, J. Guo, T. White, T. T. Y. Tan and R. Xu, *J. Phys. Chem. C*, 2007, **111**, 7893–7897.
63. R. Si, Y. W. Zhang, H. P. Zhou, L. D. Sun and C. H. Yan, *Chem. Mater.* 2007, **19**, 18–27.
64. J. Yang, C. Li, Z. Quan, C. Zhang, P. Yang, Y. Li, C. Yu and J. Lin, *J. Phys. Chem. C*, 2008, **112**, 12777–12785.
65. J. Yang, C. Li, Z. Cheng, X. Zhang, Z. Quan, C. Zhang and J. Lin, *J. Phys. Chem. C*, 2007, **111**, 18148–18154.
66. H. Huang, G. Q. Xu, W. S. Chin, L. M. Gan and C. H. Chew, *Nanotechnology*, 2002, **13**, 318.
67. T. Xie, S. Li, Q. Peng and Y. Li, *Angew. Chem., Int. Ed.* 2009, **48**, 196–200.
68. A. M. Cross, P. S. May, F. C. J. M. van Veggel and M. T. Berry, *J. Phys. Chem. C*, 2010, **114**, 14740–14747.
69. M. N. Luwang, R. S. Ningthoujam, S. K. Srivastava and R. K. Vatsa, *J. Am. Chem. Soc.* 2011, **133**, 2998–3004.
70. C. Liu, H. Wang, X. Zhang and D. Chen, *J. Mater. Chem.*, 2009, **19**, 489–496.

Nanoscale Accepted Manuscript

71. S. Rodriguez-Liviano, F. J. Aparicio, T. C. Rojas, A. B. Hungria, L. E. Chinchilla and M. Ocana, *Cryst. Growth Des.*, 2012, **12**, 635–645.
72. K. Li, D. Chen, R. Zhang, Y. Yu, J. Xu and Y. Wang, *Mater. Res. Bull.*, 2013, **48**, 1957–1960.
73. C. Li, P. Ma, P. Yang, Z. Xu, G. Li, D. Yang, C. Peng and J. Lin, *CrystEngComm*, 2011, **13**, 1003–1013.
74. B. Fan, C. Chlique, O. Merdrignac-Conanec, X. Zhang and X. Fan, *J. Phys. Chem. C*, 2012, **116**, 11652–11657.
75. Q.Y. Zhang and X.Y. Huang, *Progress in Materials Science*, 2010, **55**, 353–427.
76. X. Y. Huang, D. C. Yu, and Q. Y. Zhanga, *Journal of applied physics*, **2009**, 106, 113521.
77. D. L. Dexter, *Phys. Rev.* 1957, **108**, 630–633.
78. C. Ronda, *J. Lumin.*, 2002, **100**, 301–305.
79. J. L. Sommerdijk, A. Bril and A. W. de Jager, *J. Lumin.*, 1974, **8**, 341–343.
80. J. L. Sommerdijk, A. Bril and A. W. de Jager, *J. Lumin.* 1974, **9**, 288–296.
81. A. M. Srivastava and W. W. Beers, *J. Lumin.*, 1997, **71**, 285–290.
82. A. M. Srivastava, D. A. Doughty and W. W. Beers, *J. Electrochem Soc* 1996, **143**, 4113–4116.
83. A. M. Srivastava, D. A. Doughty and W. W. Beers, *J. Electrochem Soc* 1997, **144**, L190–192.
84. R. Pappalardo, *J. Lumin.*, 1976, **14**, 159–193.
85. Z. Yang, J. H. Lin, M. Z. Su, Y. Tao and W. Wang, *J. Alloys Compd*, 2000, **308**, 94–97.
86. Y. Zhou, S. P. Feofilov, H. J. Seo, J. Y. Jeong, D. A. Keszler and R. S. Meltzer, *Phys Rev B* 2008, **77**, 075129.
87. R. T. Wegh, E. V. D. van Loef, G. W. Burdick and A. Meijerink, *Mol Phys* 2003, **101**, 1047–1056.
88. P. S. Peijzel and A. Meijerink, *Chem Phys Lett.* 2005, **401**, 241–245.
89. A. Guille, A. Pereira, and B. Moine, *APL Mater.* 2013, **1**, 062106.
90. L. E. Brus, *J. Chem. Phys.* 1984, **80**, 4403–4409.
91. M. G. Bawendi, M. L. Steigerwald and L. E. Brus, *Annu. Rev. Phys. Chem.* 1990, **41**, 477–496.
92. K. A. S. Fernando, S. Sahu, Y. Liu, W. K. Lewis, E. A. Gulians, A. Jafariyan, P. Wang, C. E. Bunker and Y. P. Sun, *ACS Appl. Mater. Interfaces*, 2015, **7**, 8363–8376.
93. I. L. Medintz, H. T. Uyeda, E. R. Goldman and H. Mattoussi, *Nat. Mater.* 2005, **4**, 435–446.
94. B. Dubertret, P. Skourides, D. J. Norris, V. Noireaux, A. H. Brivanlou and A. Libchaber, *Science* 2002, **298**, 1759–1762.
95. X. Y. Wu, H. J. Liu, J. Q. Liu, K. N. Haley, J. A. Treadway, J. P. Larson, N. F. Ge, F. Peale and M. P. Bruchez, *Nat. Biotechnol.* 2003, **21**, 41–46.
96. M. Y. Han, X. H. Gao, J. Z. Su and S. Nie, *Nat. Biotechnol.* 2001, **19**, 631–635.
97. W. C. W. Chan, D. J. Maxwell, X. H. Gao, R. E. Bailey, M. Y. Han and S. M. Nie, *Curr. Opin. Biotechnol.* 2002, **13**, 40–46.
98. J. Zhou, Y. Yang and C. Zhang, *Chem. Rev.* 2015, **115**, 11669–11717.
99. S. Silvi and A. Credi, *Chem. Soc. Rev.*, 2015, **44**, 4275–4289.
100. Victor I. Klimov, *Los Alamos Science*, 2003, **28**, 214–220.
101. C. Carrillo-Carrion, S. Cardenas, B. M. Simonet, and M. Valcarcel, *Chem. Commun.*, 2009, 5214–5226.
102. P. G. Luo, S. K. Sonkar, S.T. Yang, F. Yang, L. Yang, J. J. Broglie, and Y. P. Sun, *RSC Adv.* 2014, **4**, 10791–10807.
103. Y. Wang and A. Hu, *J. Mater. Chem. C*, 2014, **2**, 6921–6939.
104. J. Shen, Y. Zhu, X. Yang and C. Li, *Chem. Commun.* 2012, **48**, 3686–3699.
105. Z. Zhang, J. Zhang, N. Chena and L. Qu, *Sci.* 2012, **5**, 8869–8890.
106. L. Cao, M. J. Meziani, S. Sahu and Y. P. Sun, *Acc. Chem. Res.* 2012, **46**, 171–180.
107. X. Y. Xu, R. Ray, Y. L. Gu, H. J. Ploehn, L. Gearheart, K. Raker and W. A. Scrivens, *J. Am. Chem. Soc.*, 2004, **126**, 12736–12737.
108. Y. P. Sun, B. Zhou, Y. Lin, W. Wang, K. A. S. Fernando, P. Pathak, M. J. Meziani, B. A. Harruff, X. Wang, H. F. Wang, P. G. Luo, H. Yang, M. E. Kose, B. L. Chen, L. M. Veca and S. Y. Xie, *J. Am. Chem. Soc.*, 2006, **128**, 7756–7757.
109. P. Demchenko and M. O. Dekaliuk, *Methods Appl. Fluoresc.*, 2013, **1**, 042001.
110. S. Y. Lim, W. Shen and Z. Gao, *Chem. Soc. Rev.*, 2015, **44**, 362–381.
111. W. S. Hummers, Jr. and R. E. Offeman, *J. Am. Chem. Soc.*, 1958, **80**, 1339.
112. G. Eda, Y. Y. Lin, C. Mattevi, H. Yamaguchi, H. A. Chen, I. S. Chen, C. W. Chen and M. Chhowalla, *Adv. Mater.*, 2010, **22**, 505–509.
113. K. Krishnamoorthy, M. Veerapandian, R. Mohan and S. J. Kim, *Appl. Phys. A: Mater. Sci. Process.*, 2012, **106**, 501–506.
114. T. Gokus, R. R. Nair, A. Bonetti, M. Bohmler, A. Lombardo, K. S. Novoselov, A. K. Geim, A. C. Ferrari and A. Hartschuh, *ACS Nano*, 2009, **3**, 3963–3968.
115. L. Cao, M. J. Meziani, S. Sahu and Y. P. Sun, *Acc. Chem. Res.*, 2013, **46**, 171–180.
116. J. H. Shen, Y. H. Zhu, C. Chen, X. L. Yang and C. Z. Li, *Chem. Commun.*, 2011, **47**, 2580–2582.
117. J. H. Shen, Y. H. Zhu, X. L. Yang, J. Zong, J. M. Zhang and C. Z. Li, *New J. Chem.*, 2012, **36**, 97–101.
118. A. Nourbakhsh, M. Cantoro, T. Vosch, G. Pourtois, F. Clemente, M. H. van der Veen, J. Hofkens, M. M. Heyns, S. De Gendt and B. F. Sels, *Nanotechnology*, 2010, **21**, 435203–435211.
119. J. Robertson and E. P. O'Reilly, *Phys. Rev. B: Condens. Matter Mater. Phys.*, 1987, **35**, 2946–2957.
120. C. Mathioudakis, G. Kopidakis, P. C. Kelires, P. Patsalas, M. Gioti and S. Logothetidis, *Thin Solid Films*, 2005, **482**, 151–155.
121. C. W. Chen and J. Robertson, *J. Non-Cryst. Solids*, 1998, **227–230**, 602–606.
122. S. L. James, *Chem. Soc. Rev.*, 2003, **32**, 276–288.

Cite this: DOI: 10.1039/c0xx00000x

www.rsc.org/xxxxxx

## ARTICLE TYPE

123. M. Shah, M. C. McCarthy, S. Sachdeva, A. K. Lee and Hae-Kwon Jeong, *Ind. Eng. Chem. Res.* 2012, **51**, 2179–2199.
124. Q. L. Zhu and Q. Xu, *Chem. Soc. Rev.*, 2014, **43**, 5468–5512.
125. J. L. Wang, C. Wang and W. Lin, *ACS Catal.* 2012, **2**, 2630–2640.
126. T. H. Chen, I. Popov, W. Kaveevivitchai and O. S. Miljanic, *Chem. Mater.* 2014, **26**, 4322–4325.
127. M. O’Keeffe, *Chem. Soc. Rev.*, 2009, **38**, 1215–1217.
128. D. J. Tranchemontagne, J. L. Mendoza-Cortes, M. O’Keeffe and O. M. Yaghi, *Chem. Soc. Rev.*, 2009, **38**, 1257–1283.
129. J. J. Perry Iv, J. A. Perman and M. J. Zaworotko, *Chem. Soc. Rev.*, 2009, **38**, 1400–1417.
130. Y. Ikezoe, G. Washino, T. Uemura, S. Kitagawa and H. Matsui, *Nat. Mater.*, 2012, **11**, 1081–1085.
131. G. Ferey, C. Serre, T. Devic, G. Maurin, H. Jovic, P. L. Llewellyn, G. De Weireld, A. Vimont, M. Daturi and J.-S. Chang, *Chem. Soc. Rev.*, 2011, **40**, 550–562.
132. Q.-L. Zhu, T.-L. Sheng, R.-B. Fu, S.-M. Hu, L. Chen, C.-J. Shen, X. Ma and X.-T. Wu, *Chem.–Eur. J.*, 2011, **17**, 3358–3362.
133. M. Kurmoo, *Chem. Soc. Rev.*, 2009, **38**, 1353–1379. 41 N. Stock and S. Biswas, *Chem. Rev.*, 2011, **112**, 933–969.
134. S.-L. Li and Q. Xu, *Energy Environ. Sci.*, 2013, **6**, 1656–1683.
135. S. Horike, D. Umeyama and S. Kitagawa, *Acc. Chem. Res.*, 2013, **46**, 2376–2384.
136. A. Carne, C. Carbonell, I. Imaz and D. MasPOCH, *Chem. Soc. Rev.*, 2011, **40**, 291–305.
137. Y. Cui, Y. Yue, G. Qian and B. Chen, *Chem. Rev.* 2012, **112**, 1126–1162.
138. M. D. Allendorf, C. A. Bauer, R. K. Bhaktaa and R. J. T. Houka, *Chem. Soc. Rev.*, 2009, **38**, 1330–1352.
139. E. G. Moore, A. P. S. Samuel and K. N. Raymond, *Acc. Chem. Res.* 2009, **42**, 542–552.
140. S. I. J. Weissman, *Chem. Phys.* 1942, **10**, 214–217.
141. C. L. Cahill, D. T. de Lilla and M. Frisch, *CrystEngComm*, 2007, **9**, 15–26.
142. J. P. Zou, Q. Peng, Z. Wen, G. S. Zeng, Q. J. Xing and G. C. Guo, *Cryst. Growth Des.* 2010, **10**, 2613–2619.
143. M. Xue, G. Zhu, Y. Zhang, Q. Fang, I. J. Hewitt and S. Qiu, *Cryst. Growth Des.* 2008, **8**, 427–434.
144. J. An, C. M. Shade, D. A. Chengelis-Czegán, S. P. Petoud and N. L. Rosi, *J. Am. Chem. Soc.* 2011, **133**, 1220–1223.
145. L. M. Liz-Marzan, C. J. Murphyc and J. Wangd, *Chem. Soc. Rev.*, 2014, **43**, 3820–3822.
146. M. L. Brongersma, *Faraday Discuss.* 2015, **178**, 9–36.
147. V. Giannini, A. I. Fernandez-Domínguez, S. C. Heck and S. A. Maier, *Chem. Rev.* 2011, **111**, 3888–3912.
148. T. W. Odom and G. C. Schatz, *Chem. Rev.* 2011, **111**, 3667–3668.
149. K. L. Kelly, E. Coronado, L. L. Zhao, and G. C. Schatz, *J. Phys. Chem. B*, 2003, **107**, 668–677.
150. S. Eustis and M. A. El-Sayed, *Chem. Soc. Rev.*, 2006, **35**, 209–217.
151. S. A. Maier, *Plasmonics: Fundamentals and Applications*, Springer, New York, NY, USA, 2007.
152. S. K. Ghosh and T. Pal, *Chem. Rev.*, 2007, **107**, 4797–4862.
153. P. Zijlstra and M. Orrit, *Rep. Prog. Phys.*, 2011, **74**, 106401.
154. N. C. Lindquist, P. Nagpal, K. M. McPeak, D. J. Norris and S. H. Oh, *Rep. Prog. Phys.*, 2012, **75**, 036501.
155. K. M. Mayer and J. H. Hafner, *Chem. Rev.*, 2011, **111**, 3828–2857.
156. J. N. Anker, W. P. Hall, O. Lyandres, N. C. Shah, J. Zhao and R. P. Van Duyne, *Nat. Mater.*, 2008, **7**, 442–453.
157. M. Hu, J. Chen, Z.-Y. Li, L. Au, G. V. Hartland, X. Li, M. Marquez and Y. Xia, *Chem. Soc. Rev.*, 2006, **35**, 1084–1094.
158. X. Huang and M. A. El-Sayed, *Journal of Advanced Research*, 2010, **1**, 13–28.
159. M. W. Knight, N. S. King, L. Liu, H. O. Everitt, P. Nordlander and N. J. Halas, *ACS nano*, 2014, **8**, 834–840.
160. D. Yang, Y. Dai, P. Ma, X. Kang, Z. Cheng, C. Li and J. Lin, *Chem.–Eur. J.*, 2013, **19**, 2685–2694.
161. D. Yang, X. Kang, P. a. Ma, Y. Dai, Z. Hou, Z. Cheng, C. Li and J. Lin, *Biomaterials*, 2013, **34**, 1601–1612.
162. Q. Ju, D. T. Tu, Y. S. Liu, R. F. Li, H. M. Zhu, J. C. Chen, Z. Chen, M. D. Huang and X. Y. Chen, *J. Am. Chem. Soc.*, 2012, **134**, 1323–1330.
163. J. H. Zeng, J. Su, Z. H. Li, R. X. Yan and Y. D. Li, *Adv. Mater.*, 2005, **17**, 2119–2123.
164. H. Qiu, G. Chen, L. Sun, S. Hao, G. Han and C. Yang, *J. Mater. Chem.*, 2011, **21**, 17202–17208.
165. J. Sun, X. Mi, L. Lei, X. Pan, S. Chen, Z. Wang, Z. Bai and X. Zhang, *CrystEngComm*, 2015, **17**, 7888–7895.
166. G. S. Yi and G. M. Chow, *Adv. Funct. Mater.*, 2006, **16**, 2324–2329.
167. L. Wang and Y. Li, *Chem. Mater.* 2007, **19**, 727–734.
168. J. Lin, M. Yu, C. K. Lin and X. M. Liu, *J. Phys. Chem. C*, 2007, **111**, 5835–5845.
169. B. Dunn and J. I. Zink, *Acc. Chem. Res.*, 2007, **40**, 729.
170. W. Q. Luo, C. Y. Fu, R. F. Li, Y. S. Liu, H. M. Zhu and X. Y. Chen, *Small*, 2011, **7**, 3046–3056.
171. A. Patra, C. S. Friend, R. Kapoor and P. N. Prasad, *J. Phys. Chem. B*, 2002, **106**, 1909–1912.
172. A. Patra, C. S. Friend, R. Kapoor and P. N. Prasad, *Chem. Mater.*, 2003, **15**, 3650–3655.
173. J. Dhanaraj, R. Jagannathan, T. R. N. Kutty, and Chung-Hsin Lu, *J. Phys. Chem. B*, 2001, **105**, 11098–11105.

Nanoscale Accepted Manuscript

174. B. K. Gupta, T. N. Narayanan, S. A. Vithayathil, Y. Lee, S. Koshy, A. L. M. Reddy, A. Saha, V. Shanker, V. N. Singh, B. A. Kaiparettu, A. A. Marti and P. M. Ajayan, *Small*, 2012, **8**, 3028–3034.
175. R. Lorenzi, A. Paleari, N. V. Golubev, E. S. Ignateva, V. N. Sigaev, M. Niederberger and A. Lauria, *J. Mater. Chem. C*, 2015, **3**, 41–45.
176. T. Grzyb and S. Lis, *Inorg. Chem.*, 2011, **50**, 8112–8120.
177. W. Li and J. Lee, *J. Phys. Chem. C*, 2008, **112**, 11679–11684.
178. Y. W. Zhang, X. Sun, R. Si, L. P. You and C. H. Yan, *J. Am. Chem. Soc.*, 2005, **127**, 3260–3261.
179. V. Mahalingam, F. Vetrone, R. Naccache, A. Speghini and J. A. Capobianco, *Adv. Mater.*, 2009, **21**, 4025–4028.
180. V. Mahalingam, R. Naccache, F. Vetrone and J. A. Capobianco, *Chem.–Eur. J.*, 2009, **15**, 9660–9663.
181. G. Y. Chen, T. Y. Ohulchanskyy, A. Kachynski, H. Agren and P. N. Prasad, *ACS Nano*, 2011, **5**, 4981–4986.
182. B. F. Zhang, M. Frigoli, F. Angiuli, F. Vetrone and J. A. Capobianco, *Chem. Commun.*, 2012, **48**, 7244–7246.
183. J. C. Boyer, F. Vetrone, L. A. Cuccia and J. A. Capobianco, *J. Am. Chem. Soc.*, 2006, **128**, 7444–7445.
184. J. C. Boyer, L. A. Cuccia and J. A. Capobianco, *Nano Lett.*, 2007, **7**, 847–852.
185. R. Kumar, M. Nyk, T. Y. Ohulchanskyy, C. A. Flask and P. N. Prasad, *Adv. Funct. Mater.*, 2009, **19**, 853–859.
186. G. S. Yi and G. M. Chow, *Adv. Funct. Mater.*, 2006, **16**, 2324–2329.
187. G. Y. Chen, T. Y. Ohulchanskyy, R. Kumar, H. Agren and P. N. Prasad, *ACS Nano*, 2010, **4**, 3163–3168.
188. Y. L. Dai, D. M. Yang, P. A. Ma, X. J. Kang, X. Zhang, C. X. Li, Z. Y. Hou, Z. Y. Cheng and J. Lin, *Biomaterials*, 2012, **33**, 8704–8713.
189. J. Zhao, Z. Lu, Y. Yin, C. McRae, J. A. Piper, J. M. Dawes, D. Jin and E. M. Goldys, *Nanoscale*, 2013, **5**, 944–952.
190. A. Podhorodecki, M. Banski, J. Misiewicz, M. Afzaal, P. O'Brien, D. Cha and X. Wang, *J. Mater. Chem.*, 2012, **22**, 5356–5361.
191. G. Chen, J. Shen, T. Y. Ohulchanskyy, N. J. Patel, A. Kutikov, Z. Li, J. Song, R. K. Pandey, H. Ågren, P. N. Prasad and G. Han, *ACS Nano*, 2012, **6**, 8280–8287.
192. F. Vetrone, R. Naccache, V. Mahalingam, C. G. Morgan and J. A. Capobianco, *Adv. Funct. Mater.*, 2009, **19**, 2924–2929.
193. R. Naccache, F. Vetrone, V. Mahalingam, L. A. Cuccia and J. A. Capobianco, *Chem. Mater.*, 2009, **21**, 717–723.
194. M. Banski, A. Podhorodecki, J. Misiewicz, M. Afzaal, A. L. Abdelhady and P. O'Brien, *J. Mater. Chem. C*, 2013, **1**, 801–807.
195. Q. Liu, Y. Sun, T. S. Yang, W. Feng, C. G. Li and F. Y. Li, *J. Am. Chem. Soc.*, 2011, **133**, 17122–17125.
196. F. Vetrone, V. Mahalingam and J. A. Capobianco, *Chem. Mater.*, 2009, **21**, 1847–1851.
197. C. M. Zhang, P. A. Ma, C. X. Li, G. G. Li, S. S. Huang, D. M. Yang, M. M. Shang, X. J. Kang and J. Lin, *J. Mater. Chem.*, 2011, **21**, 717–723.
198. V. Mahalingam, F. Vetrone, R. Naccache, A. Speghini and J. A. Capobianco, *J. Mater. Chem.*, 2009, **19**, 3149–3152.
199. D. M. Yang, C. X. Li, G. G. Li, M. M. Shang, X. J. Kang and J. Lin, *J. Mater. Chem.*, 2011, **21**, 5923–5927.
200. Y. P. Du, X. Sun, Y. W. Zhang, Z. G. Yan, L. D. Sun and C. H. Yan, *Cryst. Growth Des.*, 2009, **9**, 2013–2019.
201. Z. W. Quan, D. M. Yang, P. P. Yang, X. M. Zhang, H. Z. Lian, X. M. Liu and J. Lin, *Inorg. Chem.*, 2008, **47**, 9509–9517.
202. G. S. Yi, Y. F. Peng and Z. Q. Gao, *Chem. Mater.*, 2011, **23**, 2729–2734.
203. X. Sun, Y. W. Zhang, Y. P. Du, Z. G. Yan, R. Si, L. P. You and C. H. Yan, *Chem.–Eur. J.*, 2007, **13**, 2320.
204. Y. P. Du, Y. W. Zhang, L. D. Sun and C. H. Yan, *J. Phys. Chem. C*, 2008, **112**, 405–415.
205. X. Ye, J. E. Collins, Y. Kang, J. Chen, D. T. N. Chen, A. G. Yodh, and C. B. Murray, *PNAS*, 2010, **107**, 22430–22435.
206. J. W. Stouwdam and F. C. J. M. van Veggel, *Nano Lett.*, 2002, **2**, 733–737.
207. G. S. Yi, H. C. Lu, S. Y. Zhao, G. Yue, W. J. Yang, D. P. Chen and L. H. Guo, *Nano Lett.*, 2004, **4**, 2191–2196.
208. Z. Q. Li and Y. Zhang, *Nanotechnology*, 2008, **19**, 345606.
209. Z. Li, Y. Zhang and S. Jiang, *Adv. Mater.*, 2008, **20**, 4765–4769.
210. M. Wang, C. C. Mi, S. Wang, F. Li, J. L. Liu and S. K. Xu, *Spectrosc. Spectral Anal.*, 2009, **29**, 3327–3331.
211. G. C. Jiang, J. Pichaandi, N. J. J. Johnson, R. D. Burke and F. C. J. M. van Veggel, *Langmuir*, 2012, **28**, 3239–3247.
212. H. Schafer, P. Ptacek, H. Eickmeier and M. Haase, *Adv. Funct. Mater.*, 2009, **19**, 3091–3097.
213. P. Ptacek, H. Schafer, K. Kompe and M. Haase, *Adv. Funct. Mater.*, 2007, **17**, 3843–3848.
214. G. Chen, T. Y. Ohulchanskyy, S. Liu, W.-C. Law, F. Wu, M. T. Swihart, H. Ågren and P. N. Prasad, *ACS Nano*, 2012, **6**, 2969–2977.
215. H. S. Jang, K. Woo and K. Lim, *Opt. Express*, 2012, **20**, 17107–17118.
216. S. L. Gai, G. X. Yang, X. B. Li, C. X. Li, Y. L. Dai, F. He and P. P. Yang, *Dalton Trans.*, 2012, **41**, 11716–11724.
217. T. Yang, Y. Sun, Q. Liu, W. Feng, P. Yang and F. Li, *Biomaterials*, 2012, **33**, 3733–3742.
218. H. T. Wong, F. Vetrone, R. Naccache, H. L. W. Chan, J. H. Hao and J. A. Capobianco, *J. Mater. Chem.*, 2011, **21**, 16589–16596.
219. X. Teng, Y. Zhu, W. Wei, S. Wang, J. Huang, R. Naccache, W. Hu, A. I. Y. Tok, Y. Han, Q. Zhang, Q. Fan, W. Huang, J. A. Capobianco and L. Huang, *J. Am. Chem. Soc.*, 2012, **134**, 8340–8343.
220. Y. Dai, C. Zhang, Z. Cheng, P. a. Ma, C. Li, X. Kang, D. Yang and J. Lin, *Biomaterials*, 2012, **33**, 2583–2592.
221. F. Wang, Y. Zhang, X. P. Fan and M. Q. Wang, *J. Mater. Chem.*, 2006, **16**, 1031–1034.
222. A. Valizadeh, H. Mikaeili, M. Samiei, S. M. Farkhani, N. Zarghami, M. kouhi, A. Akbarzadeh and S. Davaran, *Nanoscale Research Letters*, 2012, **7**, 480.

Cite this: DOI: 10.1039/c0xx00000x

www.rsc.org/xxxxxx

## ARTICLE TYPE

223. J. Drbohlavova, V. Adam, R. Kizek and J. Hubalek, *Int. J. Mol. Sci.* 2009, **10**, 656-673.
224. D. Bera, L. Qian T. K. Tseng and P. H., 2010, **3**, 2260–2345.
225. A. Scherer, H. G. Craighead and E. D. Beebe, *Journal of Vacuum Science & Technology B*, 1987, **5**, 1599-1605.
226. K. Tsutsui, E. L. Hu and C. D. W. Wilkinso, *Jpn. J. Appl. Phys.*, 1993, **32**, 6233-6236.
227. L. Qu and X. Peng, *J. Am. Chem. Soc.*, 2002, **124**, 2049-2055.
- 10 228. C. B. Murray, D. J. Noms, and M. G. Bawendi, *J. Am. Chem. Soc.* 1993, **115**, 8706-8715.
229. L. Qu, Z. A. Peng and X. Peng, *Nano Lett.*, 2001, **1**, 333-337.
230. L. Li, H. Qian and J. Ren, *Chem. Commun.*, 2005, 528–530.
- 15 231. S. H. Xin, P. D. Wang, A. Yin, C. Kim, M. Dobrowolska, J. L. Merz and J. K. Furdyna, *Applied Physics Letters*, 1996, **69**, 3884-3886.
232. J. H. Liu, J. B. Fan, Z. Gu, J. Cui, X. B. Xu, Z. W. Liang, S. L. Luo and M. Q. Zhu, *Langmuir*, 2008, **24**, 5241-5444.
- 20 233. S. J. Yu, M. W. Kang, H. C. Chang, K. M. Chen and Y. C. Yu, *J. Am. Chem. Soc.*, 2005, **127**, 17604–17605.
234. J. G. Zhou, C. Booker, R. Y. Li, X. T. Zhou, T.-K. Sham, X. L. Sun and Z. F. Ding, *J. Am. Chem. Soc.*, 2007, **129**, 744–745.
- 25 235. Y. Q. Dong, N. N. Zhou, X. M. Lin, J. P. Lin, Y. W. Chi and G. N. Chen, *Chem. Mater.*, 2010, **22**, 5895–5899.
236. Q. L. Wang, H. Z. Zheng, Y. J. Long, L. Y. Zhang, M. Gao and W. J. Bai, *Carbon*, 2011, **49**, 3134–3140.
237. H. P. Liu, T. Ye and C. D. Mao, *Angew. Chem., Int. Ed.*, 30 2007, **46**, 6473–6475.
238. (a) H. Ming, Z. Ma, Y. Liu, K. M. Pan, H. Yu, F. Wang and Z. H. Kang, *Dalton Trans.*, 2012, **41**, 9526–9531. (b) R. Ye, C. Xiang, J. Lin, Z. Peng, K. Huang, Z. Yan, N. P. Cook, E. L.G. Samuel, C. C. Hwang, G. Ruan, G. Ceriotti, A. R. O. Raji, A. A. Marti and J. M. Tour, *Nature Communications*, 2013, **4**, 1-6.
- 35 239. B. Bourlinos, A. Stassinopoulos, D. Anglos, R. Zboril, M. Karakassides and E. P. Giannelis, *Small*, 2008, **4**, 455–458.
240. H. Peng and J. Travas-Sejdic, *Chem. Mater.*, 2009, **21**, 40 5563–5565.
241. H. T. Li, X. D. He, Y. Liu, H. Huang, S. Y. Lian, S. T. Lee and Z. H. Kang, *Carbon*, 2010, **49**, 605–609.
242. R. L. Liu, D. Q. Wu, S. H. Liu, K. Koynov, W. Knoll and Q. Li, *Angew. Chem., Int. Ed.*, 2009, **48**, 4598–4601.
- 45 243. H. Zhu, X. L. Wang, Y. L. Li, Z. J. Wang, F. Yang and X. R. Yang, *Chem. Commun.*, 2009, 5118–5120.
244. H. T. Li, H. Ming, Y. Liu, H. Yu, X. D. He, H. Huang, K. M. Pan, Z. H. Kang and S. T. Lee, *New J. Chem.*, 2011, **35**, 2666–2670.
- 50 245. Y. M. Guo, Z. Wang, H. W. Shao and X. Y. Jiang, *Carbon*, 2013, **52**, 583–589.
246. Z. C. Yang, X. Li and J. Wang, *Carbon*, 2011, **49**, 5207–5212.
247. H. Y. Wu, C. C. Mi, H. Q. Huang, B. F. Han, J. Li and S. K. Xu, *J. Lumin.*, 2012, **132**, 1603–1607.
- 55 248. B. Zhang, C. Y. Liu and Y. Liu, *Eur. J. Inorg. Chem.*, 2010, 4411–4414.
249. Z. C. Yang, M. Wang, A. M. Yong, S. Y. Wong, X. H. Zhang, H. Tan, A. Y. Chang, X. Li and J. Wang, *Chem. Commun.*, 2011, **47**, 11615–11617.
- 60 250. S. Chandra, P. Das, S. Bag, D. Laha and P. Pramanik, *Nanoscale*, 2011, **3**, 1533–1540.
251. S. C. Ray, A. Saha, N. R. Jana and R. Sarkar, *J. Phys. Chem. C*, 2009, **113**, 18546–18551.
- 65 252. J. J. Zhou, Z. H. Sheng, H. Y. Han, M. Q. Zou and C. X. Li, *Mater. Lett.*, 2012, **66**, 222–224.
253. W. B. Lu, X. Y. Qin, S. Liu, G. H. Chang, Y. W. Zhang, Y. L. Luo, A. M. Asiri, A. O. Al-Youbi and X. P. Sun, *Anal. Chem.*, 2012, **84**, 5351–5357.
- 70 254. S. Sahu, B. Behera, T. K. Maiti and S. Mohapatra, *Chem. Commun.*, 2012, **48**, 8835–8837.
255. H. Huang, J. J. Lv, D. L. Zhou, N. Bao, Y. Xu, A. J. Wang and J. J. Feng, *RSC Adv.*, 2013, **3**, 21691–21696.
256. V. N. Mehta, S. Jha and S. K. Kailasa, *Mater. Sci. Eng. C*, 75 2014, **38**, 20–27.
257. J. Wang, C. F. Wang and S. Chen, *Angew. Chem., Int. Ed.*, 2012, **51**, 9297-9301.
258. Y.H. Yang, J. H. Cui, M. T. Zheng, C. F. Hu, S. Z. Tan, Y. Xiao, Q. Yang and Y. L. Liu, *Chem. Commun.*, 2012, **48**, 380–382.
- 80 259. D. Chowdhury, N. Gogoi and G. Majumdar, *RSC Adv.*, 2012, **2**, 12156–12159.
260. J. R. Neabo, C. Vigier-Carriere, S. Rondeau-Gagne and J. F. Morin, *Chem. Commun.*, 2012, **48**, 10144–10146.
- 85 261. Q. H. Liang, W. J. Ma, Y. Shi, Z. Li and X. M. Yang, *Carbon*, 2013, **60**, 421–428.
262. A. C. Sanchez, I. Imaz, M. C. Sarabia and D. Maspoch, *Nat. Chem.*, 2013, **5**, 203–211.
263. N. Stock and S. Biswas, *Chem. Rev.* 2012, **112**, 933–969.
- 90 264. Y. R. Lee, J. Kim and W. S. Ahn, *Korean J. Chem. Eng.*, 2013, **30**, 1667-1680.
265. Y. Lu and B. Yan, *J. Mater. Chem. C*, 2014, **2**, 7411–7416.
266. A. X. Wang and X. Kong, *Materials*, 2015, **8**, 3024-3052.
267. X. Lu, M. Rycenga, S. E. Skrabalak, B. Wiley and Y. Xia, *Annu. Rev. Phys. Chem.* 2009, **60**, 167–192.
- 95 268. M. B. Cortie and A. M. McDonagh, *Chem. Rev.*, 2011, **111**, 3713–3735.

269. M. Rycenga, C. M. Cobley, J. Zeng, W. Li, C. H. Moran, Q. Zhang, D. Qin and Younan Xia, *Chem. Rev.* 2011, **111**, 3669–3712.
270. W. A. Murray and W. L. Barnes, *Adv. Mater.*, 2007, **19**, 3771–3782.
271. U. Y. Qazi and R. Javaid, *Advances in Nanoparticles*, 2016, **5**, 27-43.
272. F. Kretschmer, S. Muhlig, S. Hoepfener, A. Winter, M. D. Hager, C. Rockstuhl, T. Pertsch, and U. S. Schubert, *Part. Part. Syst. Charact.* 2014, **31**, 721–744.
273. Z. Fan, X. Huang, C. Tan and H. Zhang, *Chem. Sci.*, 2015, **6**, 95–111.
274. M. R. Jones, K. D. Osberg, R. J. Macfarlane, M. R. Langille and C. A. Mirkin, *Chem. Rev.*, 2011, **111**, 3736–3827.
275. I. Pastoriza-Santos and L. M. Liz-Marzán, *Adv. Funct. Mater.* 2009, **19**, 679–688.
276. M. Behera and S. Ram, *Int. Nano Lett.*, 2013, **3**, 17, pp1-7.
277. Y. Borodko, S. E. Habas, M. Koebel, P. Yang, H. Frei and G. A. Somorjai, *J. Phys. Chem. B*, 2006, **110**, 23052–23059.
278. W. A. Al-Saidi, H. Feng and K. A. Fichthorn, *Nano Lett.* 2012, **12**, 997–1001.
279. X. Xia, J. Zeng, L. K. Oetjen, Q. Li and Y. Xia, *J. Am. Chem. Soc.* 2012, **134**, 1793–1801.
280. W. A. Saidi, H. Feng and K. A. Fichthorn, *J. Phys. Chem. C*, 2013, **117**, 1163–1171.
281. A. Kedia and P. S. Kumar, *J. Phys. Chem. C*, 2012, **116**, 23721–23728.
282. P. C. Angelomé, H. H. Mezerji, B. Goris, I. P. Santos, J. P. Juste, S. Bals and L. M. L. Marzán, *Chem. Mater.*, 2012, **24**, 1393–1399.
283. Q. Zhang, N. Li, J. Goebel, Z. Lu and Y. Yin, *J. Am. Chem. Soc.* 2011, **133**, 18931–18939.
284. M. R. Langille, M. L. Personick and J. Zhang and C. A. Mirkin, *J. Am. Chem. Soc.* 2012, **134**, 14542–14554.
285. X. Ye, L. Jin, H. Caglayan, J. Chen, G. Xing, C. Zheng, V. Doan-Nguyen, Y. Kang, N. Engheta, C. R. Kagan and C. B. Murray, *ACS Nano*, 2012, **6**, 2804–2817.
286. K. C. Ng and W. Cheng, *Nanotechnology*, 2012, **23**, 105602.
287. C. Damm, D. Segets, G. Yang, B. F. Vieweg, E. Spiecker and W. Peukert, *Small*, 2011, **7**, 147–156.
288. M. Min, C. Kim, Y. I. Yang, J. Yi and H. Lee, *Chem. Commun.*, 2011, **47**, 8079–8081.
289. C. R. Bridges, P. M. DiCarmine, A. Fokina, D. Huesmann and D. S. Seferos, *J. Mater. Chem. A*, 2013, **1**, 1127–1133.
290. D. Nykypanchuk, M. M. Maye, D. van der Lelie and O. Gang, *Nature*, **451**, 549–552.
291. N. G. Bastus, J. Comenge and V. Puntes, *Langmuir*, 2011, **27**, 11098–11105.
292. Z. Wang, L. Tang, L. H. Tan, J. Li and Y. Lu, *Angew. Chem Int. Ed.* 2012, **51**, 9078–9082.
293. R. Fan, S. W. Chew, V. V. Cheong and B. P. Orner, *Small*, 2010, **6**, 1483–1487.
294. T. Blumenthal, J. Meruga, P. S. May, J. Kellar, W. Cross, K. Ankireddy, S. Vunnam and Q. N. Luu, *Nanotechnology*, 2012, **23**, 185305.
295. M. You, J. Zhong, Y. Hong, Z. Duan, M. Lin and F. Xu, *Nanoscale*, 2015, **7**, 4423–4431.
296. Z. Lu, Y. Liu, W. Hu, X. Wen (David) Loub and C. M. Li, *Chem. Commun.*, 2011, **47**, 9609–9611.
297. L. L. da Luz, R. Milani, J. F. Felix, I. R. B. Ribeiro, M. Talhavini, B. A. D. Neto, J. Chojnacki, M. O. Rodrigues and S. A. Júnior, *ACS Appl. Mater. Interfaces*, 2015, **7**, 27115–27123.
298. C. C. Cuerva, M. Zieba, V. Sebastian, G. Martínez, J. Sese, S. Irusta, V. Contamina, M. Arruebo and J. Santamaria, *Nanotechnology*, 2016, **27**, 095702.
299. [http://www.optomec.com/wp-content/uploads/2014/04/AJ\\_Printed\\_Electronics\\_Overview\\_whitepaper.pdf](http://www.optomec.com/wp-content/uploads/2014/04/AJ_Printed_Electronics_Overview_whitepaper.pdf).
300. J. M. Meruga, A. Baride, W. Cross, J. J. Kellara and P. S. May, *J. Mater. Chem. C*, 2014, **2**, 2221–2227.
301. M. Singh, H. M. Haverinen, P. Dhagat, and G. E. Jabbour, *Adv. Mater.* 2010, **22**, 673–685.
302. OE-A Roadmap for Organic and Printed Electronics, Organic Electronics Association OE-A, Frankfurt, 2008.
303. E. Tekin, P. J. Smith and U. S. Schubert, *Soft Matter*, 2008, **4**, 703–713.
304. D. Pesach and A. Marmur, *Langmuir*, 1987, **3**, 519–524.
305. J. A. Lim, W. H. Lee, H. S. Lee, J. H. Lee, Y. D. Park and K. Cho, *Adv. Funct. Mater.*, 2008, **18**, 229–234.
306. (a) J. Perelaer, P. J. Smith, E. van den Bosch, S. S. C. van Grootel, P. H. J. M. Ketelaars and U. S. Schubert, *Macromol. Chem. Phys.* 2009, **210**, 495–502. (b) J. Perelaer, P. J. Smith, M. M. P. Wijnen, E. van den Bosch, R. Eckardt, P. H. J. M. Ketelaars, U. S. Schubert, *Macromol. Chem. Phys.* 2009, **210**, 387–393.
307. L. Chen, Y. Zhang, A. Luo, F. Liu, Y. Jiang, Q. Hu, S. Chen and R. S. Liu, *Phys. Status Solidi RRL*, 2012, **6**, 321–323.
308. M. Wang, M. Li, M. Yang, X. Zhang, A. Yu, Y. Zhu and P. Qiu, *Nano Research*, 2015, **8**, 1800–1810.
309. Y. Zhang, L. Zhang, R. Deng, J. Tian, Y. Zong, D. Jin and Xiaogang Liu, *J. Am. Chem. Soc.* 2014, **136**, 4893–4896.
310. N. M. Sangeetha, P. Moutet, D. Lagarde, G. Sallen, B. Urbaszek, X. Marie, G. Viau and L. Ressler, *Nanoscale*, 2013, **5**, 9587–9592.
311. J. M. Ramos, J. C. R. Morales, P. A. Mora and N. M. Khaidukov, *J. Mater. Chem. C*, 2016, **4**, 801–806.
312. A. Baride, J. M. Meruga, C. Douma, D. Langerman, G. Crawford, J. J. Kellar, W. M. Cross and P. S. May, *RSC Adv.*, 2015, **5**, 101338–101346.
313. Y. Liu, K. Ai and L. Lu, *Nanoscale*, 2011, **3**, 4804–4810.
314. S. K. Singh, A. K. Singh and S. B. Rai, *Nanotechnology*, 2011, **22**, 275703.
315. B. Bao, M. Li, Y. Li, J. Jiang, Z. Gu, X. Zhang, L. Jiang and Y. Song, *Small*, 2015, **11**, 1649–1654.
316. Y. Gao, Q. Dong, S. Lan, Q. Cai, O. Simalou, S. Zhang, G. Gao, H. Chokto and A. Dong, *ACS Appl. Mater. Interfaces*, 2015, **7**, 10022–10033.
317. L. Zhou, A. Zhao, Z. Wang, Z. Chen, J. Ren and Xiaogang Qu, *ACS Appl. Mater. Interfaces*, 2015, **7**, 2905–2911.

Cite this: DOI: 10.1039/c0xx00000x

www.rsc.org/xxxxxx

## ARTICLE TYPE

318. J. Cui, S. Xu, C. Guo, R. Jiang, T. D. James and L. Wang, *Anal. Chem.*, 2015, **87**, 11592–11598. 50
319. F. Wang, Z. Xie, B. Zhang, Y. Liu, W. Yang and C. Liu, *Nanoscale*, 2014, **6**, 3818–3823.
- 5 320. X. Wen, L. Shi, G. Wen, Y. Li, C. Dong, J. Yang and S. Shuang, *Sensors and Actuators B*, 2015, **221**, 769–776.
321. J. Wang, C. F. Wang and S. Chen, *Angew. Chem. Int. Ed.*, 2012, **51**, 9297–9301.
322. B. Wang, A. Song, L. Feng, H. Ruan, H. Li, S. Dong and J. 55  
Hao, *ACS Appl. Mater. Interfaces*, 2015, **7**, 6919–6925. 10
323. S. Gao, Y. Chen, H. Fan, X. Wei, C. Hu, L. Wang and L. Qu, *J. Mater. Chem. A*, 2014, **2**, 6320–6325.
324. K. A. White, D. A. Chengelis, K. A. Gogick, J. Stehman, N. L. Rosi, and S. Petoud, *J. Am. Chem. Soc.* 2009, **131**, 18069–18071. 15
325. W. J. Li, J. F. Feng, Z. J. Lin, Y. L. Yang and Y. Yang, X. S. Wang, S. Y. Gao and R. Cao, *Chem. Commun.*, 2016, **52**, 3951–3954. 60
326. Y. Zhou and B. Yan, *J. Mater. Chem. C*, 2015, **3**, 8413–8418. 20
327. J. Zhang, Y. Yuan, G. Liang, M. N. Arshad, H. A. Albar, T. R. Sobahic and S. H. Yu, *Chem. Commun.*, 2015, **51**, 10539–10542. 65
328. C. F. Huebner, J. B. Carroll, D. D. Evanoff, Jr., Y. Ying, B. J. Stevenson, J. R. Lawrence, J. M. Houchins, A. L. Foguth, J. Sperry and S. H. Foulger, *J. Mat. Chem.*, 2008, **18**, 4942–4948. 25
329. L. Xu, Z. Zhou, C. Zhang, Y. He and B. Su, *Chem. Commun.*, 2014, **50**, 9097–9100. 70
- 30 330. L. Xu, Y. Li, Y. He and B. Su, *Analyst*, 2013, **138**, 2357–2362.
331. L. Xu, Y. Li, S. Wu, X. Liu and B. Su, *Angew. Chem.*, 2012, **124**, 8192–8196.
332. Z. Zhou, L. Xu, S. Wu and B. Su, *Analyst*, 2014, **139**, 4934–4939. 35
333. J. Tan, L. Xu, T. Li, B. Su and J. Wu, *Angew. Chem.*, 2014, **53**, 9822–9826. 75

40

80

45

85

## Author(s) Biography

### Pawan Kumar



Pawan Kumar received his B. Sc. and M. Sc. degree in 2009 and 2011 from Guru Nanak Dev University, Amritsar, Punjab, India. Currently, he is pursuing his Ph.D. from Academy of Innovative and Scientific Research (AcSIR) in CSIR-National Physical Laboratory, New Delhi, India. He is a recipient of prestigious national RGNF fellowship in Physical Sciences (2011-2012). He has more than 26 research publications in reputable international journals. His research interest is focused on the synthesis of luminescent nanomaterials (0D-3D) and their multifunctional applications in security inks, bio-labeling and phosphor based spectral converter to enhance the efficiency of Si solar cell.

### Satbir Singh



Satbir Singh received his B. Sc. and M. Sc. degree in 2011 and 2013 from Guru Nanak Dev University, Amritsar, Punjab, India. Currently, he is pursuing his Ph.D. degree from Academy of Innovative and Scientific Research (AcSIR) in CSIR-National Physical Laboratory, New Delhi, India. He is a recipient of prestigious national MANF fellowship in Physical Sciences (2014-2015). His research interest is focused on the synthesis of advanced multifunctional luminescent nanomaterials particularly; rare-earth/rare-earth free based nanomaterials for their applications in invisible luminescent security ink, optoelectronic devices, biological fluorescence labeling, field emission displays and luminomagnetic nanophosphors for drug delivery and magnetic tracking.

45

### Bipin Kumar Gupta



50

Dr. Bipin Kumar Gupta received his B.Sc., M.Sc. and Ph.D. degrees in Physics 1996, 1998 and 2004, respectively from Banaras Hindu University, Varanasi, Uttar Pradesh, India. Presently, he is Scientist in CSIR-National Physical Laboratory, New Delhi, India. He is a recipient of INDO-US fellowship in Physical Sciences (2010-11). He has more than 85 publications in reputable international journals. His current research interests are luminescent materials (0-D, 1-D, 2-D and 3D) for applications in invisible luminescent security ink, security codes, optoelectronic devices, biological fluorescence labeling, fluorescence quenching, luminescent paint, field emission displays and luminomagnetic nanophosphors for drug delivery and magnetic tracking.

65

40